Terms and Conditions of Use of Digitised Theses from Trinity College Library Dublin

Copyright statement

All material supplied by Trinity College Library is protected by copyright (under the Copyright and Related Rights Act, 2000 as amended) and other relevant Intellectual Property Rights. By accessing and using a Digitised Thesis from Trinity College Library you acknowledge that all Intellectual Property Rights in any Works supplied are the sole and exclusive property of the copyright and/or other IPR holder. Specific copyright holders may not be explicitly identified. Use of materials from other sources within a thesis should not be construed as a claim over them.

A non-exclusive, non-transferable licence is hereby granted to those using or reproducing, in whole or in part, the material for valid purposes, providing the copyright owners are acknowledged using the normal conventions. Where specific permission to use material is required, this is identified and such permission must be sought from the copyright holder or agency cited.

Liability statement

By using a Digitised Thesis, I accept that Trinity College Dublin bears no legal responsibility for the accuracy, legality or comprehensiveness of materials contained within the thesis, and that Trinity College Dublin accepts no liability for indirect, consequential, or incidental, damages or losses arising from use of the thesis for whatever reason. Information located in a thesis may be subject to specific use constraints, details of which may not be explicitly described. It is the responsibility of potential and actual users to be aware of such constraints and to abide by them. By making use of material from a digitised thesis, you accept these copyright and disclaimer provisions. Where it is brought to the attention of Trinity College Library that there may be a breach of copyright or other restraint, it is the policy to withdraw or take down access to a thesis while the issue is being resolved.

Access Agreement

By using a Digitised Thesis from Trinity College Library you are bound by the following Terms & Conditions. Please read them carefully.

I have read and I understand the following statement: All material supplied via a Digitised Thesis from Trinity College Library is protected by copyright and other intellectual property rights, and duplication or sale of all or part of any of a thesis is not permitted, except that material may be duplicated by you for your research use or for educational purposes in electronic or print form providing the copyright owners are acknowledged using the normal conventions. You must obtain permission for any other use. Electronic or print copies may not be offered, whether for sale or otherwise to anyone. This copy has been supplied on the understanding that it is copyright material and that no quotation from the thesis may be published without proper acknowledgement.

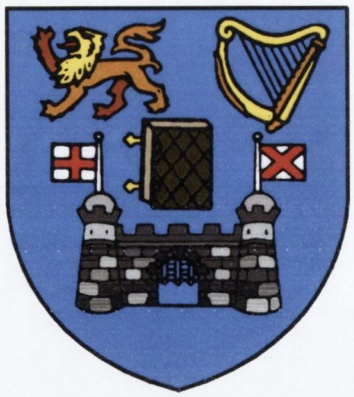

Nonlinear Optical Extinction in Organic and Inorganic Nanomaterials

by

James Joseph Doyle

A thesis submitted in partial fulfilment for the degree of

Doctor of Philosophy

School of Physics

Trinity College Dublin

September 2006

Declaration

I declare that the work in this dissertation has not been previously submitted as an exercise for a degree to this or any other university.

The work described herein is entirely my own, except for the assistance mentioned in the acknowledgements and collaborative work mentioned in the list of publications.

I agree that Trinity College Dublin may lend or copy this dissertation on request.

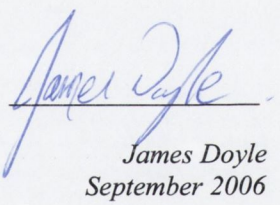

James Doyle
September 2006

"We need men who can dream of things that never were."

John F. Kennedy
Dublin, Ireland, 28th June 1963
(1971-1963)

"Invention is the talent of youth, as judgment is of age."

Jonathan Swift
Writer, Satirist, Poet
(1667-1745)

Acknowledgements

First and foremost I wish to express my deep gratitude and appreciation to Prof. Werner Blau for his supervision, understanding, financial support and continuous scientific guidance throughout the term of my studies. His relentless enthusiasm to this scientific field remains a source of personal inspiration and motivation. Secondly I wish to thank Dr. Jonathan Coleman for guidance with joint research projects and constant availability for fruitful scientific discussion. Scientific supervision could not be fully acknowledged without mentioning Dr. Sean O'Flaherty. In freely donating his time, knowledge, proficiency and professional approach to science, I can only offer him my most sincere gratitude, respect and appreciation, both as a past colleague and true friend.

To the wider Group Bu community I thank you for helping to fashion and merge this magnificent atmosphere of learning, friendship and pleasure. Firstly to the past members who paved the way: Bernd, Catriona, Christian, Colin, Eleni, Eva, Eveann, Gavin, Grace, Kevin, Manuel, Margaret, Martin, Nacho, Patrick, Rebekah, Rob, Sandy, Shweta, Silvia, Stefanie, Stephen and Valerie. For present members, Adam, Anna, Christopher, Darren, David B., David, Denis, Donal, Eimhin, Fiona, Helen, Ian, Javier, Jun, Martin, Niall, Paula, Ronan, Rory, Shane, Sharon, Takeyuki, Umar, Valeria, Yenny, I wish you all success in future endeavours. To past and present members of Materials Ireland, Cathal, Ciara, Chris, Emer, Geraldine, Jenny, Keith, Manuel, Marie, Ramesh, Una, Tony and Trevor, I wish to extend my deep appreciation. Special thank must go to Jeanette Cummins for her constant work behind the scenes which has never gone unnoticed.

Both the administrative and technical staff in the school of physics have always been very helpful and efficient when I have needed their assistance. Special thanks must go to Mr. Kelly, Dave, Jemmer, Joe, Ken, Mick, Nigel, Patrick and Robbie. Equally I must mention Michelle, Susan, Suzanne, Rebecca and Úna.

For proof reading, I wish to thank Dr. Kevin Ryan, Dr. Sean O'Flaherty and Prof. Werner Blau. For financial support I wish to thank Enterprise Ireland. The materials were synthesised and produced by various individuals and their invaluable contribution is acknowledged: Dr. Martin Cadek (ex-TCD) for "MWNTs", Anna Drury (TCD) for "PmPV". Thanks to the network partners, Prof M. Hanack (Universität Tübingen, Germany), Prof. M. Cook (University of East Anglia, UK), Prof T. Torres (Universidad Autónoma de Madrid, Spain), Prof. Whorle (Universität Bremen, Germany), Prof R. Norte (Universiteit Nijmegen, The Netherlands). I wish to thank the postgraduate students and researchers in these groups, both past and present, for producing phthalocyanine compounds. I wish to especially thank Prof. Yu Chen (East China University of Science and Technology, China) and his researchers for synthesizing and supplying phthalocyanines. For supplying MoSI nanowires I gratefully acknowledge Prof. Dragan Mihailovic and his group (Institut "Jozef Stefan", Slovenia). Thanks to Tadgh Hegarty for his lab assistance during his final year project. For interferometry imaging and microscopy studies, I wish to acknowledge Neal Leddy (TCD).

Finally I wish to sincerely thank my family, without which I wouldn't attain my goals: my parents, Susan, Raymond and Mary, for their unwavering support, continuous contact, sacrifices, laughs and understanding, thoughtfulness, constant love and belief. I love you all deeply.

Abstract

This thesis will focus on the nonlinear optical dissipation of high intensity nanosecond laser irradiation by polymer-phthalocyanine films and nano-structured dispersions. The nonlinear optical investigation of a selection of solid-state polymer-phthalocyanine films is initially presented. Using the straightforward method of sequentially deposited spin cast phthalocyanine doped polymer films, the resulting nonlinear optical response was characterized by the use of the open aperture Z-scan technique. Molecular engineering of metallophthalocyanine compounds, through both axial and peripheral substitutes has led to an optimisation the nonlinear optical response of the compound in the nanosecond regime. Effective optical coefficients with a nonlinear absorption based model are calculated, and their intensity dependence is investigated. Mechanistic implications of the optical dissipation are also discussed and examined in three separate case studies. For the optical limiting experiments the open aperture Z-scan technique was used probing total transmittance through the sample. The second harmonic, 532nm, of a Q-switched Nd:YAG laser was used with a pulse repetition rate of 10Hz. The beam was spatially filtered to remove the higher order modes and tightly focused with a 9cm focal length lens.

Experimental measurements of $Mo_6S_{4.5}I_{4.5}$ nanowires investigating the nonlinear optical extinction (NLE) of nanosecond laser pulses are also reported. These studies were performed using the open aperture Z-scan technique at 532nm and 1064nm, in an identical geometry as outlined above. Concentration dependent studies were performed for $Mo_6S_{4.5}I_{4.5}$ nanowires dispersed in isopropanol at sequentially decreasing concentrations, showing direct correlation between the NLE response and nanowire bundle diameter. Intensity dependent scattering experiments are presented for $Mo_6S_{4.5}I_{4.5}$ nanowire dispersions at 532nm and 1064nm. The NLE was compared with that for a stabilized Multi-Walled Carbon Nanotube (MWNT)-polymer composite dispersion.

Table of Contents

Chapter 5:

Chapter 6:

Appendix I:

Table of Figures

CHAPTER 1

INTRODUCTION

1.1 Scientific Overview

The advancement of individual research fields through scientific interdisciplinary co-operation has led to a more profound understanding of present day scientific objectives. The exploitation of the intrinsic properties of materials is a constant goal and motivation amongst material scientists. The ultimate challenge remains the harnessing of the resulting properties in order to meet varying complex social and industrial issues. In conjunction with technological developments, the advancement of synthetic materials research capable of imitating highly advanced natural structures is of paramount importance.

With the invention of the laser[1, 2] experimental investigations into non-classical physical properties of material systems were finally realised, leading to the birth of the nonlinear optical era. Further development into this rapidly advancing photonic field led to the possibility of controlling the high energy electron excited state dynamics of individual molecular compounds. Such compounds include organic based polymers and nanomaterials which, through their straightforward architectural flexibility, can be modified specific to target properties. Nano-structured materials such as carbon nanotubes,[3] defined as nanometre sized cylinders composed of graphitic carbon, are the focus of ongoing research interest to exploit their potential multi-functionality.

The main theme of this thesis report involves the concept of optical limiting, defined as "*the nonlinear dissipation of high intensity light, whilst allowing for the high transmission of ambient light*". At low incident energies the transmitted intensity increases linearly as a function of the incident intensity. Ideally above an incident intensity threshold the transmitted light remains constant and is independent of the increasing incident light irradiation. This intensity threshold marks the onset of nonlinear absorption and scattering processes which are specific to molecular structure. This concept may be achieved through harnessing the physical properties of materials, including nonlinear absorption and scattering processes. Phthalocyanines and C_{60} fullerene are examples of passive materials with relatively high optical damage threshold, a low intensity activation threshold and a fast nonlinear optical response to incident nanosecond laser irradiation.[4-19] Bohren[20]

defines optical dissipation of light in this fashion as *nonlinear optical extinction* (NLE), which includes all nonlinear optical processes involved. Potential uses for such processes include the protection of optical sensors, pulse shaping and optical regulation.

1.2 Thesis Outline

The overall aim of this thesis report is to investigate the linear and nonlinear optical properties of various nanoscale materials and structures including polymer-phthalocyanine films, $Mo_6S_{4.5}I_{4.5}$ nanowires, phthalocyanine nanoparticles and multi-walled carbon nanotubes. Various experimental techniques including spectroscopy, microscopy and the open aperture Z-scan technique for both nonlinear optical and scattering investigations will be employed.

Chapter 2 will review the theory of harmonic light-matter interactions, beginning at a classical level with Maxwells Equations and the Lorentz Model and expanding into a comprehensive discussion on anharmonic interactions. The Z-scan technique will also be introduced together with relevant theory.

Continuing on from the theoretical discussion, **Chapter 3** will introduce the materials to be investigated. The scientific background and material synthesis will be discussed for each system, in conjunction with electronic configuration and the standard nomenclature for sample labelling and identification.

The experimental investigations, literature reviews, results and conclusions will be presented in the following two chapters. A series of chemically modified polymer-phthalocyanine composite films were prepared to study the resulting linear and nonlinear optical properties. Sample preparation and film surface imaging, in conjunction with the linear optical properties will be detailed and discussed in **Chapter 4**. The nonlinear optical properties will also be examined for the polymer-phthalocyanine films, highlighted by three case studies, each representing a phthalocyanine molecular structural modification. **Chapter 5** is entitled "*Nonlinear Optical Response from $Mo_6S_{4.5}I_{4.5}$ Nanowires & Phthalocyanine Nanoparticles*".

This chapter will explore the nonlinear optical extinction from such systems and investigate the mechanisms of such optical dissipation. Multi-walled carbon nanotube dispersions are employed as a reference system for comparison purposes.

Finally **Chapter 6** will highlight the main scientific conclusions from this research, discussing future work, potential exploitation and realisation of the various nonlinearly responsive media in working device structures.

References

1 A. L. Schawlow, and C. H. Townes, *Physical Review* **112**, (6), 1940 (1958).
2 G. Gould, *US Patent* 19 (1977).
3 S. Iijima, *Nature* **354**, 56-58 (1991).
4 P. Miles, *Applied Optics* **38**, (3), 566-570 (1999).
5 P. A. Miles, *Applied Optics* **33**, (30), 6965-6979 (1994).
6 F. Z. Henari, K. H. Cazzini, D. N. Weldon, and W. J. Blau, *Applied Physics Letters* **68**, (5), 619-621 (1996).
7 F. Z. Henari, S. Macnamara, O. Stevenson, J. Callaghan, D. Weldon, and W. J. Blau, *Advanced Materials* **5**, (12), 930-934 (1993).
8 F. Henari, J. Callaghan, H. Stiel, W. Blau, and D. J. Cardin, *Chemical Physics Letters* **199**, (1-2), 144-148 (1992).
9 Y. Kajii, T. Nakagawa, S. Suzuki, Y. Achiba, K. Obi, and K. Shibuya, *Chemical Physics Letters* **181**, (2-3), 100-104 (1991).
10 W. J. Blau, H. J. Byrne, D. J. Cardin, T. J. Dennis, J. P. Hare, H. W. Kroto, R. Taylor, and D. R. M. Walton, *Physical Review Letters* **67**, (11), 1423 (1991).
11 D. R. Coulter, V. M. Miskowski, J. W. Perry, T. H. Wei, E. W. V. Stryland, and D. J. Hagan, *SPIE Proc.* **1105**, 42 (1989).
12 H. S. Nalwa, A. Kakuta, and A. Mukoh, *Journal of Physical Chemistry* **97**, (6), 1097-1100 (1993).
13 H. S. Nalwa, T. Saito, A. Kakuta, and T. Iwayanagi, *Journal of Physical Chemistry* **97**, (41), 10515-10517 (1993).
14 J. S. Shirk, R. G. S. Pong, F. J. Bartoli, and A. W. Snow, *Applied Physics Letters* **63**, (14), 1880-1882 (1993).
15 J. W. Perry, K. Mansour, S. R. Marder, K. J. Perry, D. J. Alvarez, and I. Choong, *Optics Letters* **19**, (9), 625-627 (1994).
16 H. S. Nalwa, and A. Kakuta, *Thin Solid Films* **254**, (1-2), 218-223 (1995).
17 G. de la Torre, P. Vazquez, F. Agullo-Lopez, and T. Torres, *Journal of Materials Chemistry* **8**, (8), 1671-1683 (1998).
18 N. B. McKeown, *Phthalocyanine Materials: Synthesis, Structure and Function (Eds: B. Dunn, J.W. Goodby, A.R. West)*. Cambridge University Press: 1998.
19 S. R. Mishra, and S. C. Mehendale, *Handbook of advanced electronic and photonic materials and devices*. Academic Press: San Diego, CA ; London, 2001; Vol. 9, p 347-364.
20 C. F. Bohren, and D. R. Huffman, *Absorption and Scattering of Light by Small Particles*. Wiley-Interscience: 1983; p 1-11.

CHAPTER 2

LINEAR & NONLINEAR OPTICAL INTERACTION WITH MATERIALS

2.1 Introduction

In the most basic form, absorption in optics can be considered as the process by which the energy of a photon is taken up by another entity. We define the absorbance of an object as the degree of incident light dissipated via vibronic electron excited state dynamics. This may be related to other material properties through the Beer-Lambert law in which the absorption of light is directly related to the material through which the light is travelling. In **Figure 2.1** the incident light intensity, I_0, is reduced through absorption processes in the solution, of path length l, (with absorbance α and concentration C) resulting in a transmitted intensity of I_1.

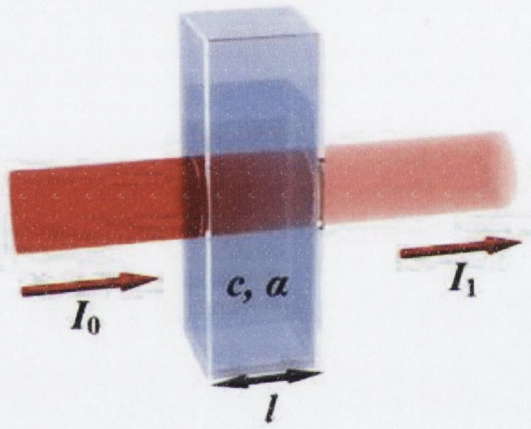

Figure 2.1 Schematic showing the absorption of incident light intensity, I_0, by a solution contained in a glass cuvette. (c-molar concentration, α-absorbance).

The Beer-Lambert Law [1] states that there is an exponential dependence between the transmission of light and the concentration of the substance and the length of material that the light travels through,

$$T = \frac{I_1}{I_0} = -\exp \alpha_0 l \qquad 2\text{-}1$$

where α_0, the absorption coefficient is equal to the product of the absorbance,α, and the molar concentration, *C*.

Absorption spectroscopy involves passing a monochromatic beam of light through a sample and measuring the absorption of the material at this wavelength. Absorption is measured as a function of wavelength over a range extending from the infrared to ultraviolet. As the light passes through the material, it is possible that photons of a suitable energy can interact with the material, resulting in an electron being excited to a higher energy state and the photon being absorbed. By measuring the amount of light absorbed for a particular wavelength, it is possible to deduce information about the electronic structure of the material. At room temperature molecules which are in thermal equilibrium generally reside in the lowest vibrational level of the ground state. The vast majority of the excitation transitions therefore occur from the S_0 level in the ground state. Since excitation occurs from only one level in the ground state to the vibrational levels in the excited state, an absorption spectrum yields information on the vibrational energy distribution of the first excited state. Hence the linear absorption spectrum of a material yields information on the vibrational energy distribution of one photon excited states.

Optical Extinction can be defined as the attenuation of electromagnetic waves by scattering and absorption processes as it traverses a medium. [2] This extinction depends on such parameters as the particle shape, size, orientation, the particle's local environment, number of particles in the system and the frequency of the incident beam. In homogeneous media the dominant optical dissipation is generally absorption. If multiple scattering is negligible, the irradiance of a beam of light is exponentially attenuated from I_0 to I_t in traversing a distance h through a particulate system is similar to **Eqn. 2-1**,

$$\frac{I_t}{I_0} = \exp(-\alpha_{ext} h) \qquad 2\text{-}2$$

where the extinction is a result of both absorption and scattering processes. To correlate scattering intensity with particle size and shape, several scattering models have been developed. When the light is scattered by particles much smaller than the

wavelength of the light (length, $r << \lambda/10$), Rayleigh scattering occurs, which treats the particles as though they are point scatterers. It occurs when light travels in transparent solids and liquids. The amount of Rayleigh scattering is dependent upon the wavelength of the light; in particular, the dependence of scattering intensity on wavelength, such that, $I_s \propto \frac{1}{\lambda^4}$ (where I_s is the scattering intensity, λ is wavelength). Conversely, Mie theory, named after the German physicist Gustav Mie, provides rigorous solutions for light scattering by an isotropic sphere embedded in a homogeneous medium. It is applicable to spheres of all sizes, refractive indices and for radiation at all wavelengths.

2.2 Nonlinear Optics

2.2.1 Introduction

Under an increasingly intense incident light, the optical response of a material changes from a linear regime to that of a nonlinear form. In this linear regime, the influence of an electromagnetic field on matter is manifested as an induced polarisation in the material. In linear optics the dipoles generally oscillate at the same frequency as the applied field in what can be classified as harmonic behaviour. This low intensity approximation is only valid when the electric field remains sufficiently low to avoid inducing appreciably large oscillation in the electric dipoles of the material. If the intensity of light is increased, the electronic dipoles can become hyperpolarized and multiphoton interactions can take place. Consequently radiation can occur at frequencies which are higher harmonics of the fundamental incident frequency. This *anharmonic* response of materials at high incident optical intensities can be identified with observable optical spectroscopic phenomena. In order to theoretically investigate such a system, classical model for light-matter interactions can be applied and can actually support both harmonic and anharmonic processes involved with increasing amplitude of electromagnetic waves.

2.2.2 Lorentz Model

The propagation of light through an optical medium can be modelled by treating light as electromagnetic waves and the atoms or molecules of the medium as classical dipole oscillators. The classical model of light propagation was developed at the end of the 19th century following Maxwell's theory of electromagnetic waves and the introduction of the concept of the dipole oscillator. The model assumes that there are several different types of oscillators within a medium, each with their own characteristic resonant frequency. At optical frequencies, the most important contribution is from the oscillations of the *bound electrons* within the atoms and so we now consider atomic oscillators. The concept of dipole oscillators was introduced soon after Maxwells electromagnetic theory. Fundamental interactions between electromagnetic fields and matter are described classically by Maxwell's Equations, (**Eqns. 2-3→2-5**). These equations form the foundation for electromagnetic and optics fields and an appreciation of their significance is crucial for a full understanding of electromagnetic theory and phenomena.

For a neutral dielectric and non-magnetic medium Maxwell's Equations may be expressed as

$$\vec{\nabla}.\vec{D} = 0 \qquad 2\text{-}3$$

$$\vec{\nabla}.\vec{B} = 0 \qquad 2\text{-}4$$

$$\vec{\nabla}\mathrm{x}\vec{\mathrm{E}} = -\frac{\partial\vec{\mathrm{B}}}{\partial \mathrm{t}} \qquad 2\text{-}5$$

$$\vec{\nabla}\mathrm{x}\vec{\mathrm{H}} = \frac{\partial\vec{\mathrm{D}}}{\partial \mathrm{t}} \qquad 2\text{-}6$$

where ***E*** and ***H*** represent the electric and magnetic field strengths and ***B*** and ***D*** represent the magnetic and electric displacement vectors. P is the polarization or *electric dipole moment per unit volume*. By performing differential operations and re-arranging the above equations it is possible to derive the following equation,

$$\vec{\nabla}^2\vec{\mathrm{E}} - \frac{1}{\mathrm{c}}\frac{\partial^2\vec{\mathrm{E}}}{\partial \mathrm{t}^2} = \mu\frac{\partial^2\vec{\mathrm{P}}}{\partial \mathrm{t}^2} \qquad 2\text{-}7$$

This is the inhomogeneous wave equation and is the fundamental equation for classical electromagnetic field propagation and light-matter interactions. It can be noted that the polarization term on the right hand side of **Eqn. 2-7** acts as a source term and the significance of this will be discussed later.

For free space, the polarization may be neglected and **Eqn. 2-7** becomes the homogeneous wave equation. This can be shown to support only transverse wave solutions which propagate with a phase velocity equal to c. One such solution is the plane wave in the form,

$$\vec{E}(z,t) = \varepsilon E_0 \cos(\omega t - kz) \qquad 2\text{-}8$$

where ε represents the polarization of the wave, ω the radial frequency and k is the propagation constant and satisfies the dispersion relation,

$$k^2 = \frac{\omega^2}{c^2} \qquad 2\text{-}9$$

As previously mentioned the polarization induced in a medium under the influence of an electromagnetic field is a property of the medium in which the electric field propagates. It is related to how a material will respond to excitation by a light field and has enormous significance when considering nonlinear optics. In discussing this concept it is necessary to review a model for light-matter interactions. Henrick Lorentz originally proposed the concept of atoms as dipole oscillators in 1878. It was shown theoretically that an oscillating electric dipole would emit electromagnetic waves. The electrons are expected to reside at the equilibrium position of the potential well associated with the atoms and when subjected to a perturbation (which causes displacement) they are influenced by the restoring force of the potential. The situation regarding the electron in the potential well can be seen as analogous to that of a mass on a spring which obeys Hooke's Law, where the restoring force is proportional to the displacement,

$$\vec{F}_r = -k\vec{x} \qquad 2\text{-}10$$

where k is the spring constant and x is the displacement from equilibrium.

Lorentz considered the interaction with electromagnetic radiation as providing the perturbation to displace electrons. The force the electrons experience in this instance is the *Lorentz Force*,

$$\vec{F}_L = e\left(\vec{E} + \vec{v} \times \vec{B}\right) \qquad 2\text{-}11$$

where v is the velocity. However the magnetic contribution to the force may be ignored as the velocities of the changes involved do not normally approach relativistic magnitudes. Applying Newton's Second Law the following equation of motion for the electrons is obtained

$$m\frac{\mathrm{d}^2\vec{x}}{\mathrm{d}t^2} + k\vec{x} = e\vec{E} \qquad 2\text{-}12$$

where the electron's natural frequency of oscillation has been defined as $\omega_0 = \sqrt{k/m}$. Assuming an incident field of the form of **Eqn 2-8** the following is obtained,

$$\frac{\mathrm{d}^2\vec{x}}{\mathrm{d}t^2} + \omega_0^2\vec{x} = \frac{e}{m}\varepsilon E_0 \cos(\omega t - kz) \qquad 2\text{-}13$$

which has the particular solution:

$$\vec{x} = \varepsilon\left(\frac{eE_0}{m\left(\omega_0^2 - \omega^2\right)}\right)\cos(\omega t - kz) \qquad 2\text{-}14$$

This is the expression for the displacement from equilibrium of an electron due to the interaction with an electromagnetic field, which may be used to determine the polarization induced in the medium. Since the polarization has already been defined as the dipole per unit volume and the dipole moment is simply the product of the electric charge and the displacement of the charge, the expression for polarization is

$$\vec{P} = Ne\vec{x} = \varepsilon\left(\frac{Ne^2E_0}{m\left(\omega_0^2 - \omega_0\right)}\right)\cos(\omega t - kz) \qquad 2\text{-}15$$

where N is the number density of electrons. This is the source term for the polarization which may be substituted into the right hand side of the wave equation, **Eqn 2-7**. Making this substitution allows for a new dispersion equation for the propagation constant in a medium such that,

$$k^2 = n^2(\omega)\frac{\omega^2}{c^2} \qquad 2\text{-}16$$

where $n(\omega)$ is the frequency dependent refractive index and can be expressed as

$$n(\omega) = \left(1 + \frac{Ne^2/m\varepsilon_o}{(\omega_0^2 - \omega_0)}\right)^{1/2} \qquad 2\text{-}17$$

The polarization introduced previously may also be expressed in the form

$$\vec{P} = \varepsilon_0 \chi \vec{E} \qquad 2\text{-}18$$

where χ is the electric susceptibility and is a tensor whose symmetry properties will reflect those of the medium it represents.

In describing the expression for the polarization in terms of the displacement the restoring force was assumed to be linear in the displacement. Should the extension be large and the elastic limit approached, the restoring force will display some dependence on higher order quadratic and cubic terms. Similarly if the electromagnetic excitation is suitable strong, it is no longer adequate to approximate as previously done. In this case higher terms in the restoring force must be considered, such that,

$$\vec{F}_R = -k\vec{x} - \tfrac{1}{2}k'\vec{x}^2 - \tfrac{1}{3}k''\vec{x}^3 - \ldots \qquad 2\text{-}19$$

These terms expressed as a Taylor expansion of the restoring force about the equilibrium position in the displacement, relate to a potential energy function where,

$$U(x) = -\int \vec{F}_R . d\vec{x} = \tfrac{1}{2}k\vec{x}^2 + \tfrac{1}{6}k\vec{x}^3 + \ldots \qquad 2\text{-}20$$

In order to investigate the response of the electrons to a strong excitation, these anharmonic terms are now introduced. Initially we will limit this discussion to the first order correction term. The equation of motion describing the system is

$$\frac{d^2\vec{x}}{dt^2} + \omega_0^2\vec{x} + b\vec{x}^2 = \frac{e}{m}\varepsilon E_0 \cos(\omega t - kz) \qquad 2\text{-}21$$

where the coefficient of the quadratic term is now represented as b. Except when the displacement is very large, it can be assumed that the nonlinear term is small

compared to the linear term. The nonlinear term can then be treated as a perturbation of the linear equation obtained in the limit $b = 0$. The first approximation to $x(t)$ can be obtained by ignoring the nonlinear term and obtaining a first order solution identical, $x^{(1)}t$, with **Eqn 2-14** such that,

$$x^{(1)}(t) = \frac{e/m}{\omega_0^2 - \omega^2} E_0 \cos(\omega t - kz) \qquad 2\text{-}22$$

A better approximation of x(t), denoted by $x^2(t)$ can then be obtained by solving,

$$\frac{d^2 x^{(2)}}{dt^2} + \omega_0^2 x^{(2)} = \frac{e}{m} \varepsilon E_0 \cos(\omega t - kz) - a\left[x^{(1)}\right]^2 \qquad 2\text{-}23$$

By squaring the expression of **Eqn 2-22** it can be seen that the result contains a DC term and one oscillating at twice the driving frequency. Following this substitution, the steadily driven case can be expressed as,

$$\begin{aligned} x^{(2)}(t) = &\left(\frac{e/m}{\omega_0^2 - \omega^2}\right) E_0 \cos(\omega t - kz) - \frac{b}{2\omega_0^2}\left(\frac{e/m}{\omega_0^2 - \omega^2}\right)^2 E_0^2 \\ &- \frac{b}{2}\frac{1}{\omega_0^2 - 4\omega^2}\left(\frac{e/m}{\omega_0^2 - \omega^2}\right)^2 E_0^2 \cos(2\omega\omega - kz) \end{aligned} \qquad 2\text{-}24$$

This significant anharmonic term shows that the displacement includes oscillatory terms at both the fundamental and second harmonic of the driving frequency. Since the polarization is dependent upon the electron displacement through the dipole moment it can be seen that the polarization also includes a term oscillating at 2ω. When this form of polarization is introduced into the wave equation, (**Eqn 2-8**), it acts as a source for electromagnetic radiation which has as its origin the anharmonic response of the electrons to a perturbation in the Lorentz Model.

2.2.3 Nonlinear Polarization

The optical response of a material is usually formally defined by the polarisation vector, $\vec{P}$. Under low irradiation intensity this polarization is linearly dependent on the electric field strength, $\vec{E}$, and under high intensity the linear dependence can be expressed as a series, such that,

$$\vec{P} = \vec{P}_0 + \varepsilon_0\left(\chi^{(1)}\vec{E} + \chi^{(2)}\vec{E}.\vec{E} + \chi^{(3)}\vec{E}.\vec{E}.\vec{E}\right) + \ldots \qquad 2\text{-}25$$

where $\vec{P}_0$ is the static, spontaneous polarization, ε_0 is the permittivity of free space, $\chi^{(1)}$ is the linear susceptibility of the material and is a second rank tensor of the form $\chi^{(m)}$ for $m>1$ (denoting the m^{th} order nonlinear susceptibility, a m+1 rank tensor). The symmetry relationship $\vec{P}(\vec{E}) = -\vec{P}(-\vec{E})$ indicated that even order susceptibilities vanish in materials with *centrosymmetry*, such as phthalocyanine molecules, a topic which is experimentally investigated in **Chapter 5.** Thus the third order susceptibility, $\chi^{(3)}$, is the first nonlinear term for such isotropic systems. It involves the reaction of three photons to produce a fourth and is of interest since it is responsible for several important applications, including phase conjugation, self focusing and defocusing.

In general the susceptibilities are complex in form and the real part of the susceptibility defines parametric processes, which implies that the initial and final quantum mechanical states involved in the multiphoton interactions are the same and the photon energy is conserved. The imaginary part of the susceptibility implies damping of the optical wave in the medium resulting from the exchange of energy between the optical field and nonlinear medium. These non-parametric processes can occur under resonant conditions with incident frequency and involve the redistribution of electrons among the electronic states.

2.2.4 Effective Susceptibilities

The imaginary part of the third order optical susceptibility involves the modification of the absorption coefficient of a material. The total absorption coefficient (α_{tot}) can be expressed in terms of both the linear and non liner terms, where,

$$\alpha_{tot} = \alpha_0 + \alpha_{NL} \qquad 2\text{-}26$$

If the absorption coefficient is considered a function of the optical field intensity, it can be written in the form

$$\alpha_{tot} = \alpha_0 + f(I) + O(I^2) + O'(I^3) \qquad 2\text{-}27$$

where $f(I)$ represents an intensity dependent nonlinear absorption and there may be terms of orders of I^n in the expansion of $O(I^n)$. If it assumed that the dominant nonlinearity is described by $f(I)$, then under certain conditions it may be possible to expand $f(I)$ as a term linearly dependent on I. The total absorption coefficient then becomes,

$$\alpha_{tot} = \alpha_0 + \beta I \qquad 2\text{-}28$$

where β is constant. One can consider the material behaving as an effective $\chi^{(3)}$ material and relate the nonlinear absorption coefficient β to an effective imaginary third order susceptibility $Im\{\chi^{(3)}_{eff}\}$. The $Im\{\chi^{(3)}_{eff}\}$ coefficient can be used to relate the material to other parametric $\chi^{(3)}$ responses exhibited by other materials in terms of the magnitude of the observed optical dissipation.

Practically one can discuss the response of a saturable absorber where the light intensity at which the material saturates is defined as I_{sat}. If we consider optical pumping where, $I<<I_{sat}$, then the total absorption coefficient can be expressed as,

$$\alpha_{tot} = \frac{\alpha_0}{1 + I/I_{sat}} \approx \alpha_0(1 - I/I_{sat}) = \alpha_0 - \frac{\alpha_0}{I_{sat}} I \qquad 2\text{-}29$$

The nonlinear term is then linearly dependent on the intensity and the response can be described as an effective $\chi^{(3)}$ effect.

2.3 Z-Scan & Optical Limiting

The Z-scan technique was first published by Sheik-Bahae et al [3] and has since become a standard tool for the determination of both real and imaginary third order susceptibility coefficients. Its strength derives from an ability to translate changes in beam curvature, induced by the nonlinear response of the sample under study, into transmission changes. The Z-scan principle involves the sequential movement of a sample through the focus of an incident Gaussian beam thereby subjecting it to a symmetric range of intensities about the focal point.

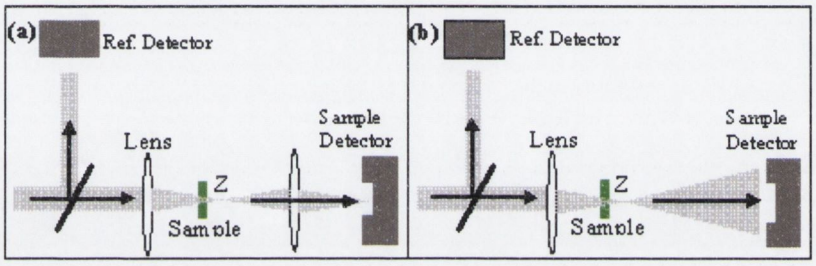

Figure 2.2 (a) Open aperture Z-scan experimental set-up. **(b)** Closed Aperture Z-scan experimental set-up

A schematic of the two main arrangements used in Z-scan is shown in **Figure 2.2(a)&(b)**. Nonlinear optical changes where all the transmitted light is collected (**Figure 2.2a**) is termed the "open aperture Z-scan" probing the imaginary part of $\chi^{(3)}$, as outlined in **Section 2.4**. The transmitted light measured as a function of sample position in the *far field*, using two detectors is presented in **Figure 2.2(b).** The sensitivity of the experiment to the nonlinear refractive index, a real $\chi^{(3)}$ response, is due to the presence of the aperture in place in the far field, referred to as 'closed aperture Z-scan'.

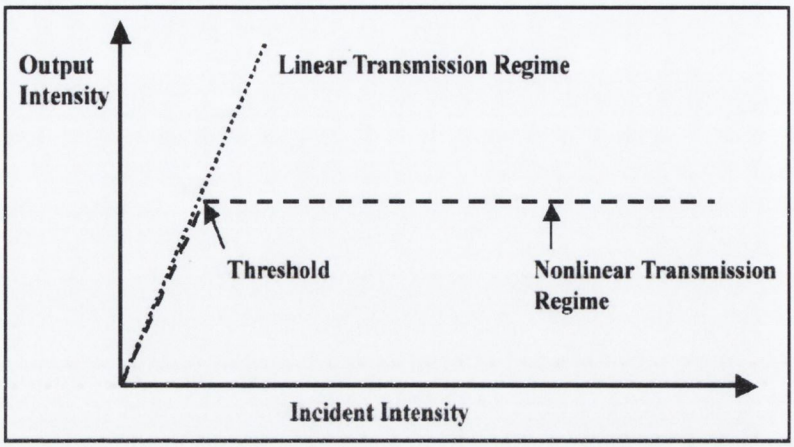

Figure 2.3 Plot of output intensity as a function of input intensity for a theoretical optical limiting system. Above an intensity threshold the output repose remains constant and independent of the input.

For materials which absorb light nonlinearly, the concept of saturable and reverse saturable absorption will be briefly introduced. Materials possessing strong electronic absorptions can behave as saturable absorbers as long as the rate of populating the excited state exceeds the rate of decay to the ground state. As the excited states are populated there is a corresponding depletion in the ground-state population leading to a decrease in the ground state absorption coefficient. The opposite of this process is defined as *Reverse Saturable Absorption*, which is characterized by decreasing transmission with increasing light intensity. This occurs when the excited state absorption cross section is greater than that of the ground state, $\sigma_{ex} > \sigma_0$. Theoretically, at a certain energy threshold, the output energy remains constant with increasing input energy (see **Fig 2.3**). This process known also as *optical limiting* has several potential uses, one of which involves the protection of sensor or optical equipment, including the human eye. Nonlinear optical behaviour can be induced in a system above an intensity threshold, noted for optical limiters in **Figure 2.3**, which plots the output intensity as a function of input intensity. Due to material dependent nonlinear processes, above this intensity threshold the ideal output remains constant and independent of the input intensity.

Prior to a discussion on the theory of the Z-scan technique, outlining the spatial decomposition of an incident laser pulse and the resulting transmitted power, the profile of the incident light beam will be briefly introduced.

2.3.1 Gaussian Beam Profile

Most optical beams propagating in free space are almost pure TEM (Transverse Electric and Magnetic) waves. A **Gaussian beam** can be considered as a beam of electromagnetic radiation whose transverse electric field and intensity distributions are described by Gaussian functions.

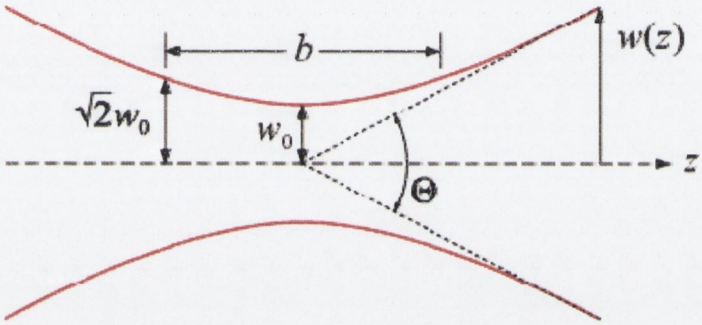

Figure 2.4 Generalized Gaussian beam profile, including various physical parameters of the beam, including waist radius, beam spot size varying with z, the confocal parameter and Rayleigh range.

For a Gaussian beam propagating in free space, the spot size $w(z)$ will be at a minimum value w_0 at one place along the beam axis, known as the *beam waist*. As presented in **Figure 2.4,** for a beam of wavelength λ at a distance z along the beam from the beam waist, the variation of the spot size is given by

$$\omega(z) = \omega_0 \sqrt{1 + \left(\frac{z}{z_0}\right)^2} \qquad 2\text{-}30$$

where the origin of the z-axis is defined to coincide with the beam waist, and where

$$z_0 = \frac{\pi\omega_0^2}{\lambda} \qquad 2\text{-}31$$

is known as the *Rayleigh Range*. At a distance from the waist equal to the Rayleigh Range z_0,the width, ω, of the beam is defined as

$$\omega(\pm z_0) = \omega_0\sqrt{2} \qquad 2\text{-}32$$

The distance between these two points, *b*, is called the *confocal parameter* of the beam,

$$b = 2z_0 = \frac{2\pi\omega_0^2}{\lambda} \qquad 2\text{-}33$$

2.3.2 Z-Scan Technique

There is considerable interest in investigating the fast and large optical nonlinearities of organic π–conjugated systems and this topic will be the focus of interest in **Chapter 4**, entitled "*Polymer-Phthalocyanine Composites*". For such investigations, the Z-scan technique is a method for rapidly measuring such properties as the nonlinear optical absorption and refraction of a material in order to calculate various nonlinear optical coefficients.

Considering both the open and closed aperture Z-scan geometry (**Figures 2.2a & 2.2b**), and assuming the fundamental mode, TEM_{00} Gaussian beam, of beam waist radius w_0 travelling in the z+ direction, we can write the peak electric field as:

$$E(z,r,t) = E_0(t)\frac{\omega_0}{\omega(z)}\exp\left(-\frac{r^2}{\omega^2(z)} - ik\frac{r^2}{2R(z)}\right)e^{-i\phi(z,t)} \qquad 2\text{-}34$$

where, $\omega^2(z) = \omega_o^2\left(1 + z^2/z_0\right)$ is the beam radius; ω_0 is the waist radius; $z_0 = k\omega_o^2/2$ is the diffraction length of the beam; $k = 2\pi/\lambda$ is the wave number and $R = z\left(1 + z_0^2/z^2\right)$; $\tan\phi = z/z_0$ and λ is the wavelength of the laser irradiation. $E_o(t)$ denotes the radiation electric field at the focus and contains the temporal

envelope of the laser pulse. The $e^{-i\phi(z,t)}$ term contains all the radially uniform phase variations. As the radial phase variation calculations are the only concern specific to this report, $\Delta\phi(r)$, the Slowly Varying Envelope Approximation (**SVEA**) applies and all other phase changes that are uniform in r are ignored. The SVEA judges that the laser pulse envelope varies slowly in time and space compared to a period and wavelength of light. If the sample thickness is small so that changes in the beam diameter within the sample due to refraction and diffraction are negligible, we then can regard the medium as *thin*. This implies that for linear diffraction, the path length $L << z_0$ and for nonlinear refraction, the path length $L << z_0 / \Delta\phi(0)$. The second criterion is automatically met in most standard Z-scan experiments as $\Delta\phi_0$ is small. It has also been found experimentally that the first criterion for linear diffraction is more restrictive than necessary and the condition $L < n_0 z_0$ is sufficient. Thus the amplitude $\sqrt{I}$ and phase ϕ of the electric field as a function of z are now governed in the **SVEA** by a pair of simultaneous equations,

$$\frac{d\Delta\phi}{dz'} = \Delta n(I)k \qquad 2\text{-}35$$

and

$$\frac{dI}{dz'} = -\alpha(I)I \qquad 2\text{-}36$$

where z' is the propagation depth in the sample and $\alpha(I)$ in general includes both linear and nonlinear absorption terms. In the case of a cubic nonlinearity and negligible nonlinear absorption, the previous two equations can be solved to give the phase shift $\Delta\phi$ at the exit surface of the sample which simply follows the radial variation of the incident radiation at a given position z. Thus,

$$\Delta\phi(z,r,t) = \Delta\phi_0(z,t)\exp\left(-\frac{2r^2}{\omega^2(z)}\right) \qquad 2\text{-}37$$

with

$$\Delta\phi_0(z,t) = \frac{\Delta\Phi_0(t)}{1 + z^2/z_o^2} \qquad 2\text{-}38$$

$\Delta\Phi_0(t)$ is the on-axis phase shift at the focus and is defined as,

$$\Delta\Phi_0(t) = k\Delta n_0(t) L_{eff} \qquad 2\text{-}39$$

where $L_{eff} = (1 - \exp(-\alpha_0 L))/\alpha_0$ is the effective sample length defined in terms of the linear absorption coefficient, α_0, and $\Delta n_0 = n_2 I_0(t)$, with $I_0(t)$ being the on-axis irradiance at the focus, i.e. $z = 0$. The electric field exiting the sample E_{exit} now contains the nonlinear phase distortion

$$E_{exit}(r,z,t) = E(z,r,t) e^{-\alpha_0 L/2} e^{i\Delta\phi(z,r,t)} \qquad 2\text{-}40$$

A treatment method known as Gaussian Decomposition[4] can now be applied. This involves the decomposition of the complex electric field at the exit plane into a summation of Gaussian beams through a Taylor series expansion of the nonlinear phase term $e^{i\Delta\phi(z,r,t)}$ from **Eqn 2-40**,

$$e^{i\Delta\phi(z,r,t)} = \sum_{m=0}^{\infty} \frac{[i\Delta\phi_0(z,t)]^m}{m!} e^{-2mr^2/w^2(z)} \qquad 2\text{-}41$$

Each Gaussian beam can now be propagated to the aperture plane and there be re-summed to reconstruct the beam. The resultant electric field pattern at the aperture becomes

$$E_a(r,t) = E(z, r = 0, t) e^{-\alpha L/2} \sum_{m=0}^{\infty} \frac{[i\Delta\phi_0(z,t)]^m}{m!} \frac{\omega_{mo}}{\omega_m} \exp\left(-\frac{r^2}{\omega_m^2} - \frac{ikr^2}{2R_m} + i\theta_m \right) \qquad 2\text{-}42$$

By defining d as the propagation distance in free space from the sample to the aperture plane and $g = 1 + d/R(z)$, the remaining parameters in **Eqn. 2-42** can be expressed as

$$\omega_{m0}^2 = \frac{\omega^2(z)}{2m+1}, \; d_m = \frac{k\omega_{m0}^2}{2}, \; \omega_m^2 = \omega_{m0}^2 \left[g^2 + \frac{d^2}{d_m^2} \right],$$

$$R_m = d\left[1 - \frac{g}{g^2 + d^2/d_m^2}\right]^{-1} \text{ and } \theta_m = \tan^{-1}\left[\frac{d/d_m}{g}\right] \qquad 2\text{-}43$$

The transmitted power through the aperture is obtained by spatially integrating $E_a(r,t)$ up to the aperture radius r_a, giving

$$P_T(\Delta\phi_0(t)) = c\varepsilon_0 n_0 \pi \int_0^{r_a} |E_a(r,t)|^2 r dr \qquad 2\text{-}44$$

where ε_0 is the permittivity in a vacuum. The normalized transmission, $T(z)$, can be calculated as

$$T(z) = \frac{\int_{-\infty}^{\infty} P_T(\Delta\phi_0(t))dt}{S\int_{-\infty}^{\infty} P_i(t)dt} \qquad 2\text{-}45$$

where $P_i(t) = \pi\omega_0^2 I_0(t)/2$ is the instantaneous input power within the sample and $S = 1 - \exp(-2r_a^2/\omega_a^2)$ is the aperture linear transmittance, with ω_a denoting the beam radius at the aperture in the linear regime and r_a is the aperture radius. In the case of cubic nonlinearity and in the limit of small nonlinear phase change ($|\Delta\phi_0| << 1$) and with $r = 0$, the far-field condition $d >> z_0$ can be used to further simplify **Eqn. 2-45** to give a geometry-independent normalized transmittance as

$$T(z, \Delta\varphi_0) = 1 - \frac{4\Delta\phi_0 z/z_0}{(z/z_0{}^2 + 9)(z/z_0{}^2 + 1)} \qquad 2\text{-}46$$

2.3.3 Numerical Resolution & Beam Spatial Energy Profile

To discuss the importance of the various parameters that influence reverse saturable absorption in a nonlinear absorbing system, a general 5-level model such as that shown in **Figure 2.5** has been considered. For this investigation, approximations suitable for the nonlinear optical absorbing phthalocyanine system under

nanosecond irradiation have been applied to an aromatic dye compound which will be discussed in depth in **Chapter 3**.

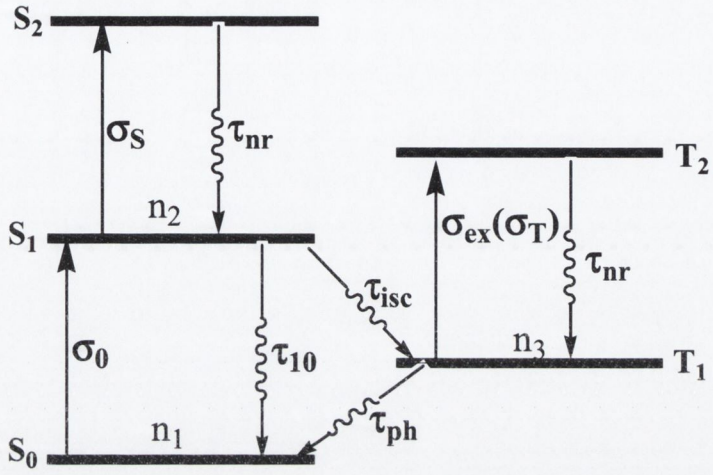

Figure 2.5 Generalized five-level system used in deriving the excited state absorption model used to simulate RSA in the phthalocyanine system. Si represents singlet levels and Ti represents triplet levels. Solid arrows imply an excitation resulting from photon absorption and jagged arrows represent relaxations

For simplicity at this juncture, it is sufficient to acknowledge that phthalocyanine systems[5-7] are well reported to nonlinearly absorb high intensity light through excited state electron charge transfer processes.[8-16] The vibrational levels of the electronic states are ignored and, for the sake of simplicity, the laser pulse width is assumed to be longer than any of the lifetimes associated with the higher order singlet (S_2, S_3...) and triplet (T_2, T_3,....) levels. To further simplify matters it was assumed that relaxation out of states S_2 (second excited singlet energy state, spin quantum number = 0) and T_2 (second triplet energy state, spin quantum number = 1) is very rapid so that the population of these two levels may be neglected.[3, 17-19] **Table 1** presents a selection of numerical photophysical values for *t*Bu_4PcInCl, representative of the excitation process described in **Figure 2.5**.

Metal	τ_s (ns)[a]	Φ_t[b]	f_t (8 ns)
Al	6.9	0.35	0.18
Ga	3.3	0.51	0.42
In	0.3	0.88	0.95
Si	4.5[c]	0.35[d]	0.25
Ge	4.2[c]	0.37[d]	0.28
Sn	2.0[c]	0.62	0.63
Pb	0.35	0.92	0.95

Table 1. Photophysical properties for a series of Group III & IV metallophthalocyanines. τ_s=first excited-singlet lifetime, Φ_t[b]=triplet quantum yield, f_t= Average fractional population of the excited-triplet states during the pulse.
[a]First excited-state lifetimes determined by picosecond pump-probe measurements at 700 nm; uncertainty is ± 10%; [b]Triplet quantum yields determined from ground-state bleaching recovery at 700 nm; uncertainty is ±0.10; [c]Values determined by use of time-correlated photon counting; [d]Values estimated from fluorescence quantum yields.
(Reproduced from J. W. Perry, K. Mansour, S. R. Marder, K. J. Perry, D. J. Alvarez, and I. Choong, Optics Letters ***19****, (9), 625-627,1994.)*

Generally for this 5-level system after initial excitation the first excited singlet state S_1 is populated, from here the electrons may be subsequently excited into S_2 within the pulse width of the laser. Once in S_2 they rapidly relax to S_1 again. From S_1 the population may undergo an intersystem crossing to the first excited triplet T_1 with a time constant τ_{isc} and thereafter undergo excitations and relaxations to and from T_2. Thus the population is exchanged cyclically between S_1 and T_1, as the lifetime of T_1 (τ_{ph}) is very long in comparison to τ_{isc}. Furthermore, stimulated emission from S_1 is excluded due to the small fluorescence quantum yield. The system now reduces to the following set of three differential rate equations,

$$\frac{\partial n_1}{\partial t} = -\frac{\sigma_0 I}{h\nu} n_1 + \frac{n_2}{\tau_{10}} + \frac{n_3}{\tau_{ph}} \qquad 2\text{-}47$$

$$\frac{\partial n_2}{\partial t} = \frac{\sigma_0 I}{h\nu} n_1 - \frac{n_2}{\tau_{isc}} - \frac{n_2}{\tau_{10}} \qquad 2\text{-}48$$

$$\frac{\partial n_3}{\partial t} = \frac{n_2}{\tau_{isc}} - \frac{n_3}{\tau_{ph}} \qquad 2\text{-}49$$

where n_1, n_2 and n_3 refer to the populations of S_0, S_1, and T_1. Attenuation of the laser beam is governed by a propagation equation where the absorption coefficient now includes the excited state absorption from S_1 and T_1

$$\frac{\partial I}{\partial z} = -\alpha I = -(\sigma_0 n_1 + \sigma_S n_2 + \sigma_T n_3) I \qquad 2\text{-}50$$

Under the steady state approximation, which is valid when the pulse width is much longer than any relaxation time, all the time derivatives may be set to zero. This is a valid assumption under nanosecond irradiation as the lifetimes in phthalocyanines are typically of order picoseconds, for example tetrasubstituted indium phthalocyanines.[20] In this case, the equation can be easily solved analytically and the intensity dependent absorption coefficient,

$$\alpha(I, I_{Sat}, \kappa) = \frac{\alpha_0}{1 + \frac{I}{I_{Sat}}}\left(1 + \kappa \frac{I}{I_{Sat}}\right) \qquad 2\text{-}51$$

by defining $\kappa = \sigma_{ex}/\sigma_0$, and noting that σ_{ex} and σ_0 are the absorption cross-sections of the ground and the excited transitions respectively, and $I_{Sat} = h\nu / (\sigma_0 \tau_{10})$.
Thus this effectively reduces the 5-level model to a 3-level model. This model, though simple, reproduces the gross effects of reverse saturable absorption and highlights the crucial role that the excited state absorption plays in the overall absorption coefficient. This steady state model approximates to a dynamic model in the limit of temporally long pulse widths, ie. nanosecond irradiation when all other lifetimes in the material are of the order of picoseconds.

Before application of the nonlinear absorption coefficient to experimental data $\alpha(I, I_{Sat}, \kappa)$ has to be substituted back into the propagation formalism. One can consider an integral over a homogeneous sample of thickness L where the integration is performed with limits on dz going from $z = 0 \rightarrow L$ and the limits on dI going from $I = I_{In} \rightarrow I_T$:

$$\int_{I_{In}}^{I_T}\left(\frac{1}{1+I/I_{Sat}}+\frac{\kappa I/I_{Sat}}{1+I/I_{Sat}}\right)^{-1}\frac{dI}{I}=-\alpha_0\int_0^L dz \qquad 2\text{-}52$$

This expression can then be sequentially integrated and by defining the transmission T as $T = I_T/I_{In}$ a transcendental equation for T, where T is essentially a function of I, κ and I_{Sat} can be readily derived.

$$T(I,\kappa,I_{Sat})=\exp(-\alpha_0 L)\left(\frac{I_{Sat}+\kappa T(I,\kappa,I_{Sat})I}{I_{Sat}+\kappa I}\right)^{1-\frac{1}{\kappa}} \qquad 2\text{-}53$$

It can be noted that the intensity (I) and the pulse energy density defined as $F = E_{Tot}/(\pi w(z)^2)$, where E_{Tot} is the energy per pulse and $\pi w(z)^2$ is the surface area through which the portion of the pulse is propagating at any position denoted by z, are directly related to each other and consequently the parameter I/I_{Sat} can be replaced with F/F_{Sat} in Eqn. 2-52 where in this case F_{Sat} is the energy density saturation. The parameter F_{sat} (also defined as F_c, marking the onset of the nonlinear absorption process) has previously been reported my Mclean et al.[21] and can be mathematically expressed as $F_c=\hbar w(\sigma_{ex}-\sigma_0)$, where $\hbar w$ is the photon energy and σ_{ex} and σ_0 are the excited triplet state and ground state cross sectional areas, respectively.

The intensity- (and energy density-) dependent absorption coefficient was incorporated into computer code and a least-squares regression algorithm was employed to fit this to experimental data.

Within this expression for the nonlinear absorption coefficient one can then state that higher κ values combined with lower F_{Sat} values define optimized optical limiters.

If an optical pulse is considered to be propagating in the z-direction in space then it will possess a certain spatial distribution of its energy in the x-y plane perpendicular to its propagation. Frequently, this energy profile is symmetric in the x and y directions and Gaussian in its radial distribution. If one defines w as the half-width at e^{-1} times the maximum intensity within the distribution, then one can

consider the entire energy in the pulse at any instant E_{Tot} being composed of energy contributions $E(r, \delta r, \delta\theta)$ contained within the discrete spatial regions defined by θ to $\theta+\delta\theta$ and r to $r+\delta r$ in the (r,θ) plane.

$$E(r,\delta r,\delta\theta)=\frac{E_{Tot}}{w^2\pi}\int_{\theta=\theta}^{\theta+\delta\theta}d\theta\int_{r=r}^{r=r+\delta r}r\exp\left\{-\frac{r^2}{w^2}\right\}dr \qquad 2\text{-}54$$

Additionally, symmetry implies that θ is somewhat redundant as for any given r the energy is equal for all θ and exploiting such symmetry the double integral can be reduced to a single integral over r. Therefore one can consider the energy increments contained within the annular sections defined by the radial values contained within r and $r+\delta r$. The entire energy E_{Tot} can be formulated as the sum over the energy contained within each of the separate n annular regions.

$$E_{Tot}=\sum_{i=0}^{n-1}E(r_i,r_{i+1})=\sum_{i=0}^{n-1}\left\{2\frac{E_{Tot}}{w^2}\int_{r=r_i}^{r=r_{i+1}}r\exp\left\{-\frac{r^2}{w^2}\right\}dr\right\} \qquad 2\text{-}55$$

At this juncture it becomes clear that for any given pair of nonlinear optical coefficients κ and F_{Sat}, assuming that the waist size of the beam w and the pulse energy E_{Tot} are known, one can consider first a spatial decomposition the incident pulse following the method just detailed above, followed by independent analysis within the sample medium of each decomposed annular section. These transmission coefficients can then be recombined with their respective incident components to create the spatial profile of the transmitted pulse defined by its own energy and the nonlinear optical response of the sample medium.

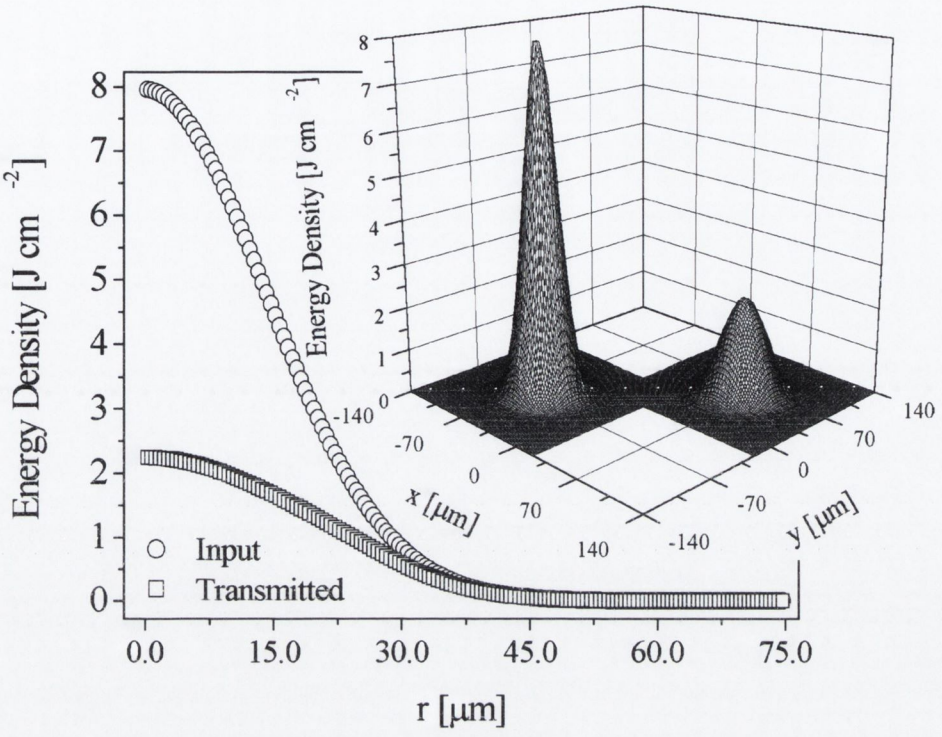

Figure 2.6 Simulation of spatial decomposition of a Gaussian pulse followed propagation of each subdivision through a sample medium with $\alpha_0 L = 0.1$, $\kappa = 20$, $F_{Sat} = 5$ J cm^{-2}, w = 20μm and total pulse energy $E_{Tot} = 100\mu J$. A three dimensional rendering of the incident and transmitted pulses are presented in the inset.

To highlight this, the spatial decomposition of a Gaussian pulse with physical parameters typical of that which will be used subsequently for experiments on nonlinear absorbing systems, followed by a propagation of each decomposed subdivision of the pulse through a sample medium and recombination after the light-medium interaction will be presented. For the purposes of producing an appreciable nonlinear response, the materials' physical properties were defined so that $\alpha_0 L = 0.1$, $\kappa = 20$ and $F_{Sat} = 5\ J\ cm^{-2}$. The waist radius was set so that $w = 20\mu m$ and the pulse was given total energy $E_{Tot} = 100\ \mu J$. One of the significant benefits of the method of splitting the pulse is that in principle any pulse shape can be considered. As an example to demonstrate this generality an unrealistic hypothetical conical pulse is presented in **Figure 2.6**. In the figure the two-dimensional shape of the Gaussian pulse discussed in the preceding paragraph is

included to allow a direct comparison of the two input pulse shapes. In the inset to **Figure 2.6** a three-dimensional rendering of the incident and transmitted pulses (shifted for clarity). After interaction within the medium it can be seen that the spatial distribution of the output pulse is no longer conical, where it has assumed a much more complicated distribution of its energy. In an optical limiting experiment one generally monitors the energy of the incident pulses in tandem with the waist diameter of the beam, and it has become somewhat commonplace to illustrate the data as output intensity, energy density (J cm^{-2}) or transmission percentage against the incident parameter. Generally the spatial component involved in the calculation of either the energy density or the intensity is governed by the active area of the beam and normally defined by πw^2, where w is the waist radius at e^{-1} times the intensity as defined above.

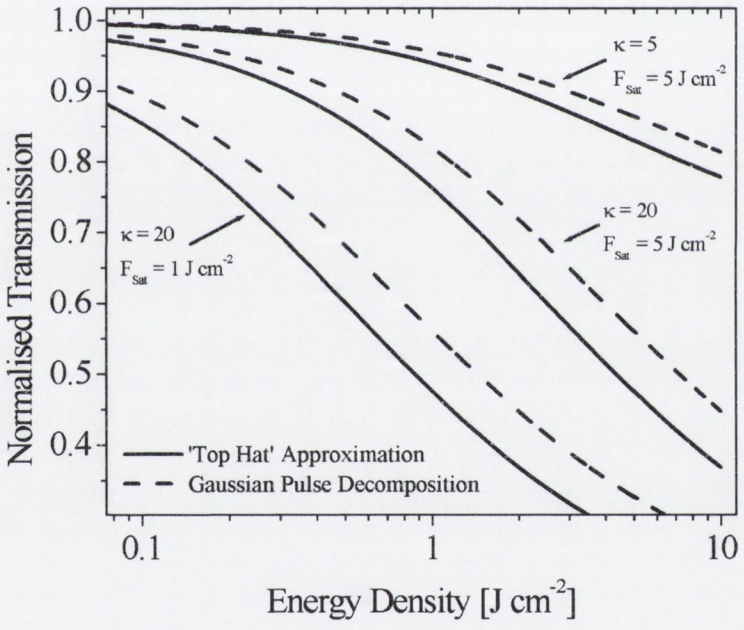

Figure 2.7 Typical optical limiting plots of transmission as a function of energy density. Solid lines represent a 'top-hat' approximation where the spatial distribution of the pulses energy is ignored and for the dashed lines the Gaussian profile of the pulse is considered using the theory detailed previously.

In **Figure 2.7** optical limiting plots of transmission as a function of energy density are simulated using **Eqn. 2-54** with the two distinctly different methods. In one case

the 'top hat' approximation is used (solid lines) and in the other the Gaussian profile of the pulse is considered using the theory detailed throughout this section (dashed line). It can be seen in the figure that if one considers the strength of the nonlinear attenuation, the 'top hat' approximated pulse outperforms the Gaussian decomposed simulation for all values of F with equal κ and F_{Sat} magnitudes. Consequently to achieve similar curves, higher magnitudes of κ and lower F_{Sat} have to be inserted into the algorithm that considers the spatial resolution of the pulses energy. Thus if one were to fit this curve ('top-hat' approximation) to a dataset then the numerical values of the yielded nonlinear coefficients (κ, F_{Sat}) would be in fact different than those produced considering the Gaussian spatial profile of the pulse, and given that high κ and low F_{Sat} are desirable one would certainly underestimate the optical limiting efficiency of the system.

Conclusion

Using the classical Lorentz Model, the linear interaction between matter and incident electromagnetic waves has been investigated and expanded to include higher order terms, representing nonlinear effects, at high incident light intensity. For all experimental procedures probing the nonlinear optical extinction of light, the Z-scan technique is employed, as outlined in **Section 3,** where the incident light has the form of a TEM_{00} Gaussian beam. Computer code was employed extensively to parameterize and characterize nonlinear optical effects under specific conditions. Spatial and temporal investigation of a high intensity beam traversing a medium and inducing reverse saturable absorption processes was outlined and investigated theoretically.

References

1 E. Hecht, *Optics* Reading, Mass. ; Harlow : Addison-Wesley: 1998.

2 C. F. Bohren, and D. R. Huffman, *Absorption and Scattering of Light by Small Particles*. Wiley-Interscience: 1983; p 1-11.

3 M. Sheik-Bahae, A. A. Said, T. H. Wei, D. J. Hagan, and E. W. Vanstryland, *IEEE Journal of Quantum Electronics* **26**, (4), 760-769 (1990).

4 D. Weaire, B. S. Wherrett, D. A. B. Miller, and S. D. Smith, *Optics Letters* **4**, 331-333 (1979).

5 C. E. Dent, R. P. Linstead, and A. R. Lowe, *Journal of the Chemical Society* 1033-9 (1934).

6 R. P. Linstead, *Journal of the Chemical Society*, 1016-17 (1934).

7 N. A. Frigerio, *Journal of Organic Chemistry* **26**, (6), 2115-& (1961).

8 H. S. Nalwa, and J. S. Shirk, *Phthalocyanines: Properties and Applications* John Wiley&Sons: New York, 1996; Vol. 4, p 83.

9 H. S. Nalwa, and A. Kakuta, *Thin Solid Films* **254**, (1-2), 218-223 (1995).

10 J. W. Perry, K. Mansour, S. R. Marder, K. J. Perry, D. J. Alvarez, and I. Choong, *Optics Letters* **19**, (9), 625-627 (1994).

11 J. S. Shirk, R. G. S. Pong, F. J. Bartoli, and A. W. Snow, *Applied Physics Letters* **63**, (14), 1880-1882 (1993).

12 H. S. Nalwa, T. Saito, A. Kakuta, and T. Iwayanagi, *Journal of Physical Chemistry* **97**, (41), 10515-10517 (1993).

13 H. S. Nalwa, A. Kakuta, and A. Mukoh, *Journal of Physical Chemistry* **97**, (6), 1097-1100 (1993).

14 J. S. Shirk, J. R. Lindle, F. J. Bartoli, and M. E. Boyle, *Journal of Physical Chemistry* **96**, (14), 5847-5852 (1992).

15 H. Matsuda, S. Okada, A. Masaki, and H. Nakanishi, *Proc. SPIE Vol. 1560, Nonlinear Optical Properties of Organic Materials IV, Kenneth D. Singer; Ed.*, 75-83 (1991).

16 D. R. Coulter, V. M. Miskowski, J. W. Perry, T. H. Wei, E. W. V. Stryland, and D. J. Hagan, *SPIE Proc.* **1105**, 42 (1989).

17 P. Miles, *Applied Optics* **38**, (3), 566-570 (1999).

18 P. A. Miles, *Applied Optics* **33**, (30), 6965-6979 (1994).

19 S. M. O'Flaherty, S. V. Hold, M. J. Cook, T. Torres, Y. Chen, M. Hanack, W. J. Blau, *Advanced Materials* **15**, (1), 19-+ (2003).

20 J. W. Perry, K. Mansour, I. Y. S. Lee, X. L. Wu, P. V. Bedworth, C. T. Chen, D. Ng, S. R. Marder, P. Miles, T. Wada, M. Tian, and H. Sasabe, *Science* **273**, 1533-1536 (1996).

21 D. G. McLean, R. L. Sutherland, M. C. Brant, D. M. Brandelik, P. A. Fleitz, T. Pottenger, *Optics Letters*, **18**, 858 (1993)

CHAPTER 3

INTRODUCTION TO MATERIALS

3.1 Organic Materials

3.1.1 Introduction

Historically the term organic material described all materials whose chemistry was related to life processes. However, with the synthesis of urea, the first organic compound to be artificially synthesized from inorganic starting materials, the definition required altering. It is generally accepted that organics are carbon based materials (e.g with carbon-carbon bonds), ranging from from methane to polymers, fullerenes and nanotubes, large macrocyclic molecules such as the phthalocyanines and most biological materials.

Carbon is an abundant non-metallic, tetravalent element, with several allotropic forms including diamond, graphite, fullerenes and carbon nanotubes. This atom can be found in one of multiple possible arrangements of the electronic states. The carbon atom has six electrons, which occupy $1s^2$, $2s^2$, and $2p^2$ atomic orbitals with the $1s^2$ orbital containing two core electrons and the remaining four electrons occupying the $2s^22p^2$ valence orbitals. The energy difference between the upper 2p and lower 2s energy levels in carbon is small and therefore the electronic wavefunctions for these four electrons can readily mix with each other in a process known as hybridisation. The chemistry of organic molecules is based on the covalent bonds between the carbon atoms. Carbon has an atomic configuration of $1s^22s^22p^2$ with four valence electrons in the n=2 atomic shell. In carbon, each carbon atom forms single covalent bonds with four adjacent carbon atoms. In organic compounds there may be single, double and triplet bonds between adjacent carbon atoms. In molecules with double or triple bonds, the valence electrons are divided between the σ-bonds and the π-bonds. Due to the high bonding energy of the σ-bonds, it takes a large amount of energy to excite these electrons and they tend to be relatively inert. In sp^2 hybridization, three of the valence electrons are involved in bonding, leaving the fourth electron on each carbon atom unaffected by the hybridized p_z orbital. The p_z orbitals are arranged in a dumbbell shape out of plane and form π-bonds, as presented diagrammatically in **Figure 3.1**. These bonds result from parallel orbital overlap, where the two combined orbitals meet

lengthwise and create more diffuse bonds than σ-bonds. Electrons in π-bonding states are referred to as π-electrons.

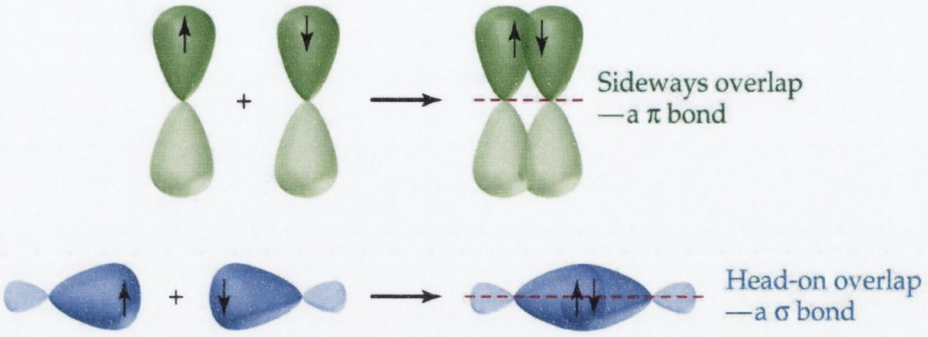

Figure 3.1 Diagram of hybridized electron orbital which forming either π-bonds (out of plane) or σ bonds (in-plane)

As mentioned, three possible hybridizations can occur for carbon: sp, sp^2 and sp^3, where the superscript indicates the number of 2p electrons which are involved. **Figure 3.2** presents sp^3 hybridisation of carbon showing the wave functions for the s and p atomic orbitals *combining* to form a new set of equivalent wave functions called hybrid orbitals. The various bonding states are related to certain structural arrangements, so that sp bonding gives rise to chain structures, sp^2 bonding to planar structures and sp^3 bonding to tetrahedral structures.

Considering the example of ethylene ($H_2C{=}CH_2$) molecule as presented in **Figure 3.3**, each carbon atom is bonded to two hydrogen atoms and has a double bond with the other carbon atom. The two 2*s* electrons *hybridize* with one of the 2*p* electrons to form three sp^2 bonds. These are the σ bonds and are arranged at an angle of about 120^0 to each other. The carbon and hydrogen atoms lie within a plane, and the other 2*p* electron forms a π orbital derived from the $2p_z$ atomic orbital, as in **Figure 3.1**. The overlap of the π-orbitals produces the second bond between the two carbon atoms.

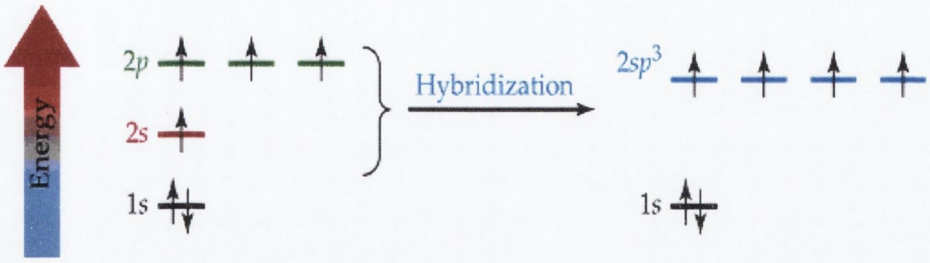

Figure 3.2 Schematic of sp^3 hybridisation in carbon atom

The versatility of carbon results in numerous conjugated structures, which span a range of dimensions and topologies. Long chain polymers are examples of one-dimensional systems. Aromatic rings form the basis of many two–dimensional structures while cage molecules, namely fullerenes, have a three-dimensional delocalization of the π-electrons. A vast array of molecular configurations can be created from these basic structures.

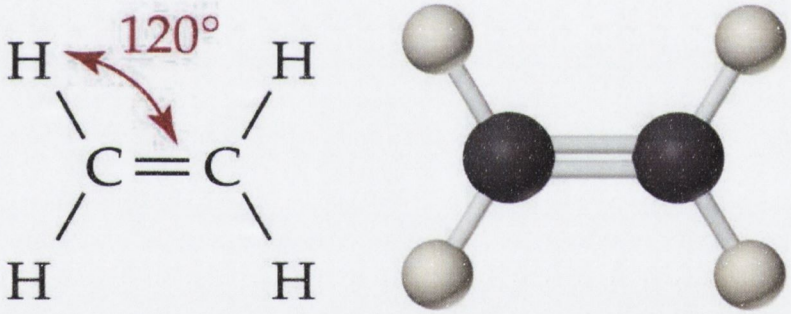

Ethylene

3-Dimensional side-view image of the planar ethylene molecule.

Figure 3.3 The structure of ethylene, in *stick* and three dimensional form. The carbon-carbon double bond consists of one s bond from the head-on overlap of sp^2 orbitals and one p bond from the sideways overlap of p orbitals.

Following on from this discussion we introduce benzene (C_6H_6), which is also a planar molecule with six carbon atoms arranged hexagonally. Each carbon atom

forms a sp^2 σ-bonds with one hydrogen atom and its two adjacent carbon atoms. The π-electrons form a ring orbital above and below the plane of the hexagon. Traditionally the structure of benzene is drawn with alternating single and double bonds between the carbon atoms. In reality the π-electrons are shared equally between the two bonds on either side of the carbon atoms. Organic molecules such as benzene with alternating single and double bonds are said to be *conjugated.* These contrast with other large molecules with only single bonds between the carbon atoms, which are known as *saturated* structures.

3.1.2 Electron Delocalization

Presented in **Figure 3.4**, benzene, is defined as an organic, aromatic hydrocarbon. Aromaticity is a chemical property in which a conjugated ring of unsaturated bonds, lone pairs, or empty orbitals exhibit a stabilization stronger than would be expected by the stabilization of conjugation alone. The model for benzene consists of two resonance forms, which corresponds to the double and single bonds' switching positions. By definition, delocalized electrons are electrons in a molecule that are not associated with a single atom or a covalent bond. These electrons form part of a π-electron system that can extend over several adjacent atoms. Delocalized electrons can be found in conjugated systems of double bonds and in aromatic systems, such as benzene. These bonds are weaker and much more delocalized, therefore requiring much less energy to excite them. Since the p-orbitals associated with π–bonds are located out of the plane of the atoms, these orbitals can interact with each other freely, and become delocalized. Excitations of the π-electrons can therefore produce a large perturbation of the molecular orbital and enable the induction of a large polarisation. It is this delocalized, extended π-conjugated system that is utilized for high intensity light induced charge transfer in such systems as porphyrins and phthalocyanines.

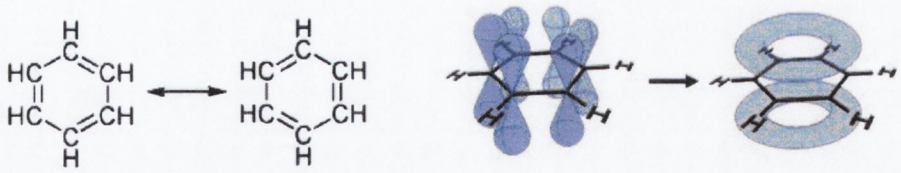

Figure 3.4 Structural diagram of benzene. Delocalization, Six π-electron orbitals and delocalized electron cloud in benzene, together with the in-plane electron cloud associated with σ bonding.

3.1.3 Multiphoton Interactions

Specific to this report, both the linear and nonlinear optical parameters of phthalocyanine molecules are strongly dependent on their conformational and chemical structure. An understanding of how molecular structure relates to its capacity for multiphoton interactions and hence its nonlinear optical performance is essential in the design of materials with enhanced nonlinear optical properties. The electronic states of the molecule can be arranged in order of increasing energy. The electrons from the constituent atoms of the molecule fill up the molecular orbitals until they are all paired off in bonds. The highest filled energy level is called the HOMO level (Highest Occupied Molecular Orbital). For π-conjugated molecules this will be a π-orbital because the electrons from the σ bond are very tightly bound. The first energy level above the HOMO level is called the LUMO level (Lowest Unoccupied Molecular Orbital). This orbital will be populated by excited, energetic electrons and is associated with the π-π* transitions. The electronic levels and photophysical processes in organic materials can be represented schematically in a Jablonski diagram such as that shown in **Figure 3.5**. In this scheme the molecular electronic levels are divided into singlet and triplet levels. The electrons in the ground state of a molecule are all paired off in bonds with their spins antiparallel. This means that the HOMO level has a spin quantum number, **S**=0. Spin quantum number is a quantum number that parametrizes the intrinsic angular momentum (or spin angular momentum) of a given particle The excited states can have either S=0,1. This is due to the excitation process putting an unpaired electron (**S**= ½, an intrinsic property of electrons) in an excited state and leaving an unpaired electron

in the HOMO level. The **S**=0 states are know as singlets and the **S**=1 states are known as triplets. Triplets tend to have lower energies as the singlet counterparts. Electronic transitions to singlet and triplet states leads to very different optical responses.

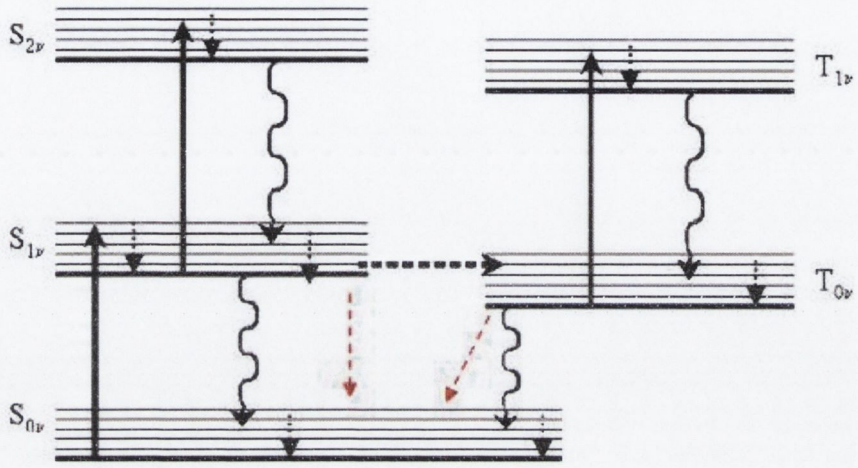

Figure 3.5 Jablonski diagram of photophysical processes. The red line indicates nonradiative decay processes from both S_1 and T_0 to S_0.

A variety of excitation and relaxation transitions can occur, which can be either radiative or non-radiative. The transitions are represented as lines; dashed lines denote non-radiative transitions while solid and wavey lines denote radiative transitions. The horizontal dashed line represents the process of electron population intersystem crossing, from singlet to triplet states. Each molecule will have a series of singlet states, (S_0, S_1, S_2, S_3...) where S_0 denoted the singlet ground state. Triplet states have a series of states, T_1, T_2, T_3 etc. Since photons carry no spin, they can only excite transitions between the same electronic states of the same spin. Therefore, in general, transitions from S_0 to T_1 are forbidden. For metallophthalocyanine systems, due to spin-orbit coupling, singlet-triplet transitions are allowed, resulting in population transfer to this relatively long lived excited state. The emission spectra are dominated by $S_1 \rightarrow S_0$ transitions. The most familiar radiative excitation is ground state absorption where a molecule is excited from its lowest ground state into a vibrational level in the first excited state. The probability

of this transition is given by the ground state absorption cross section σ_0, which is related to the ground state absorption coefficient by, $\alpha_0=\sigma_0 N_0$, where N_0 is the number density of the absorbing species. Absorption processes are extremely rapid and occur on a timescale of $\sim 10^{-15}$ s. Absorption is also possible out of an excited state in a multiphoton process known as excited state absorption. Excited states of molecules can also be populated by a multiphoton processes in which more than one photon is simultaneously absorbed from the radiation field. The probability of N photons being absorbed by a molecule at a given point in space and in time is directly proportional to the N^{th} power of the density of photons per area unit per second. It therefore follows that these processes are likely to occur only at high intensities. Following a molecule's excitation into a vibronic level of an excited state, it will rapidly cascade down the vibrational manifold. This is a thermal nonradiative process, which occurs on a timescale of 10^{-13} s. Once in the lowest vibrational level of its excited state the molecule may then relax radiatively into the ground state vibrational manifold. If both states have the same multiplicity this process is known as fluorescence. It is a spin allowed process and occurs over a timescale of 1-100 ns. Radiative relaxation from a triplet state is known as phosphorescence and is a spin forbidden process. It is therefore a slow process occurring on a time scale of microseconds to days.

Linear absorption involving transitions from the ground state to the S_1 *band* usually results in excitation into the S_1 vibration-rotation manifold. This is followed by rapid decay to the bottom of the band, whereupon the molecule is placed in an off-resonance energy state. This allows complete depletion of the ground state. Specific to metallophthalocyanine systems, the lifetimes of the S_1 to T_1 transition is of the order of nanoseconds. The singlet excited states have relatively short excited state lifetimes (of the order 1-10ns), while the lowest triplet state has a relatively long radiative lifetime because of the low probability for the $T_1 \rightarrow S_0$ transition. Singlet-singlet transitions can be noted on the optical emission spectra in the form of fluorescence, while triplet-singlet transitions describe phosphorescence emissions. There are several processes, which may compete with radiative de-

excitation, such as internal conversion, intersystem crossing and various quenching mechanisms.

3.1.4 Internal Conversion

Internal conversion refers to isoenergetic transitions where vibrationally excited molecular entity in the lower electronic state transfer may occur between a zero vibrational level of a higher state to a high lying vibrational level of a lower state.

3.1.5 Intersystem Crossing & Spin-Orbit Coupling

Intersystem crossing refers to isoenergetic transition between a vibrationally excited singlet state and a triplet state. This process is spin forbidden, however it can be achieved through orbit spin coupling between excited states of different multiplicity. In the periodic table of elements, the ionization energy decreases as you go down each group. The shielding effect with increasing number of orbiting shells makes it easier to remove the outer most electrons from those atoms that have many electrons. Incorporation of heavy metal atoms in organic materials is often used as a method of increasing nonlinear absorption through intersystem crossing and triplet-triplet absorption. This coupling increases with atomic number Z in what is known as the "Heavy Atom Effect".

3.2 Introduction to the Phthalocyanine

3.2.1 Original Discovery

The first reported synthetic aromatic dye compound was mauve, discovered at the age of 18, by Sir William Henry Perkin in 1856. He quickly realised the industrial potential of a replacement natural dye, since the work to obtain the dyes was labour intensive and expensive. The natural dyes tended to lack consistency of depth of

colour, differing in composition and concentration. With the birth of the industrial revolution, came a huge demand for mass-production of materials, the consequences of which transformed the textile industry. In 1927 de Diesbach and von der Weid [1] described new, insoluble blue compound which was most likely a copper phthalocyanine. The following year Dandridge, Drescher, and Thomas (Scottish Dyes Ltd.) filed a patent application describing new and unnamed, insoluble coloured organic compounds, which in time would be the outline for the preparation of iron phthalocyanine. The examination of these patented compounds and the determination of their structure was referred to R. P. Linstead by Prof. J.F. Thorpe, of the Imperial Institute of Science and Technology, London. [2] The determination of chemical properties, structure and the possible use as an industrial pigment and dye is attributed to Linstead. [3-5] The first report of Linstead's work to the Chemistry Section of the British Association for the Advancement of Science was made in September 1933, the beginning of a series of reports where he is also accredited with coining the name *phthalocyanine* (from the Greek, *phthalo*-rock oil; *cyanine*-blue).[6] In 1934 alone, Linstead contributed to 6 papers published by the Journal of the Chemical Society.[4-9] Between the years 1934 and 1940, 190 phthalocyanine dye related patents had been filed.

In July 1939 Miles Dahlen[10] reported that, for phthalocyanines, "The development is far from being a closed book, either scientifically or industrially, and it is possible that other additions to the ever-broadening line of pigments and dyes will come from this series". Over 60 year later, this research field remains as open and diverse as Dahlen predicted.

3.2.2 Nomenclature

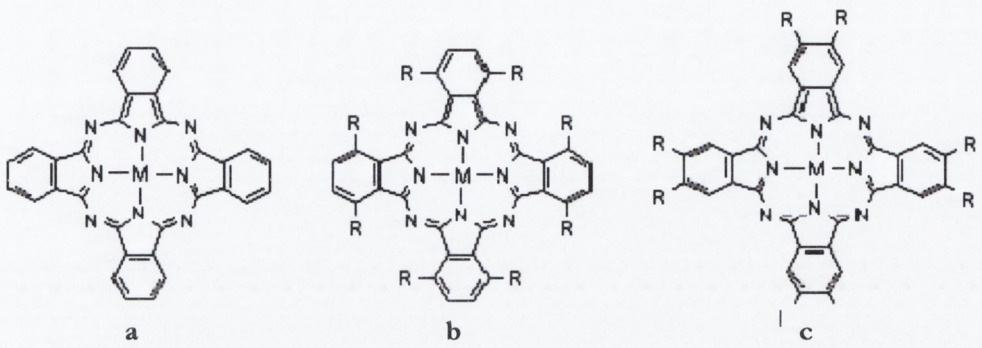

Figure 3.6 Selection of phthalocyanine chemcial structures. (a) Metal-substituted phthalocyanine; (b) Non-peripheral substituted metallophthalocyanine; (c) Peripheral substituted metallophthalocyanine

Phthalocyanines are two-dimensional conjugated arrays, which are highly architecturally flexible. [11] They can be extensively chemical tailored allowing control over their electronic and optical properties. A selection of phthalocyanine structures are shown in **Figure 3.6**, with a central metal substituted phthalocyanine in **Figure 3.6(a),** non-peripheral substituted metallophthalocyanine in **Figure 3.6(b)** and a peripheral substituted metallophthalocyanine, **Figure 3.6(c)**. From the structural diagram in **Figure 3.7**, it is clear that phthalocyanines allow for a variety of chemical modifications: the introduction of metals (M), semi-metals or hydrogen into the central cavity and peripheral and axial substitutions, all of which can dramatically alter the physical structure and chemical responses of the molecule.

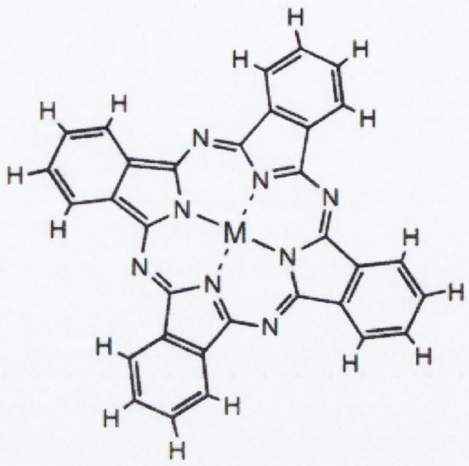

Figure 3.7 Phthalocyanine molecular structures (*Note*: M=Metal, N=Nitrogen, H= Hydrogen)

3.2.3 Electronic Structure & Photophysical Processes

The linear absorption spectrum of phthalocyanines is characterized by two strong absorption peaks; a Q-band in the red/near infrared part of the spectrum (~670nm) and a B-band in the UV/blue part of the spectrum (~350nm). The strong Q-band absorption is responsible for the characteristic intense blue-green colour of the compound. A window of high transmission exists between these two bands and is an important feature when discussing the multiphoton absorption behaviour of phthalocyanines. This high transmission region in the visible portion of the spectrum is also desirable for any potential window-type optical applications. A typical linear absorption spectrum for a metal substituted phthalocyanine is shown in **Figure 3.8**.

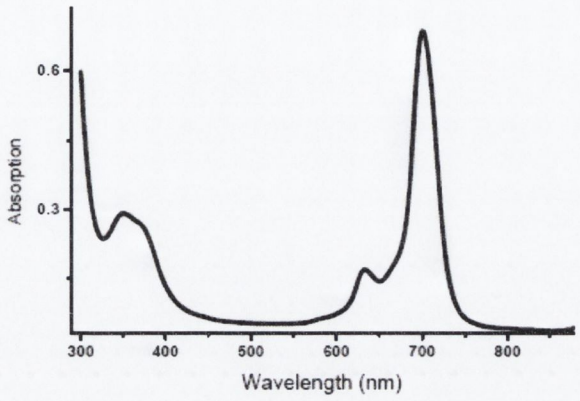

Figure 3.8 Typical UV-Visible spectrum for a metallophthalocyanine, showing the B- and Q-band peaks and the high transmission region in the visible part of the spectrum.

Metallophthalocyanines are characterized by enhanced intersystem crossing between the singlet and triplet levels. This action results in a build up of the electronic population in the triplet levels and is a mechanism, which is responsible for a nonlinear absorption process known as reverse saturable absorption. This type of multiphoton absorption is facilitated by a weak linear absorption such as that which occurs in phthalocyanines between the two main bands. Structural modifications and substitutions in phthalocyanines typically shift the linear absorption maxima and the corresponding vibronics. The main features of the linear absorption, which are due to the π-electrons within the conjugated ring, are generally retained.

3.3 Introduction to $Mo_6S_{4.5}I_{4.5}$ Nanowires

3.3.1 Introduction to Inorganic Nanowires

Interest in one-dimensional nanomaterials has increased dramatically due to their novel and remarkable chemical and physical properties compared to materials on the macroscopic scale.

In this report, we define a nanowire as a nanoscale, one dimensional anisotropic object with a large aspect ratio, being highly ordered, with repeating molecular units along the X-axis, **Figure 3.9**). In conjunction with the broad research in organic nanotubes, detailed investigations have been conducted into inorganic nanotubes, often composed of metal oxides with a morphologically similar to carbon nanotubes. As early as 1930, Linus Pauling [12] published a report on the possibility of curved layers in minerals, but it took over 30 years for experimental evidence of inorganic nanotube to confirm Pauling's work. Reshef Tenne et al.[13] reported the synthesis of nanotubes composed of tungsten disulfide in 1992. Today a wide and varied selection of materials have been synthesised in nanotube form include CdSe, MoS_2 and NbS_2. In this report the nonlinear optical extinction of laser irradiation from $Mo_6S_{4.5}I_{4.5}$ nanowires is discussed. In theoretical structural modeling, the $Mo_6S_{4.5}I_{4.5}$ nanowire is considered similar to transition metal chalcogenide cluster compounds, such as the Chevrel phases[14-16] than curled-up sheets of MoS_2. This three component anisotropic nanowire system was first synthesised by the Mihailovic group in 2004. [17]

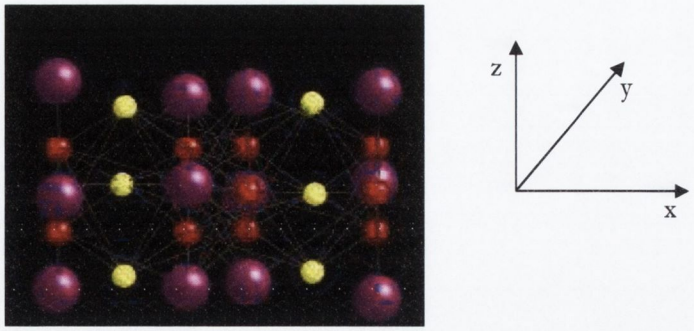

Figure 3.9 Structure of subnanometer diameter $Mo_6S_{4.5}I_{4.5}$ nanowire

3.3.2 Background

Chalcogens is the name for elements in group 6 of the periodic table. It consists of the elements oxygen (O), sulfur (S), selenium (Se), tellurium (Te), the radioactive polonium (Po), and the synthetic ununhexium (Uuh). Their compounds, particularly the sulfides, selenides and tellurides are collectively known as *chalcogenides.* Chalcogens (more specifically S, Se and Te) are ideal systems for the formation of mono-dimensional nanostructures. The S, Se or Te chains can be readily crystallized through van der Waals interactions, a consequence of which is crystallization along the x-axis, favouring the stronger covalent bonds over the relatively weak, inter-chain van der Waals forces. Thus, these materials have a tendency to form high anisotropic one dimensional structures. [13, 15, 16, 18-21] Among the conventional chalcogenides, compounds known as the "Chevrel phases" have attracted particular attention and excited solid state chemists and physicists, since they were first discussed in 1971 by Chervel et al.[22] These are ternary molybdenum chalcogenides that can be described by the formula MMo_6X_8, where X is usually S, Se or Te and M = Pb, Sn, Au, Cu, Li. Mo_6 octahedra are the fundamental building blocks in these systems. Compounds containing halogens[23] have also been prepared as well as compounds in which some molybdenum atoms are replaced by Re, Ru, and Rh.[24, 25] In her doctorate thesis V. Nicolosi discussed the atomic structure of $Mo_6S_{4.5}I_{4.5}$ nanowires using high resolution TEM.[26] She concluded that such structures can be defined as a *mono dimensional Mo-chalcogenide-halide structure,*

composed by Mo octahedrons surrounded by trimers of iodine, connected by bridging planes of 3 sulphur atoms. The peripheral sites where either S or I reside control the interaction of the wire with other wires and with its external environment. In this paper, they present this anisotropic, crystalline structure diagrammatically, reproduced in **Figure 3.10(a) & (b)**.

The main families of inorganic nanotubes are reviewed and discussed in several papers.[18, 21, 27] The basis of the growth mechanism of inorganic nanotubes is the lack of resistance in the process of wrapping the quasi two-dimensional crystal flakes.[19] This bending is spontaneous in transition metal dichalcogenide nanotubes.[20]

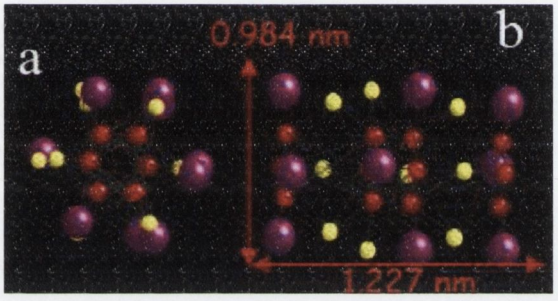

Figure 3.10 (a) front view of a single nanowire; **(b)** unit cell of the single nanowire. The red atoms represent Mo, yellow-S, purple-I.

3.3.3 Synthesis

The $Mo_6S_{4.5}I_{4.5}$ nanowires studied in this thesis are produced in the Jozef Stefan Institute of Ljubljana (Slovenia), in the laboratories of Prof. Dragan Mihailovic. Nanowires of general formula $Mo_6S_{9-x}I_x$ are obtained by direct synthesis from pure elements. Platelets of molybdenum sheet metal (foil 0.1 mm thick), sulphur powder and iodine are sealed and evacuated in a quartz ampoule with diameter of 19 mm and length 140 mm, with a remaining gas pressure of about 10^{-2} Pa. This ampoule is placed in a furnace and heated to a temperature of 1070 °C at a rate of 8 K/h. This temperature is kept stable for 72 hours. The ampoule is subsequently cooled at 1.5 K/min in the furnace. The majority of the resulting material has a fur-like

appearance, with individual needles having a diameter of about 100 nm to 1000 nm and a wide range of lengths, up to 5 mm.

3.3.4 Electronic Structure and Molecular Geometry

Electronic band structure calculations on $Mo_6S_{4.5}I_{4.5}$ nanowires have been recently performed and predict those materials to be semi-metallic. [28] In fact, while the Fermi level energy is crossing hybridized bands belonging to Mo, S and I, suggesting a metallic ground state, a band gap (~ 0.5 - 0.9 eV) above the Fermi level is also noticed (see **Figure 3.11**).

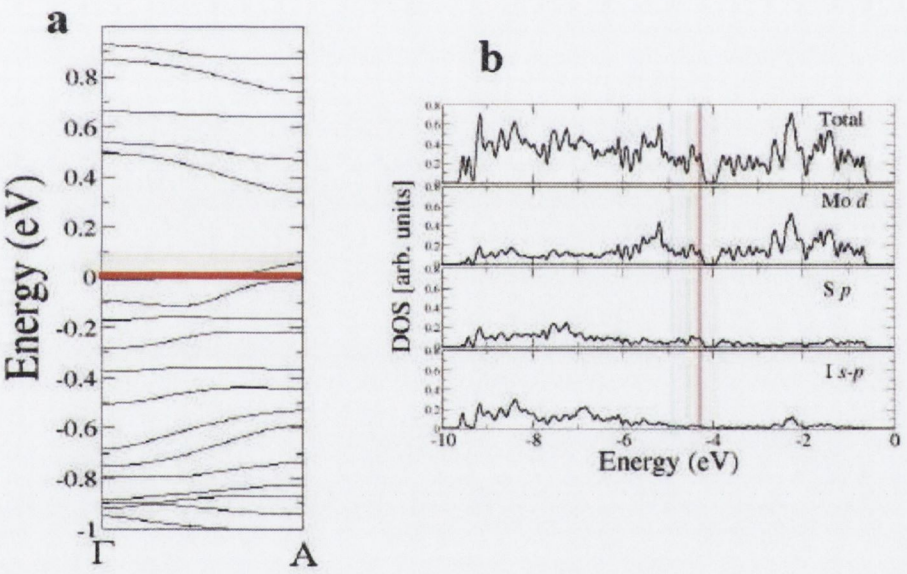

Figure 3.11 (a) Electronic band structure and **(b)** Density of States at the Fermi energy level calculated for $Mo_6S_{4.5}I_{4.5}$ single nanowires.

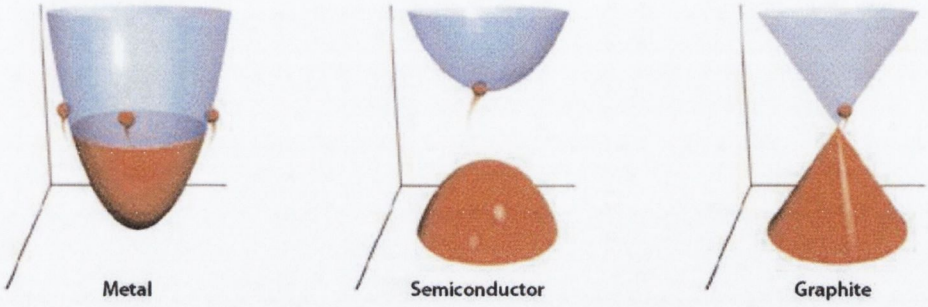

Figure 3.12 Cartoon representing the band structures for a metal, semiconductor and graphite, highlighting the means of electron transport

Figure 3.12 gives an indication of the density of states for a metal, semiconductor and graphite (an example of a semi-metal). $Mo_6S_{4.5}I_{4.5}$ nanowires can be considered as semimetals or p-type semiconductors due to existence of a bandgap (~0.5-0.9 eV), with the Fermi level existing just above the valence band, as is found in p-doped semiconductors. In such systems, the addition of acceptor impurities contributes hole levels low in the semiconductor band gap so that electrons can be easily excited from the valence band into these levels, leaving mobile holes in the valence band. This shifts the effective Fermi level to a point about halfway between this acceptor levels and the valence band. The absorption of a photon by an interband transition in a semiconductor creates an electron in the conduction band and a hole in the valence band. The oppositely charged particles are attracted through Coulombic interactions, increasing the probability of *electron-hole pair confinement*.

3.4 Introduction to Carbon Nanotubes

3.4.1 Original Discovery

The discovery of carbon nanotubes has been credited to the Japanese electron microscopist Sumio Iijima in 1991,[29] who was studying the material deposited on the cathode during the arc-evaporation synthesis of fullerenes. Formed in the cathodic deposit was a variety of closed graphitic structures including nanoparticles and nanotubes, with outer diameters of 4–30 nm a nd length of 1 μm. Since these tubes consisted of multiple shells, where many tubes are arranged in a coaxial fashion, and tube diameter is of the order of nanometres, he called these tubes Multi-walled Nanotubes (MWNTs) (**Figure 3.13b**), compared to Single-Walled Nanotubes (SWNTs), which are seamless cylinders each made of a single graphite sheet. The diameters range from 0.4 to 3 nm, and lengths are of the order of micrometres (**Figure 3.13a**). SWNTs intrinsically aggregate to form bundles, decreasing the surface area of nanotube available for interaction with the surrounding environment which in many cases is considered a physical limitation. **Figure 3.13c** presents TEM images for both SWNTs and MWNTs showing the internal cylindrical structure for both systems.

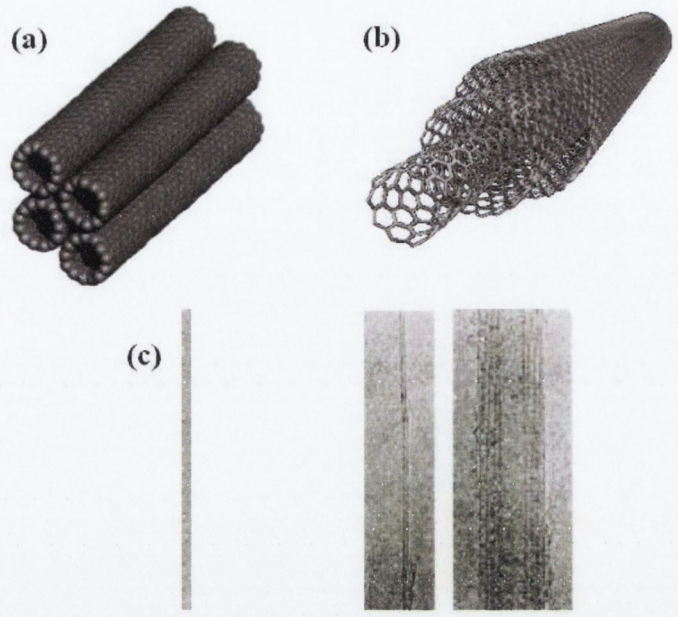

Figure 3.13 (a) Single-Walled Nanotube forming bundles through weak Van der Waals interactions, **(b)** Concentric cylinders of carbon nanotubes making up MWNT, **(c)** TEM imaging of SWNTs and MWNTs, respectively.

3.4.2 Atomic Structure of Carbon Nanotubes

Before the discovery of fullerenes in 1985,[30] ordered carbon was thought to exist in only two allotropes; diamond, a sp^3 hybridized form of carbon, and graphite, an sp^2 hybridized form (**Figure 3.14**). In 1985 Kroto, Curl, and Smalley discovered the first member of a new family of carbon structures, in the form of a spherical cage, presented in **Figure 3.14**. This was C_{60}, consisting of a mainly hexagonal lattice, with the incorporation of five pentagons giving sufficient positive curvature for it to close into a sphere.

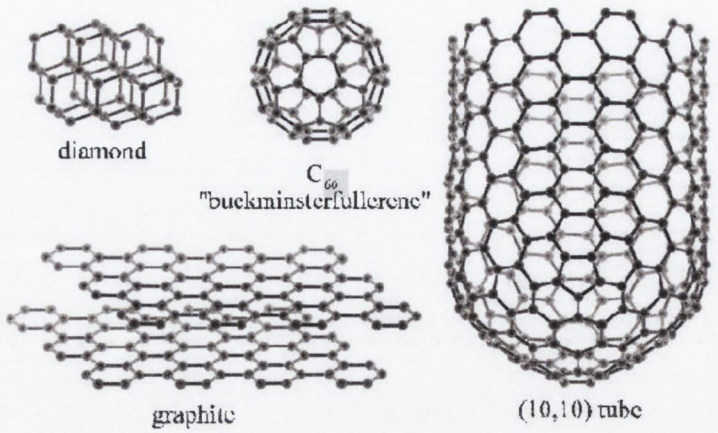

Figure 3.14 Allotropes of carbon; diamond, graphite, fullerenes and nanotubes.

This was named the Buckminster Fullerene, in honour of the architect who had used this structure in many buildings. Following this discovery, many other members of the fullerenes family were discovered, differing in radii and in shapes.

3.4.3 Physical Structure of Carbon Nanotubes

A geometrically perfect carbon nanotube consists of two-dimensional hexagonal lattices of carbon atoms scrolled to form concentric cylinders. All cylinders are terminated at both ends by *endcaps* where, as in the case of C_{60}, pentagons are introduced to give curvature and close the cylinders. There are many ways in which the graphene sheet can be scrolled to form a cylinder, depending on the angle that the lattice makes with the cylinder axis. This is characterized by the chiral vector which is defined by $\underline{C} = n\underline{a}_1 + m\underline{a}_2$ where $\underline{a}_1$ and $\underline{a}_2$ are unit vectors in the hexagonal lattice and m and n are integers, as shown on a sheet of graphite in **Figure 3.15**. The (n, m) values of the chiral vector determines all the characteristics of an ideal nanotube, including diameter, chiral angle, and all electronic properties, notably the

bandgap of the nanotube. The chiral angle is the angle between the lattice and the cylindrical axis of the nanotube.

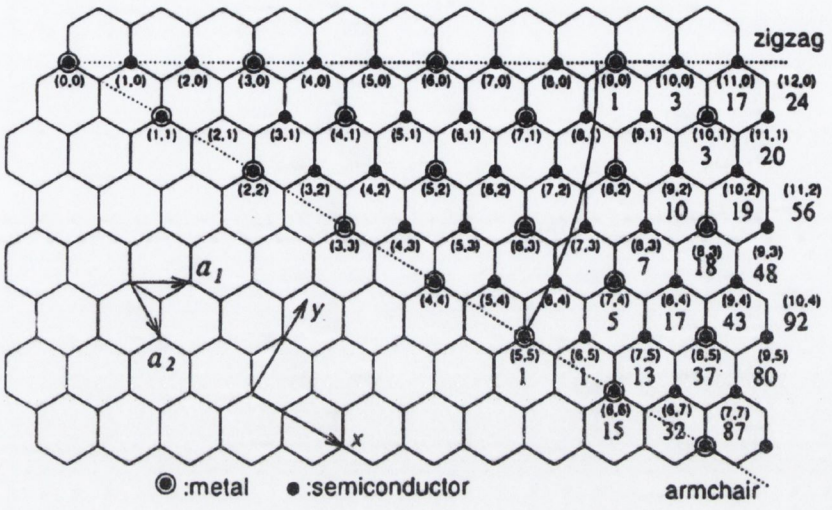

Figure 3.15 Representation of the possible chiral vectors of carbon nanotubes.

Nanotube chiralities can be divided into three broad categories: *Zigzag* nanotubes, with chiral vectors of the form (n, 0). The rows of the lattice structure are perpendicular to the nanotube axis. Secondly, *Armchair* nanotubes have chiral vectors (n, n), with bonds lying perpendicular to the nanotube axis. All other nanotubes have chiral angle between 0° and 30° and are called *chiral* nanotubes. These three general types of nanotubes are depicted in **Figure 3.16**.

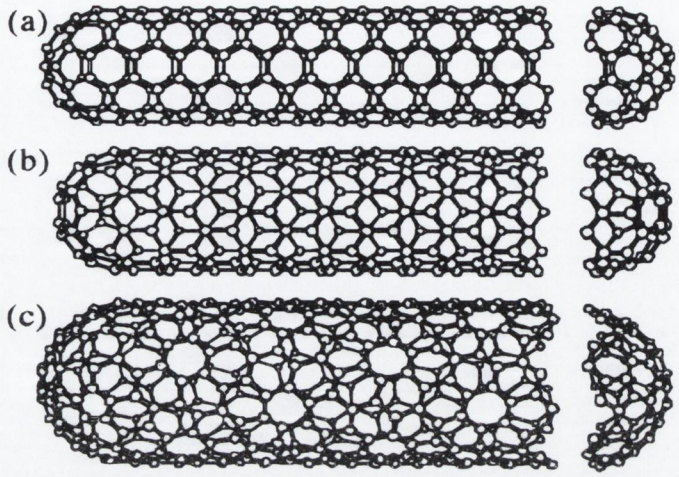

Figure 3.16 The three general types of nanotubes; (a) armchair, (b) zigzag, (c) chiral.

3.4.4 Electronic Structure of Multi-Walled Nanotubes

Specific to this thesis will be the investigation into the nonlinear optical investigation of MWNT-polymer composite systems. MWNTs consist of many close concentric cylinders, and interactions between these can greatly complicate the electronic structure. The original work on shell interactions modelled double-walled nanotubes, and suggested that interlayer coupling had little effect on the electronic structure of the individual shells.[31] Thus, individual shells were predicted to retain their semiconducting or metallic nature. The density of states for a MWNT is far more complicated than for SWNTs, however the outer shell is thought to dominate the electronic structure, as it is the shell that interacts with the external environment. Nanotubes of the type n-m=3p, where p is zero or any positive integer are metallic and thus conducting. The relationship that determines from the chiral vector which nanotubes will be metallic is relatively simple, and is

$$\frac{n-m}{3} = p \qquad 3\text{-}1$$

The fundamental gap (HUMO-LUMO) would be 0eV, and thus showed that all other nanotubes behaved as semi-conductors. The fundamental gap was ~ 0.5eV and was a function of tube diameter. Immediately apparent from this is that 1/3 of all nanotubes are metallic, and that all armchair nanotubes are metallic, as these are nanotubes where n=m. Presented in **Figure 3.17** are the theoretical band structures for a metallic, semi-metallic and semiconducting SWNT.

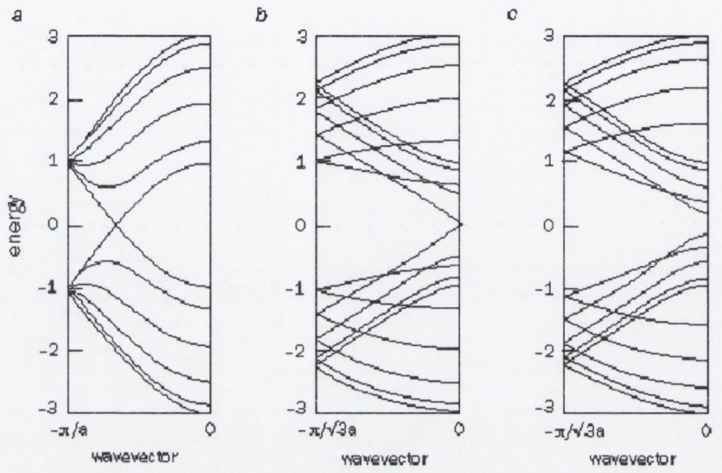

Figure 3.17 Band structure calculations for SWNTs; (a) is due to a truly metallic tube as there is a finite density of states at the Fermi energy; (b) Semi-metallic (*pseudo-metallic*) nanotube with zero bandgap; (c) Semiconducting nanotube with finite bandgap

3.4.5 Multi-Walled Carbon Nanotube Composite Systems

Nanotube-polymer composite systems have previously been prepared in the Blau group in Trinity College Dublin.[32-34] The polymer used is a functional organic polymer,poly(meta-phenylenevinylene-co-2,5-dioctyloxy-para-phenylenevinylene), or PmPV, the chemical structure of such is presented in **Figure 3.18.** It has been shown that during the composite formation, the nanotube aggregates are broken up, and the polymer coating hinders their re-aggregation. This interaction has several interesting properties which results in substantial advantages over other composites developed. The polymer binds to the lattice structure of the nanotubes, and as PmPV is soluble in many organic solvents, unlike the pure nanotubes themselves, stable solutions of these composites are readily attainable. This also allows the preferential selection of nanotubes from the raw nanotube powder.

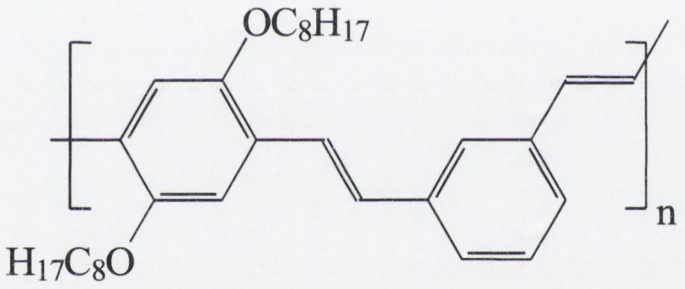

Figure 3.18 Chemical structure of poly(meta-phenylenevinylene-co-2,5-dioctyloxy-para-phenylenevinylene), PmPV

Sidegroups have significant effects on the morphology of PmPV by altering backbone conformation and thus the capability of the polymer strands to interact with each other. This morphological effect indicates that the sidegroups have critical implications for the formation of stable PmPV-nanotube composites. From a conformation viewpoint, there is a slight but noticeable helicity to the backbone of PmPV. The van der Waals interaction between the sidegroups keeps them relatively planar, and exposes the polymer backbone. Initial work on the purification abilities of the composite concentrated on characterizing the phase separation effects of the

composite, the preferential selection and suspension of nanotubes. The TEM image presented in **Figure 3.19** shows carbon nanotubes coated in PmPV protruding from the edge of a composite film.

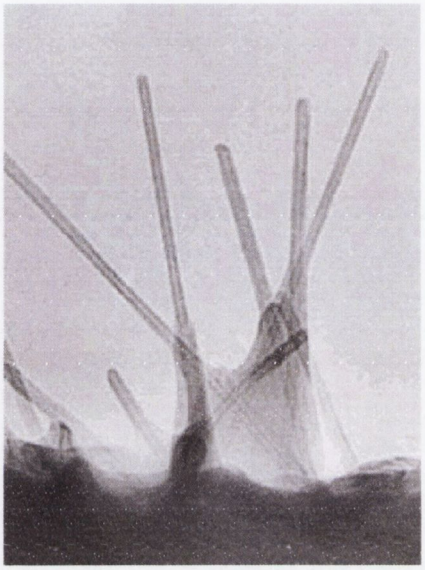

Figure 3.19 TEM image of PmPV/MWNT Composite.

The PmPV film can be clearly seen to wet the nanotubes protruding from the composite film. There are no graphitic impurities visible, despite the raw powder from which this composite is formed being about 75% graphitic particles. These particles are usually seen attached to the walls of nanotubes, suggesting that the PmPV coating the nanotube in some way displaces the graphitic particles from the nanotube. The PmPV thus acts as a filtering system removing the nanotubes from the accompanying graphitic particles and forms a stable nanotube-polymer dispersion.

References

1 E. v. d. W. Henri de Diesbach, *Helvetica Chimica Acta* **10**, (1), 886-888 (1927).
2 J. F. Thorpe, R. P. Linstead, and I. ltd., US2000052, (1933).
3 R. P. Linstead, *Journal of the Chemical Society*, 1016-17 (1934).
4 R. P. Linstead, and A. R. Lowe, *Journal of the Chemical Society* 1022-7 (1934).
5 R. P. Linstead, and A. R. Lowe, *Journal of the Chemical Society*, 1031-3 (1934).
6 R. P. Linstead, *Journal of the Chemical Society* 1016-17 (1934).
7 G. T. Byrne, R. P. Linstead, and A. R. Lowe, *Journal of the Chemical Society* 1017-22 (1934).
8 C. E. Dent, and R. P. Linstead, *Journal of the Chemical Society*, 1027-31 (1934).
9 C. E. Dent, R. P. Linstead, and A. R. Lowe, *Journal of the Chemical Society* 1033-9 (1934).
10 M. A. Dahlen, *Industrial and Engineering Chemistry* **31**, (7), 839-847 (1939).
11 N. B. McKeown, *Journal of Materials Chemistry* **10**, (9), 1979-1995 (2000).
12 L. Pauling, *Proc. Nat. Acad. Sci* **16**, 578-82 (1930).
13 R. Tenne, L. Margulis, M. Genut, and G. Hodes, *Nature* **360**, (6403), 444-446 (1992).
14 D. Mihailovic, Z. Jaglicic, D. Arcon, A. Mrzel, A. Zorko, M. Remskar, V. V. Kabanov, R. Dominko, M. Gaberscek, C. J. Gomez-Garcia, J. M. Martinez-Agudo, and E. Coronado, *Physical Review Letters* **90**, (14), (2003).
15 V. Nicolosi, D. Vrbanic, A. Mrzel, J. McCauley, S. O'Flaherty, C. McGuinness, G. Compagnini, D. Mihailovic, W. J. Blau, and J. N. Coleman, *Journal of Physical Chemistry B* **109**, (15), 7124-7133 (2005).
16 V. Nicolosi, D. Vrbanic, A. Mrzel, J. McCauley, S. O'Flaherty, D. Mihailovic, W. J. Blau, and J. N. Coleman, *Chemical Physics Letters* **401**, (1-3), 13-18 (2005).
17 D. Vrbanic, M. Remskar, A. Jesih, A. Mrzel, P. Umek, M. Ponikvar, B. Jancar, A. Meden, B. Novosel, S. Pejovnik, P. Venturini, J. C. Coleman, and D. Mihailovic, *Nanotechnology* **15**, (5), 635-638 (2004).
18 Y. Xia, P. Yang, Y. Sun, Y. Wu, B. Mayers, B. Gates, Y. Yin, F. Kim, and H. Yan, *Advanced Materials* **15**, (5), 353-389 (2003).
19 M. Remskar, Z. Skraba, F. Cleton, R. Sanjines, and F. Levy, *Applied Physics Letters* **69**, (3), 351-353 (1996).
20 M. Remskar, Z. Skraba, R. Sanjines, and F. Levy, *Applied Physics Letters* **74**, (24), 3633-3635 (1999).
21 M. Remìkar, Z. Skraba, M. Regula, C. Ballif, R. Sanjinés, and F. Lévy, *Advanced Materials* **10**, (3), 246-249 (1998).
22 R. Chevrel, M. Sergent, and J. Prigent, *Journal of Solid State Chemistry* **3**, (4), 515-519 (1971).

23 R. Knoll, S. D. Goren, C. Korn, A. Shames, C. Perrin, A. Privalov, and H. M. Vieth, *Physica B: Condensed Matter* **324**, (1-4), 157-166 (2002).
24 A. Perrin, M. Sergent, and O. Fischer, *Materials Research Bulletin* **13**, (4), 259-264 (1978).
25 A. Perrin, R. Chevrel, M. Sergent, and O. Fischer, *Journal of Solid State Chemistry* **33**, (1), 43-47 (1980).
26 V. Nicolosi, in *School of Physics*, Trinity College Dublin: Dublin, Ireland, 2006; Vol. Doctor in Philosophy, p 173.
27 C. N. R. Rao, and M. Nath, *Dalton Trans.* **1**, 24 (2003).
28 V. Nicolosi, S. Berber, J. N. Coleman, J. Sloan, D. Tomanek, D. Mihailovic, and W. J. Blau, in, NT'04 Conference, Poster Presentation: 2004.
29 S. Iijima, *Nature* **354**, 56-58 (1991).
30 H. E. Kroto, J. R. Heath, S. C. O'Brien, R. F. Curl, and R. E. Smalley, *Nature* **318**, 162 (1985).
31 R. Saito, G. Dresselhaus, and M. S. Dresselhaus, *Journal of Applied Physics* **73**, (2), 494-500 (1993).
32 J. N. Coleman, S. Curran, A. B. Dalton, A. P. Davey, B. McCarthy, W. Blau, and R. C. Barklie, *Phys. Rev. B* **58**, (Issue 12), 7492–7495 (1998).
33 S. A. Curran, P. M. Ajayan, W. J. Blau, D. L. Carroll, J. N. Coleman, A. B. Dalton, A. P. Davey, A. Drury, B. McCarthy, S. Maier, and A. Strevens, *Advanced Materials* **10**, (14), 1091-+ (1998).
34 J. N. Coleman, D. F. OBrien, B. McCarthy, B. Lahr, A. Drury, R. C. Barklie, W. J. Blau, and A. B. Dalton, *Chemical Communications* **20**, 2001-2002 (2000).

CHAPTER 4

POLYMER-PHTHALOCYANINE COMPOSITES

4.1 Introduction

The realization of photonic based technologies depends on two main factors: the existence and understanding of appropriate optical techniques and secondly, suitable optical materials for the fabrication of optical circuits, interconnects and devices. The first factor has already been realized with the development of the laser and the theory of nonlinear optics. The second factor required for photonic technologies relates to materials that can facilitate efficient nonlinear optical interactions of high conversion efficiency, and which can be fabricated into useful devices.

The protection of sensitive optical equipment has been the focus of much attention in recent times. Of great important is the protection of the human eye from potentially harmful intense beams. Numerous researchers[1-17] have advanced the field of nonlinear optics through the design of tailored molecules to absorb high intensity light, primarily via nonlinear absorption and scattering processes.[18] Organic materials, such as fullerenes[2, 4, 14, 16, 19] and organometallic materials[3, 5, 20, 21] have been shown to behave as nonlinear absorbers. Phthalocyanines and their derivatives have attracted considerable attention for *optical limiting* processes, which can be defined as the strong absorption of high intensity light whilst allowing for the high transmission of ambient light. Like fullerenes, phthalocyanines are materials that optically limit via a nonlinear absorption process due to excited state, multi-step absorption.[9, 22, 23] Due to their architectural flexibility, extended delocalized π-electron structure, high triplet yields, fast nonlinear optical response times and easy processing, phthalocyanines are ideal molecules for potential optical limiting applications.[23-31] The highly delocalized18 π-electron aromatic system of phthalocyanines can give rise to a strong nonlinear optical response. The application of metallo-phthalocyanine compounds in a practical optical limiting device such as in a 'bottleneck' or 'tandem' limiter geometry[32, 33] would almost inevitably require the casting of the optically active compounds in the solid state. In this chapter we investigate the applicability of doping phthalocyanine into a non-active polymer host to cast high quality optically active layers. The ultimate aim is to develop and

tailor a polymer-phthalocyanine composite system for the incorporation into an optical limiting device. For the compounds mentioned in this chapter, the scientific standard molecular formula for the phthalocyanine (Pc) takes the form: SPcMX. The chemical modifications include varying the central metal (M), the addition of axial ligands (X) and peripheral (and non-peripheral) substitutions (S). For this study a simplified 5-level theoretical model for the RSA process was used to calculate effective nonlinear optical parameters and has previously been reported [32-36] and discussed in chapter 2.

4.1.1 Excited Sate Dynamics: Background

To discuss the importance of the various parameters that influence reverse saturable absorption in the phthalocyanine system the general 5-level model with approximations suitable for the phthalocyanine system under nanosecond irradiation applied. As mentioned previously, to simplify matters it was assumed that relaxation out of states S_2 and T_2 is very rapid so that the population of these two levels may be neglected.

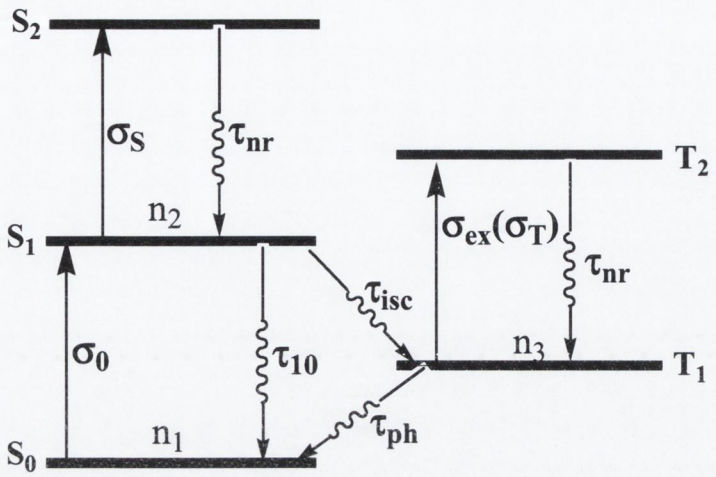

Figure 4.1 Generalized five-level system used in deriving the excited state absorption model used to simulate RSA in the phthalocyanine system. Si represents singlet levels and Ti represents triplet levels. Solid arrows imply an excitation resulting from photon absorption and jagged arrows represent relaxations

Generally for this 5-level system after initial excitation the first excited singlet state S_1 is populated, from here the electrons may be subsequently excited into S_2 within the pulse width of the laser. Once in S_2 they rapidly relax to S_1 again. From S_1 the population may undergo an intersystem crossing to the first excited triplet T_1 with a time constant τ_{isc} and thereafter undergo excitations and relaxations to and from T_2. Thus the population is exchanged cyclically between S_1 and T_1, as the lifetime of T_1 (τ_{ph}) is very long in comparison to τ_{isc}. Furthermore, stimulated emission from S_1 is excluded due to the small fluorescence quantum yield. The system now reduces to the following set of three differential rate equations,

$$\frac{\partial n_1}{\partial t} = -\frac{\sigma_0 I}{h\nu} n_1 + \frac{n_2}{\tau_{10}} + \frac{n_3}{\tau_{ph}} \qquad 4\text{-}1$$

$$\frac{\partial n_2}{\partial t} = \frac{\sigma_0 I}{h\nu} n_1 - \frac{n_2}{\tau_{isc}} - \frac{n_2}{\tau_{10}} \qquad 4\text{-}2$$

$$\frac{\partial n_3}{\partial t} = \frac{n_2}{\tau_{isc}} - \frac{n_3}{\tau_{ph}} \qquad 4\text{-}3$$

where n_1, n_2 and n_3 refer to the populations of S_0, S_1, and T_1. Attenuation of the laser beam is governed by a propagation equation where the absorption coefficient now includes the excited state absorption from S_1 and T_1

$$\frac{\partial I}{\partial z} = -\alpha I = -(\sigma_0 n_1 + \sigma_S n_2 + \sigma_T n_3) I , \qquad 4\text{-}4$$

Under the steady state approximation, which is valid when the pulse width is much longer than any relaxation time, all the time derivatives may be set to zero. This is a valid assumption for nanoseconds pulses as the lifetimes in phthalocyanines are typically of order picoseconds.[32, 33] In this case, the equation can be easily solved analytically and the intensity dependent absorption coefficient becomes:[14]

$$\alpha(I, I_{Sat}, \kappa) = \frac{\alpha_0}{1 + \frac{I}{I_{Sat}}}\left(1 + \kappa \frac{I}{I_{Sat}}\right) \qquad 4\text{-}5$$

by defining $\kappa = \sigma_{ex}/\sigma_0$, and noting that σ_{ex} and σ_0 are the absorption cross-sections of the ground and the excited transitions respectively, and $I_{Sat} = h\nu / (\sigma_0 \tau_{10})$. Thus this effectively reduces the 5-level model to a 3-level model. This model, though simple, reproduces the gross effects of RSA and highlights the crucial role that the excited state absorption plays in the overall absorption coefficient. Within this expression for the nonlinear absorption coefficient one can then state that higher κ values combined with lower F_{Sat} values define more efficient optical limiters. This steady state model approximates to a dynamic model in the limit of temporally long pulse widths, ie. nanosecond irradiation when all other lifetimes in the material are of the order of picoseconds.

4.2 Sample Preparation

The fabrication of the solid-state polymer-phthalocyanine films involves the addition of phthalocyanine molecules to a pre-prepared solution of PMMA dissolved in cyclohexanone. For this investigation, phthalocyanine compounds **1-11** & **20** were added at partial concentrations of $10gl^{-1}$ and $0.5gl^{-1}$ for samples **12-20,** to the PMMA solution. This composite was sonically agitated until a completely dissolved, homogeneous solution was formed. Solid-state film samples of freshly dissolved polymer-phthalocyanine solutions were formed on quartz glass substrates, using multi-layer conventional spin casting. These multi-layer polymer-phthalocyanine films were cast by sequentially spinning prepared composite solution with approximately one hour of baking at 60^0C in a standard oven, between each layer to facilitate the removal residual solvent.

The linear optical properties the composite systems in this study were measured using a Shimadzu UV3100 UV-VIS-NIR spectrometer. In conjunction with the linear optical investigation the morphology of the film surface was investigated using a Zygo White Light Interferometer. This technique allows for detailed three-dimensional rendering by probing the interference pattern created along a selected surface area. Film thickness measurements were made using the same technique. For the optical limiting experiments, the open aperture Z-scan technique[1] was used probing total transmittance through the samples, presented diagrammatically in **Figure 4.2**. The second harmonic, 532nm, of a Q-switched Nd:YAG laser was used with a pulse repetition rate of 10Hz. The beam was spatially filtered to remove the higher order modes and tightly focused with a 9cm focal length lens. The waist radius for all experiments was calculated as ~18-23μm.

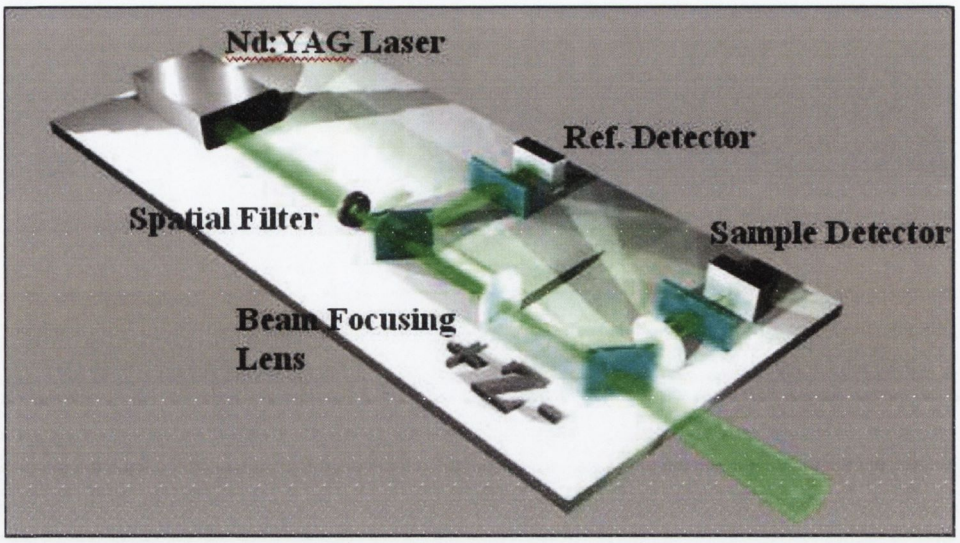

Figure 4.2 Diagram of nanosecond open aperture Z-scan experimental set-up. *Note:* Ref. Detector=Reference detector.

4.3 Surface Imaging & Linear Optical Results

4.3.1 Surface Roughness & Thickness Measurements

A selection of computer rendered surface images of the composite films is displayed in **Figure 4.3(a-c)** labelled (a) $[t\text{Bu}_4\text{PcGa}]_2\text{O}$, (b) $\text{Cu}_2(t\text{Bu}_4\text{PcIn})(t\text{Bu}_4\text{PcGa})\text{S}_2\text{TPP}$ and (c) $(\text{PhS})_4\text{PcZn}$. Two dimensional surface topography measurements and parameters were obtained to probe the average roughness (R_a, defined as the average peak-valley height on a surface) on a nanometre scale for most of the composite films in this study. (The range of films studied for surface roughness are marked with an asterix in **Tables 1-3**) Average roughness values calculated averaged between 10–100 nm for the polymer composites tested with an experimental error of ±1nm. In order to minimise optical light distortion it is imperative to significantly reduce this interfacial roughness, relative to the wavelength of incident light.[18] From this study we can then discount

the influence of surface roughness when discussing the resulting change in transmitted energy occurring at high incident intensities.

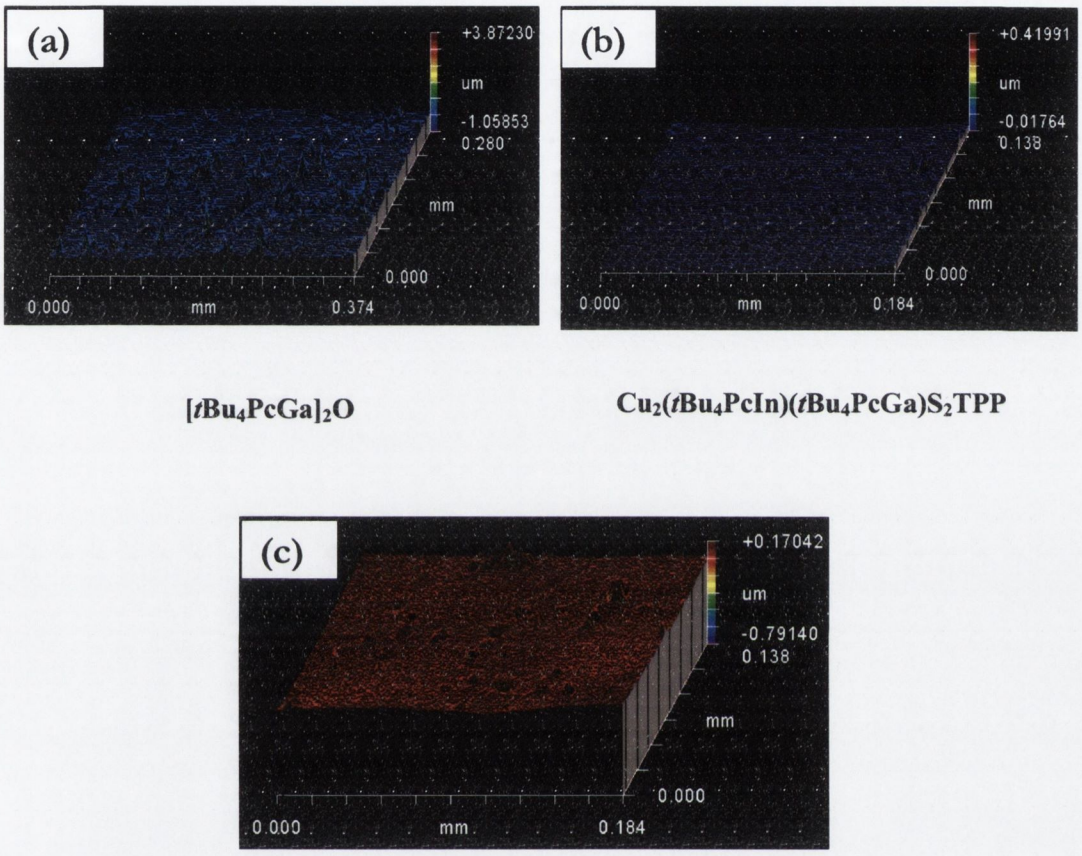

[*t*Bu$_4$PcGa]$_2$O

Cu$_2$(*t*Bu$_4$PcIn)(*t*Bu$_4$PcGa)S$_2$TPP

(PhS)$_4$PcZn

Figure 4.3 Computer rendered interferometry images for a selection of spin cast phthalocyanine-PMMA composite films.

4.3.2 Linear Optical Response

In studying the nonlinear optical response from PMMA-phthalocyanine films, a preliminary investigation into the linear absorption spectra was necessary. For each of the PMMA-phthalocyanine films listed in **Tables 1-3**, the linear absorption coefficient, α_0, is also presented. This value varies between phthalocyanine compound and is sensitive to structural modifications, phthalocyanine-phthalocyanine interactions [37] and host environment. [38] In conjunction with this study, linear spectra were obtained in both solution and solid state for all compounds. The solvents used for the solution-based linear optical experiments are indicated in brackets after each compound in each table. Spectra for single-layer cast PMMA-phthalocyanine composites are presented in **Figure 4.4** along with the complimentary solution spectrum. The Full Width Half Maximum (FWHM) value was calculated for the Q-band region, in solution (dissolved in solvent) and solid-state for each phthalocyanine sample. An overall broadening of the Q-band region was noted between the phthalocyanine in solution and solid-state PMMA-phthalocyanine films, indicative of molecular aggregation. This intrinsic aggregation of phthalocyanine molecules in solution has been reported[39] to reduce the degree of high intensity induced optical limiting. In this thesis the FWHM parameter is employed to indicate the extent of molecular aggregation or phthalocyanine-phthalocyanine interaction in various systems presented. It must also be noted that wavelength shifts in the UV-Visible absorption spectra between solution and solid-state based samples can affect the nonlinear optical response from 532nm laser irradiation.

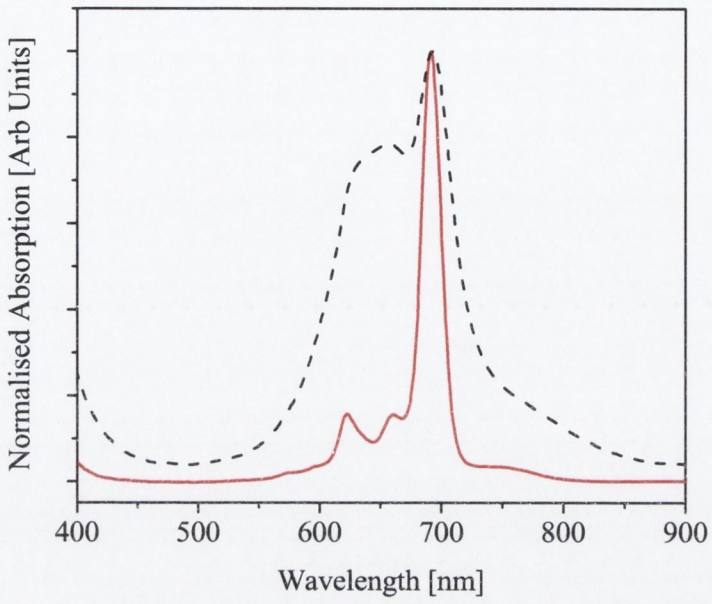

Figure 4.4 Compound $[t\text{Bu}_4\text{PcGa}]_2\text{O}$ in solution (Solid line) and embedded in the host PMMA matrix (Dashed line). Both spectra have been normalized to λ_{max}.

4.4 Nonlinear Optical Results

4.4.1 Introduction

Solution based nonlinear optical (NLO) investigations into chemically modified phthalocyanine compounds have led to a broad understanding of the sensitivity of the resulting properties on a molecular level. [2,5,8,11,19,20,26,58] It can be argued that for future industrially applicable optical limiting (OL) devices, the study of solid-state, transparent, host polymer(phthalocyanine) systems will be essential. Sections **4.4.2**, **4.4.3** and **4.4.4** will discuss the resulting NLO response of PMMA(phthalocyanine) devices as case studies. It must be mentioned at this juncture that this discussion is based on the material response, specific to the OL films prepared. Due to such

additional contributory issues including localized laser induced thermal damage, a comprehensive NLO discussion on a molecular level is not possible. In order to accurately investigate this Z-scan spectra would undertaken with simultaneous linear optical spectra to characterize any material damage. Without the addition of linear spectroscopy, the value of thermal damage quoted would greatly overestimate the effect of this damage on any resulting NLO response. However certain clear trends may be noted which appear to agree with similar solution based NLO studies reported.

4.4.2 Case Study: Overview

The third-order NLO properties with phthalocyanines were first reported in 1987 for the peripherally unsubstituted chlorogallium phthalocyanine (PcGaCl) and fluoroaluminium phthalocyanine (PcAlF).[40] The $\chi^{(3)}$ value for PcGaCl was half that of PcAlF at 1.064 μm. After this, the $\chi^{(3)}$ values of a various phthalocyanines, including PcAlCl, PcInCl and PcTiO, were measured using THG techniques.[41] Comparison of $\chi^{(3)}$ values of phthalocyanines with and without axial ligands[42, 43] indicates that phthalcoyanines with an axial ligand, for example, PcVO, PcTiO, PcAlF, PcGaCl, PcInCl show a large $\chi^{(3)}$ in THG experiments. Axial substitution in Pc complexes has provoked relevant changes on the electronic structure of the molecule by altering the π-electronic distribution due to the dipole moment of the central metal-axial ligand bond.[23, 26, 29, 39, 44-55] The third-order optical nonlinearities in charge-transfer complexes such as PcCu-C_{60} and others have been observed.[56-58] Optical limiting with phthalocyanines was first reported for the chloroaluminum phthalocyanine (PcAlCl)[43] and subsequently many other phthalocyanine compounds have also been investigated as passive optical limiting materials. Perry et al.[8] studied a series of phthalocyanine compounds, proposed a practical optical limiting device structure and fabricated this using tetrasubstituted chloroindium phthalocyanine (tBu$_4$PcInCl). Under nanosecond irradiation this device was able to attenuate laser pulses by factors up to 540. Henari et al.[55] reported the nonlinear optical properties of a series of phthalocyaninatotitanium (IV) oxide with different peripheral groups (R_xPcTiO). The optical limiting properties of a octasubstituted lead phthalocyanine $[C_{12}H_{25}O]_8$PcPb, has also been studied by Qu et al.[59] The

nanosecond optical limiting properties of nickel phthalocyanines,[60] gallium- and indium phthalocyanines and naphthalocyanines[23, 30, 44-47, 49, 51] have been reported. Shirk et al.[26] reported the effects of axial substitution at the central metal atom on the optical limiting performance of indium phthalocyanines. They found that the optical limiting properties of these materials were robust relative to structural changes in the axial position, and consequently the changing of axial substituents from chloro to *p*-trifluoromethylphenyl (*p*-TMP) results in the somewhat enhancement of the optical limiting response. Tian et al.[61] reported the nonlinear properties of non-aggregated zinc and vanadium phthalocyanines, where they found that the zinc phthalocyanine had a larger macroscopic optical nonlinearity than the vanadium phthalocyanine. The optical nonlinearities of $PcYb_2$ were reported by Mendonca et al;[62] of $PcLu_2$, $PcNd_2$, and $PcEu_2$ by Wen et al.[63] and of tin phthalocyanine thin films by Yamashita et al.[64] Previous reports into device modelling[32, 33] suggests that heavy atom phthalocyanine materials in optimized optical-limiter designs that ensure uniform saturation could produce attenuations of 10^4 for devices with 70% linear transmission.

Numerous papers have reviewed various aspects of this topic[5, 10, 11, 27, 65, 66] including investigations into the relationship between the optical limiting response and the chemical structure for both phthalocyanines and related compounds.

The use of guest-host systems, where phthalocyanines assume the role of guest inclusions in an otherwise homogeneous host polymer film is a feasible method towards the application of the phthalocyanine molecule in a solid-state passive optical limiter. All polymer-phthalocyanine composite films tested in this study displayed characteristic reverse saturable absorption curves under high intensity Z-scan experiments. **Figure 4.5** plots the normalized transmission as a function of Z-distance for PMMA([*t*Bu_4PcGa]$_2$O), at various focal intensities. The group of twenty phthalocyanine compounds analysed for this investigation has been sub-divided into three main categories: a discussion on the influence of central metal substitutions (**Compounds 1-8, Table 1, Section 4.4.3**), the effect of the chemical addition of axial substituents (**Compounds 2, 9-13, Table 2, Section 4.4.4**) and that of peripheral substitutions (**Compounds 2, 4, 14-20, Table 3, Section 4.4.5**). In each section the nonlinear optical response of the PMMA-

phthalocyanine films is characterized using known optical limiting parameters, [1, 11] including κ (ratio of excited state to ground state cross sectional areas, σ_{ex}/σ_o), the saturation fluence, F_{sat} and β_{eff}, the effective nonlinear optical coefficient. Ideally, a large κ and β_{eff} are desirable together with a low F_{sat} value, indicative of a fast, efficient and strong NL response to incident irradiation.

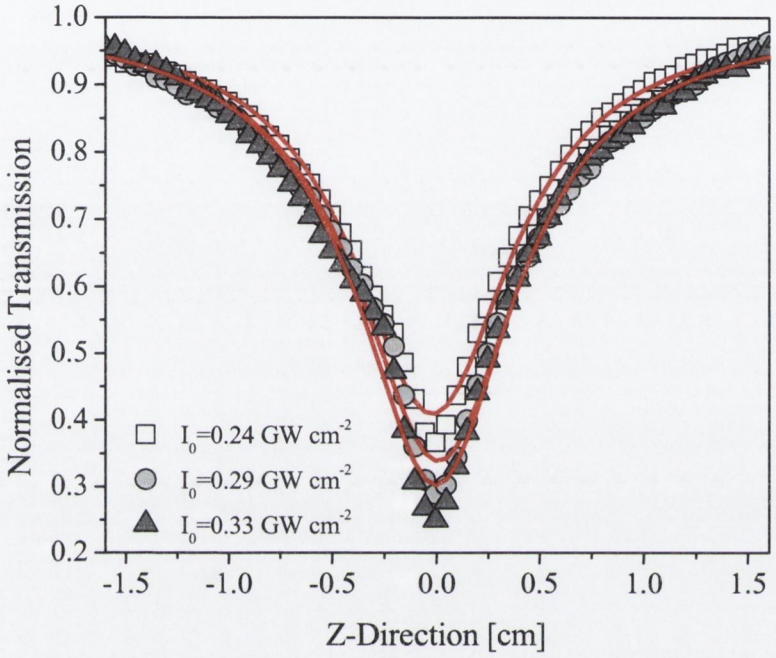

Figure 4.5 Resulting open aperture curves with normalized transmission plotted as a function of sample position, Z for the $[t\text{Bu}_4\text{PcGa}]_2\text{O}$/PMMA film, at different focal intensities.

4.4.3 Case Study I: Central Metal

In this section eight molecules are studied in four groups with each phthalocyanine of structural equivalence, except for central metal substitution. Presented in **Table 1** are four sets of metallophthalocyanines, **1** and **2** comparing In and Ga; the set of **3** and **4** , the set of **5** and **6** and **7** and **8** comparing Ge and Sn, along with the respective linear and nonlinear optical coefficients. Comparing the samples **1** and **2**, the phthalocyanine with In central metal displayed a superior NLO response

possible due to enhanced spin-orbit coupling as a result of heavy metal substitution.[67] The calculated κ value and FWHM ratio for **1** and **2** are similar. However **1** has a factor of 3 lower F_{sat}, when compared to **2**, indicative of the nonlinear absorption processes occurring for relatively lower input energies. The effective nonlinear absorption coefficient, β_{eff}, was calculated as $(5.9 \pm 1.2) \times 10^{-6}$ and $(7.8 \pm 1.6) \times 10^{-6}$ cm W^{-1}, (samples **1** and **2** respectively).

Film **4** with the Sn metal substitution displayed a superior F_{sat}, κ and β_{eff} calculated values, compared to the equivalent Ge substituted composite film **3**. Both solid-state samples exhibited similar Q-band FWHM values but sample **3** displayed over three times larger Q-band FWHM solution-solid state ratio than **4,** indicating noted aggregation upon spin casting and thus can reduce the optical limiting performance.[39, 61]

In **Figure 4.6 (a)-(d),** a plot of normalized transmission against the incident pulse energy density is presented for samples **3, 4, 7, 8**, respectively, along with the solution (Solid line) and solid-state (Dashed line) UV-Visible absorption spectra (inset). Perry et al. [67] reported the values for the triplet quantum yield and the first excited-singlet lifetime where a clear trend was noted for a series of group IIIA and group IVA metallophthalocyanines, Pb, In, Sn, Ga, Ge, Al and Si. Similar heavy metal effects on nonlinear optical response of phthalocyanines have been reported. [68] In contrast to films **3** and **4** an improved NLO response was noted with samples **5** and **7** (GePc) outperforming **6** and **8** (SnPc). For the Ge substituted composite sample **5,** a larger κ value of (9.0 ± 0.4) was calculated compared to (6.7 ± 1.3) for **6**. The difference in values of F_{sat} and β_{eff} were negligible for the two composite films. The polymer-GePc film, **7**, had a lower F_{sat} value of (3.5 ± 0.4) J cm^{-2} when compared to that of **8**. The value for κ was found to be comparable while the value for β_{eff} calculated for **7** was over twice that calculated for **8**. It must be noted that film **8** experienced a larger degree of aggregation in the solid-state form compared to that of film **7,** while **6** also displayed increased Q-band broadening when compared to **5.** The negative effect on the nonlinear optical response due to aggregation in polymer composite films does highlight the important role of further chemical modifications including axial ligand substitutions to inhibit aggregation while retaining the optical limiting properties of the system.

Film	Structure	I_0 [GW cm^{-2}]	α_0 [cm^{-1}]	Q-Band FWHM		β_{eff} [cm W^{-1}]	F_{sat} [J cm^{-2}]	κ σ_{ex}/σ_0
				[nm]	Ratio			
1	*t*Bu$_4$PcInCl* *(T)*	0.4	134.58	115	5.7	$(5.9 \pm 1.2) \times 10^{-6}$	0.5 ± 0.1	4.1 ± 0.1
2	*t*Bu$_4$PcGaCl* *(T)*	0.4	176.5	93	5.2	$(7.8 \pm 1.6) \times 10^{-6}$	1.6 ± 0.1	3.7 ± 0.1
3	$Cl_{16}GePc(O^aR)_2$ *(C)*	0.8	1959.3	130	4.8	$(8.7 \pm 1.7) \times 10^{-6}$	9.9 ± 0.8	5.7 ± 0.3
4	$Cl_{16}SnPc(O^aR)_2$ *(C)*	0.8	1540.2	126	1.4	$(2.9 \pm 0.6) \times 10^{-5}$	5.5 ± 0.8	6.6 ± 0.5
5	$^bR_4GePcCl_2$ *(C)*	0.6	1110.3	53	2.2	$(3.2 \pm 0.6) \times 10^{-5}$	6.6 ± 0.5	9.0 ± 0.4
6	$^bR_4SnPcCl_2$ *(C)*	0.2	1844	94	3.4	$(3.7 \pm 0.8) \times 10^{-5}$	6.1 ± 1.8	6.7 ± 1.3
7	$Cl_{16}GePc(O^cR)_2$ *(THF)*	0.5	2847.6	193	2.3	$(7.0 \pm 1.4) \times 10^{-5}$	3.5 ± 0.4	3.9 ± 0.2
8	$Cl_{16}SnPc(O^cR)_2$ *(THF)*	0.8	4492.6	156	2.9	$(2.7 \pm 0.5) \times 10^{-5}$	10.6 ± 0.7	3.5 ± 0.1

Table 1 Linear and nonlinear optical coefficients for a various central metal substituted phthalocyanine molecules embedded in a PMMA matrix. [a] R = 3,5-Di-tert-butylphenyl, [b] R = p-aldehydphenoxy, , [c] R= -$(C_2H_4O)_3CH_3$. (T) = Toluene, (C) = Chloroform, (THF) = Tetrahydrofuran.

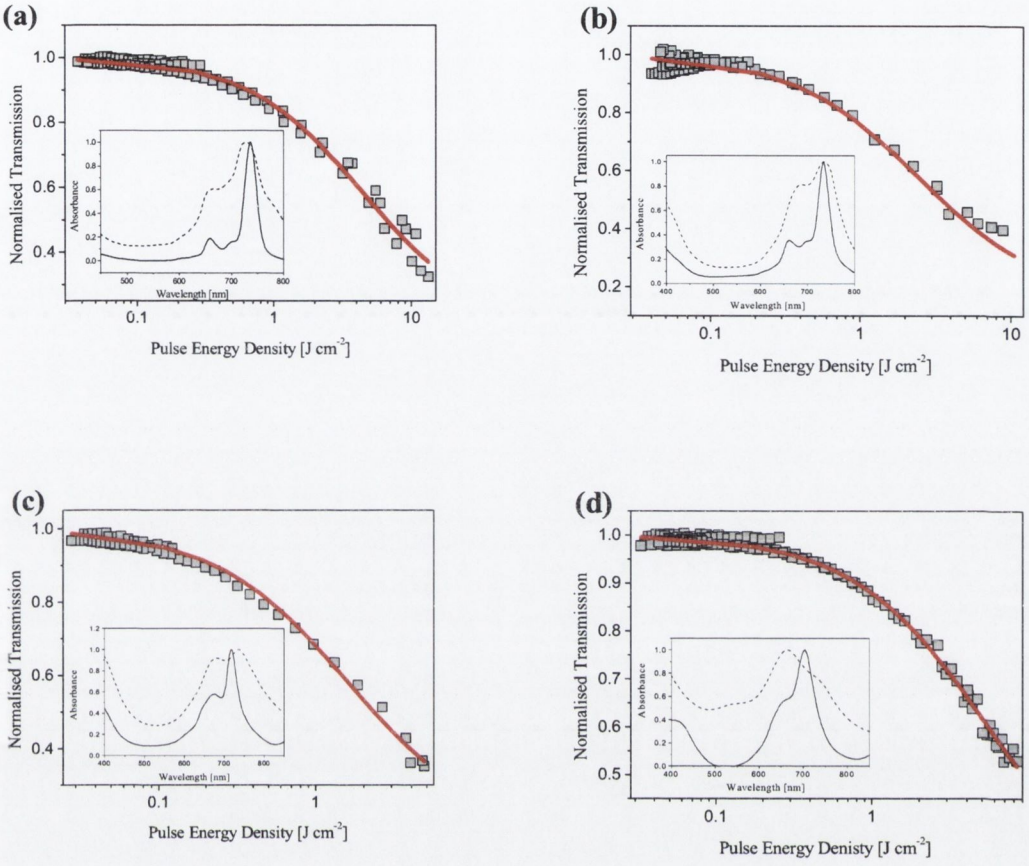

Figure 4.6 (a)-(d) Plot of normalized transmission against the incident pulse energy density for films 3, 4, 7, 8 respectively, along with the solution (Solid line) and solid-state (Dashed line) UV-Visible absorption spectra (inset)

4.4.4 Case Study II: Axial Substitution

The influence of *Metal-to-Ligand* electron transfer can dramatically affect the resulting nonlinear optical properties of phthalocyanine systems. [23, 26, 29, 35, 45, 46, 53, 58] Comparing the PMMA-phthalocyanine samples **2**, **9** and **10**, (presented in **Table 2**) the strongest electron withdrawing nature of the (P-TMP) axial ligand, with the CF_3 bonded to the benzene unit, in **10** resulted in the largest κ value when compared to

(3.7 ± 0.1) for **2** and (5.0 ± 0.1) for **9**. This sample also displayed the largest β_{eff} of the three composite films. The degree of strength of electron withdrawing capabilities of the axial ligand in **10** (largest), **9** and **2** (lowest) resulted in sequentially decreasing κ values from **10** to **2**. Sample **2** had the lowest calculated F_{sat} value, of (1.6 ± 0.1) J cm^{-2}, compared to (2.3 ± 0.1) J cm^{-2} for **9** and (3.1 ± 0.2) J cm^{-2} for **10**. As a low F_{sat} value is desirable for optimal optical limiting response, film **2,** with the direct Ga-Cl axial bond displayed an optimised optical limiting response. The highest F_{sat} value was calculated for **10**, which has the less efficient, Ga-benzene-CF_3, axial ligand. For axial ligand substitution, it appears that κ may be influenced by the strength of electron withdrawing in the axial group, while F_{sat} may be mainly influenced by the efficiency of this electron transfer process.

Film **11** is composed of a commercially available phthalocyanine (*Aldrich Product Code: 393894*) with two separate bulky peripheral substitutes and a vanadium-oxygen axial ligand embedded in the PMMA film. Though it displayed one of the highest κ values, of (10.0±0.2) it also had one of the highest F_{sat} values of (11.5±0.5) J cm^{-2} with a β_{eff} of (6.4 ± 1.3) x10^{-6} cm W^{-1}. The relatively poor electron withdrawing strength of the axial ligand may have played a role in resulting nonlinear optical response but future research will involve the characterisation of VnPc composite systems with various axial ligand substituted electron withdrawing groups.

Other interesting axial ligand structures have been developed and display noted nonlinear optical properties. The dopant in film **12** was originally designed for enhanced charge transfer processes in solar cells. Organic ligand triphenyl phosphines (TPP) are located outside the $Cu_2In_2GaS_7$ central core. This sample displayed a relatively large β_{eff} of (1.5 ± 0.3) x10^{-4} cm W^{-1}, together with a large κ value of (8.7±0.2). This enhanced nonlinear optical response was also noted in the low F_{sat} value of (2.0±0.1) J cm^{-2}. Comparing these values with the results from the other phthalocyanine based composite films in this study, only films **1** and **2** have lower F_{sat} values. Film **12** displayed a far larger κ value when compared to these films. The FWHM of the Q-band region in solution and solid-state was also similar to that of film **1** and **2**. The structure needs further confirmation by X-ray single

crystal analysis, but could be of potential significance incorporated in future optical limiting device design.

Film	Structure	I_0 [GW cm^{-2}]	α_0 [cm^{-1}]	Q-Band FWHM		β_{eff} [cm W^{-1}]	F_{sat} [J cm^{-2}]	κ σ_{ex}/σ_0
				[nm]	Ratio			
2	tBu$_4$PcGaCl* *(T)*	0.4	176.5	93	5.2	$(7.8 \pm 1.6) \times 10^{-6}$	1.6 ± 0.1	3.7 ± 0.1
9	tBu$_4$PcGa(OPhCl)* *(T)*	0.4	96.48	100	1.2	$(4.5 \pm 0.9) \times 10^{-6}$	2.3 ± 0.1	5.0 ± 0.1
10	tBu$_4$PcGa(P-TMP)* *(T)*	0.4	145.7	85	4.5	$(10.1 \pm 2.0) \times 10^{-6}$	3.1 ± 0.2	8.2 ± 0.3
11	tBu$_4$t(Me$_2$N)PcVO* *(T)*	1.1	301	144	2.4	$(6.4 \pm 1.3) \times 10^{-6}$	11.5 ± 0.5	10.0 ± 0.2
12	$Cu_2In_2Ga_2S_7TPP_2^*$ *(THF)*	0.4	135.23	100	5.0	$(1.5 \pm 0.3) \times 10^{-5}$	2.0 ± 0.1	8.7 ± 0.2
13	Cu_2(tBu$_4$PcIn)(tBu$_4$PcGa)$S_2TPP_2^*$ *(T)*	0.5	145.35	100	3.0	$(4.9 \pm 1.0) \times 10^{-6}$	3.2 ± 0.2	4.4 ± 0.1

Table 2 Linear and nonlinear optical coefficients for a various axially substituted phthalocyanine molecules embedded in a PMMA matrix. (T) =Toluene, (THF) = Tetrahydrofuran

4.4.5 Case Study III: Peripheral Substitution

In order to increase solubility and decrease aggregation effects of phthalocyanine molecules in solution, bulky peripheral side-group have been attached to the main phthalocyanine ring. **Table 3** presents the linear and NLO results for various peripheral substituted phthalocyanine-polymer composite systems. Comparing the three peripheral substituted PMMA-$SnPcCl_2$ films (**4**, **14** and **15**), the κ values calculated for each of the composites were (6.7 ± 1.3), (10.4 ± 1.0) and (9.1 ± 0.4) respectively. The highly concentrated, electron withdrawing fluorine side-group out-performed **4** and displayed comparable results as **15**. The F_{sat} values for **4** and **15** were approximately equal, but sample **15** displayed the lowest value of the three, with a value of (3.7 ± 0.3) J cm^{-2}. The electron withdrawing nitrophenoxy substituted PMMA-$SnPcCl_2$ film also exhibited the highest nonlinear absorption coefficient, β_{eff}, of the three samples with a value of (1.5 ± 0.3) x10^{-4} cm W^{-1}. The two bulky peripheral substituents in samples **4** and **15** do minimise aggregation more effectively than the fluorine atoms, which can be noted in a lower Q-Band FWHM ratio of ~3.3 for both samples. Therefore, considering an optical limiting device based on these polymer-SnPc films, **15** exhibited the optimal nonlinear optical properties: minimised aggregation, relatively high κ and β_{eff} together with a low F_{sat}. This response can be related to the double Cl axial ligand bond and the nitrophenoxy peripheral substitute on the SnPc macrocycle. Alternative central metal substitutions may lead to a further increase in the nonlinear optical response.

Zinc phthalocyanines have long been studied for their photophysical properties and optical limiting response [69] [14] and two commercially available compounds were chosen, with a tert-butyl (*Aldrich Product Code: 430994*, film **16**) and a sulphurphenyl peripheral substitute (*Aldrich Product Code: 418234*, film **17**). In this study, samples **16** and **17** have similar calculated values for κ, β_{eff} and F_{sat} but PMMA-$(SPh)_4PcZn$ displayed more prominent Q-band broadening in solid-state. The *tert*-butyl peripheral substituted phthalocyanine was therefore considered for the majority of future phthalocyanine-polymer composite samples prepared.

Included in this section on peripheral substituents is the possibility of extending the π–conjugated phthalocyanine system by the addition of benzene rings to the phthalocyanine macrocycle. This structure forms a naphthalocyanine which in solution, has been reported to exhibit enhanced optical limiting properties at 532nm compared to the phthalocyanine equivalent.[39, 43, 70] Film **2** is an example of a PMMA-phthalocyanine film with the naphthalocyanine counterpart prepared in film **18**. The latter film does display a larger κ values of (4.5 ± 0.1) compared to that of **2,** which has a value calculated at (3.7 ± 0.1). The same is true for **18** when relating the nonlinear absorption coefficient to that of **2**. However when considering the saturation fluence parameter, F_{sat}, the PMMA-phthalocyanine film **2** had a lower value than that of sample **18**. Both samples display relatively similar Q-band FWHM values and solution to solid-state FWHM ratios, indicative of minimised aggregation in the composite film. Both films exhibited individually favourable optical limiting coefficients, highlighting the need to compare the optical limiting quality of a material using multiple nonlinear optical parameters.

The composition of phthalocyanine dopant in film **13** is that of a more complex dimer-type phthalocyanine structure. This sample links the *t*Bu_4PcGa and *t*Bu_4PcIn phthalocyanine molecules axially via a sulphur and copper-TPP central bridge. The resulting nonlinear optical response showed a κ value of (4.4 ± 0.1), F_{sat} value of (3.2 ± 0.2) J cm^{-2} and a β_{eff} value of (4.9±1.0) x10^{-6} cm W^{-1}. Overall this material displayed an inferior nonlinear response when compared to film **1** and **2** individually, due perhaps to the competing electron accepting In and Ga metals and thus the overall resulting charge transfer efficiency. Though the aggregation was lower than film **1** and **2**, there may also be excited singlet-singlet state population transfer between the phthalocyanines which can hinder the efficiency of the triplet state charge transfer.

In **Table 3** the phthalocyanine compound in film **19** contains a μ-oxo bridge, joining two phthalocyanine units and film **20** joins two naphthalocyanine units. The structures of both compounds has been previously investigated in solution for enhance nonlinear optical response.[30, 46, 47, 49, 51] Comparing the two samples embedded in the host PMMA matrix, sample **19** exhibited a higher κ (5.1 ± 0.1), lower F_{sat}, (2.0 ± 0.1) J cm^{-2} but a lower β_{eff} value of (4.8±1.0) x10^{-6} cm W^{-1}. This

sample also displayed only half the Q-band FWHM broadening when compared to **20**. Furthermore the large FWHM in the PMMA-naphthalocyanine film indicates larger intrinsic aggregation in the solution form. The relatively poor nonlinear optical response may be attributed to this molecular interaction.

Number	Structure	I_0 [GW cm^{-2}]	α_0 [cm^{-1}]	Q-Band FWHM [nm]	Ratio	β_{eff} [cm W^{-1}]	F_{sat} [J cm^{-2}]	κ σ_{ex}/σ_0
4	[a]$R_4SnPcCl_2$ *(THF)*	0.2	1844	94	3.4	$(3.7 \pm 0.8) \times 10^{-5}$	6.1 ± 1.8	6.7 ± 1.3
14	$F_{16}SnPcCl_2$ *(THF)*	0.5	2304.9	90	4.7	$(9.9 \pm 2.0) \times 10^{-5}$	6.3 ± 0.9	10.4 ± 1.0
15	[d]$R_4SnPcCl_2$ *(THF)*	0.7	2782.4	75	3.3	$(1.5 \pm 0.3) \times 10^{-4}$	3.7 ± 0.3	9.1 ± 0.4
16	tBu$_4$PcZn* *(T)*	0.4	207.1	36	1.3	$(5.7 \pm 1.1) \times 10^{-6}$	3.1 ± 0.3	3.2 ± 0.1
17	$(SPh)_4PcZn^*$ *(T)*	0.5	207.49	93	4.9	$(5.0 \pm 1.0) \times 10^{-6}$	2.5 ± 0.1	3.4 ± 0.1
2	tBu$_4$PcGaCl* *(T)*	0.4	176.5	93	5.2	$(7.8 \pm 1.6) \times 10^{-6}$	1.6 ± 0.1	3.7 ± 0.1
18	tBu$_4$NcGaCl* *(T)*	1.1	232.09	117	5.9	$(10.3 \pm 2.1) \times 10^{-6}$	2.4 ± 0.1	4.5 ± 0.1
19	$[t\text{Bu}_4\text{PcGa}]_2O^*$ *(T)*	0.3	81.53	104	5.5	$(4.8 \pm 1.0) \times 10^{-6}$	2.0 ± 0.1	5.1 ± 0.1
20	$[t\text{Bu}_4\text{NcGa}]_2O^*$ *(T)*	0.2	311.65	223	1.6	$(9.4 \pm 1.9) \times 10^{-6}$	3.1 ± 0.6	3.9 ± 0.1

Table 3 Linear and nonlinear optical coefficients for a various peripherally substituted phthalocyanine molecules embedded in a PMMA matrix.[a] R = p-aldehydphenoxy, [d] R= p-nitrophenoxy, (T) =Toluene, (THF) = Tetrahydrofuran

Conclusion

Various chemically modified phthalocyanine based structures have been embedded in a host PMMA polymer matrix and investigated for surface topographical features, linear and nonlinear optical response at 532nm. The main aspiration in this study for solid-state based nonlinear optically responsive composite films was the potential inclusion in a working optical limiting device. Phthalocyanines offer a high architectural flexibility in structure, which facilitates the tailoring of their physical, optoelectronic and chemical parameters over a very broad range. The spectral bandwidth over which the excited state absorption occurs along can be altered by molecularly engineering the phthalocyanine macrocycle as outlined and discussed in the case studies. In order to optimize the optical limiting response from phthalocyanine-polymer film, the basic considerations included homogeneity of phthalocyanine dispersion in solid-state form, surface diffusivity, linear spectral bandwidth and minimization of molecular aggregation effects. The combination and inclusion of molecular engineered of phthalocyanine structures in novel optical limiting device concepts would potentially lead to the development of industrially applicable systems.

References

1 M. Sheik-Bahae, A. A. Said, T. H. Wei, D. J. Hagan, and E. W. Vanstryland, *IEEE Journal of Quantum Electronics* 26, (4), 760-769 (1990).

2 W. J. Blau, H. J. Byrne, D. J. Cardin, T. J. Dennis, J. P. Hare, H. W. Kroto, R. Taylor, and D. R. M. Walton, *Physical Review Letters* 67, (11), 1423 (1991).

3 N. Hari Singh, *Applied Organometallic Chemistry* 5, (5), 349-377 (1991).

4 F. Henari, J. Callaghan, H. Stiel, W. Blau, and D. J. Cardin, *Chemical Physics Letters* 199, (1-2), 144-148 (1992).

5 H. S. Nalwa, *Advanced Materials* 5, (5), 341-358 (1993).

6 J. S. Shirk, R. G. S. Pong, F. J. Bartoli, and A. W. Snow, *Applied Physics Letters* 63, (14), 1880-1882 (1993).

7 J. Zyss, *Nonlinear Optics: Materials, Physics, and Devices*. Academic Press: Boston, MA, 1993.

8 J. W. Perry, K. Mansour, I. Y. S. Lee, X. L. Wu, P. V. Bedworth, C. T. Chen, D. Ng, S. R. Marder, P. Miles, T. Wada, M. Tian, and H. Sasabe, *Science* 273, 1533-1536 (1996).

9 H. Nalwa, and S. Miyata, *Nonlinear optics of molecules and polymers*. CRC Press: Boca Raton, FL, 1997.

10 G. de la Torre, P. Vazquez, F. Agullo-Lopez, and T. Torres, *Journal of Materials Chemistry* 8, (8), 1671-1683 (1998).

11 S. M. O'Flaherty, S. V. Hold, M. J. Cook, T. Torres, Y. Chen, M. Hanack, and W. J. Blau, *Advanced Materials* 15, (1), 1-14 (2003).

12 D. Chemla, and J. Zyss, *Nonlinear optical properties of organic molecules and crystals*. Academic Press Vol.2: Orlando, FL, 1987.

13 V. Georgakilas, D. M. Guldi, R. Signorini, R. Bozio, and M. Prato, *J. Am. Chem. Soc.* 125, (47), 14268-14269 (2003).

14 M. Meneghetti, F. Fantinel, and R. Bozio, *Synthetic Metals* 137, (1-3), 1495-1496 (2003).

15 E. Collini, C. Ferrante, R. Bozio, A. Lodi, and G. Ponterini, *Journal of Materials Chemistry* 16, (16), 1573-1578 (2006).

16 M. Meneghetti, R. Signorini, M. Zerbetto, R. Bozio, M. Maggini, G. Scorrano, M. Prato, G. Brusatin, E. Menegazzo, and M. Guglielmi, *Synthetic Metals* 86, (1-3), 2353-2354 (1997).

17 R. Bozio, M. Meneghetti, D. Pedron, and C. Pecile, *Synthetic Metals* 27, (3-4), B109-B114 (1988).

18 C. F. Bohren, and D. R. Huffman, *Absorption and Scattering of Light by Small Particles*. Wiley-Interscience: 1983; p 1-11.

19 L. W. Tutt, and T. F. Boggess, *Progress in Quantum Electronics* 17, (4), 299-338 (1993).

20 F. Z. Henari, *Journal of Optics a-Pure and Applied Optics* 3, (3), 188-190 (2001).

21 S. Wang, W. Huang, R. Liang, Q. Gong, H. Li, H. Chen, and D. Qiang, *J. Phys. Chem. B* 105, (44), 10784-10787 (2001).

22 H. S. Nalwa, and J. S. Shirk, *Phthalocyanines. Properties and Applications*. Publishers (LSK) Ltd: Cambridge, U.K, 1996; Vol. 4, p 79.
23 J. S. Shirk, R. G. S. Pong, S. R. Flom, H. Heckmann, and M. Hanack, *Journal of Physical Chemistry A* 104, (7), 1438-1449 (2000).
24 N. B. Mckeown, *Phthalocyanine Materials: Synthesis, Structure and Function*. Cambridge University Press: Cambridge, 1998.
25 G. de la Torre, C. G. Claessens, and T. Torres, *European Journal of Organic Chemistry*, (16), 2821-2830 (2000).
26 J. S. Shirk, R. G. S. Pong, S. R. Flom, H. Heckmann, and M. Hanack, *Journal of Physical Chemistry A* 104, 1438 (2000).
27 C. G. Claessens, W. J. Blau, M. Cook, M. Hanack, R. J. M. Nolte, T. Torres, and D. Wohrle, *Monatshefte Fur Chemie* 132, (1), 3-11 (2001).
28 M. Hanack, *Abstracts of Papers of the American Chemical Society* 222, U242-U242 (2001).
29 Y. Chen, L. R. Subramanian, M. Fujitsuka, O. Ito, S. O'Flaherty, W. J. Blau, T. Schneider, D. Dini, and M. Hanack, *Chemistry-a European Journal* 8, (18), 4248-4254 (2002).
30 Y. Chen, S. O´Flaherty, M.Fujitsuka, M. Hanack, L.R. Subramanian, O. Ito, and W. J. Blau, *Chem.Mater* 14, 5163-5168 (2002).
31 D. Dini, and M. Hanack, *Journal of Porphyrins and Phthalocyanines* 8, (7), 915-933 (2004).
32 P. Miles, *Applied Optics* 38, (3), 566-570 (1999).
33 P. A. Miles, *Applied Optics* 33, (30), 6965-6979 (1994).
34 S. M. O'Flaherty, J. J. Doyle, and W. J. Blau, *Journal of Physical Chemistry B* 108, (45), 17313-17319 (2004).
35 S. M. O'Flaherty, S. V. Hold, M. J. Cook, T. Torres, Y. Chen, M. Hanack, and W. J. Blau, *Advanced Materials* 15, (1), 19-+ (2003).
36 T. J. Xia, D. J. Hagan, A. Dogariu, A. A. Said, and E. W. VanStryland, *Applied Optics* 36, (18), 4110-4122 (1997).
37 A. R. Monahan, J. A. Brado, and A. F. DeLuca, *Journal of Physical Chemistry* 76, (3), 446 - 449 (1972).
38 R. M. Christie, *Dyes and Pigments* 27, (1), 35-43 (1995).
39 M. Hanack, T. Schneider, M. Barthel, J. S. Shirk, S. R. Flom, and R. G. S. Pong, *Coordination Chemistry Reviews* 219-221, 235-258 (2001).
40 Z. Z. Ho, C. Y. Ju, and W. M. Hetherington, *Journal of Applied Physics* 62, (2), 716-718 (1987).
41 H. Matsuda, S. Okada, A. Masaki, and H. Nakanishi, *Proc. SPIE Vol. 1560, Nonlinear Optical Properties of Organic Materials IV, Kenneth D. Singer; Ed.*, 75-83 (1991).
42 H. S. Nalwa, and J. S. Shirk, *Phthalocyanines: Properties and Applications* John Wiley&Sons: New York, 1996; Vol. 4, p 83.
43 D. R. Coulter, V. M. Miskowski, J. W. Perry, T. H. Wei, E. W. V. Stryland, and D. J. Hagan, *SPIE Proc.* 1105, 42 (1989).
44 Y. Chen, M. Barthel, Michael Seiler, L. R. Subramanian, H. Bertagnolli, and M. Hanack, *Angewandte Chemie-International Edition* 41, (17), 3239-3242 (2002).
45 Y. Chen, S. M. O'Flaherty, M. Hanack, and W. J. Blau, *Journal of Materials Chemistry* 13, (10), 2405-2408 (2003).

46 Y. Chen, S. O'Flaherty, M. Fujitsuka, M. Hanack, L. R. Subramanian, O. Ito, and W. J. Blau, *Chemistry of Materials* 14, (12), 5163-5168 (2002).
47 Y. Chen, M. Hanack, Y. Araki, and O. Ito, *Chemical Society Reviews* 34, (6), 517-529 (2005).
48 D. Dini, M. Hanack, H. J. Egelhaaf, J. C. Sancho-Garcia, and J. Cornil, *Journal of Physical Chemistry B* 109, (12), 5425-5432 (2005).
49 Y. Chen, Y. Araki, M. Fujitsuka, M. Hanack, O. Ito, S. M. O'Flaherty, and W. J. Blau, *Solid State Communications* 131, (12), 773-778 (2004).
50 Y. Chen, D. Dini, M. Hanack, M. Fujitsuka, and O. Ito, *Chemical Communications*, (3), 340-341 (2004).
51 Y. Chen, M. Fujitsuka, S. M. O'Flaherty, M. Hanack, O. Ito, and W. J. Blau, *Advanced Materials* 15, (11), 899-+ (2003).
52 M. Barthel, D. Dini, S. Vagin, and M. Hanack, *European Journal of Organic Chemistry*, (22), 3756-3762 (2002).
53 M. Barthel, and M. Hanack, *Journal of Porphyrins and Phthalocyanines* 4, (7), 635-638 (2000).
54 D. Schlettwein, H. Tada, and S. Mashiko, *Thin Solid Films* 331, (1-2), 117-130 (1998).
55 F. Henari, A. Davey, W. Blau, P. Haisch, and M. Hanack, *Journal of Porphyrins and Phthalocyanines* 3, (5), 331-338 (1999).
56 W. Huang, S. Wang, R. Liang, Q. Gong, W. Qiu, Y. Liu, and D. Zhu, *Chemical Physics Letters* 324, (5-6), 354-358 (2000).
57 T. H. Tran-Thi, T. Fournier, A. Y. Sharonov, N. Tkachenko, H. Lemmetyinen, P. Grenier, K. D. Truong, and D. Houde, *Thin Solid Films* 273, (1-2), 8-13 (1996).
58 J. J. Doyle, B. Ballesteros, G. de la Torre, D. A. McGovern, J. M. Kelly, T. Torres, and W. J. Blau, *Chemical Physics Letters* 428, (4-6), 307-311 (2006).
59 S. Qu, Y. Chen, Y. Wang, Y. Song, S. Liu, X. Zhao, and D. Wang, *Materials Letters* 51, (6), 534-538 (2001).
60 Y. Chen, Y. L. Song, S. L. Qu, and D. Y. Wang, *Optics Materials* 18, 219 (2001).
61 M. Tian, S. Yanagi, K. Sasaki, T. Wada, and H. Sasabe, *J. Opt. Soc. Am. B* 15, 846 (1998).
62 C. R. Mendonca, L. Gaffo, L. Misoguti, W. C. Moreira, O. N. Oliveira Jr, and S. C. Zilio, *Chemical Physics Letters* 323, (3-4), 300-304 (2000).
63 T. C. Wen, and I. D. Lian, *Synthetic Metals* 83, (2), 111-116 (1996).
64 M. Yamashita, F. Inui, K. Irokawa, A. Morinaga, T. Tako, A. Mito, and H. Moriwaki, *Applied Surface Science* 130-132, 883-888 (1998).
65 R. C. Hollins, *Current Opinion in Solid State & Materials Science* 4, (2), 189-196 (1999).
66 G. de la Torre, P. Vaquez, F. Agullo-Lopez, and T. Torres, *Chemical Reviews* 104, (9), 3723-3750 (2004).
67 J. W. Perry, K. Mansour, S. R. Marder, K. J. Perry, D. J. Alvarez, and I. Choong, *Optics Letters* 19, (9), 625-627 (1994).
68 C. Yu, S. Yinglin, Q. Shiliang, and W. Duoyuan, *Optical Materials* 18, (2), 219-223 (2001).
69 M. Calvete, G. Y. Yang, and M. Hanack, *Synthetic Metals* 141, (3), 231-243 (2004).

70 H. S. Nalwa, M. Hanack, G. Pawlowski, and M. K. Engel, *Chemical Physics* 245, (1-3), 17-26 (1999).

CHAPTER 5

NONLINEAR OPTICAL RESPONSE FROM $MO_6S_{4.5}I_{4.5}$ NANOWIRES & PHTHALOCYANINE NANOPARTICLES

5.1 Introduction

The attenuation of high intensity laser irradiation for optical sensor protection can be achieved through several nonlinear processes. In two papers published in 1994[1] and 1999[2] Miles et al. outlined the most plausible geometeries to encorporate optically active materials for nonlinear dissipation of light. He suggested that potential optical limiting device structures, such as *tandem limiters*, can theoretically achieve very large excited state absorption of light, through the design of a sequential array of optical limiting elements. Thus pure nonlinear optical (NLO) absorbers such as C_{60} fullerenes,[3-7] prophyrins[7, 8] and phthalocyanines[7, 9-14] can be incorporated into device architectures to enhance the nonlinear extinction of light. Through continued progress in nanomaterial fabrication, nonlinear scattering responses from particular nanostructured systems (nanotubes, nanowires, nanoparticles etc.) can potentially be harnessed for incorporation into optical limiting devices. **Chapter 4** presented the NLO investigation into PMMA(phthalocyanine) films for potential incorporation in optical limiting devices. Detrimental effects, such as phthalocyanine dimerization were highlighted which results in less efficient NLO responses. As an alternative approach to developing optical limiting (OL) devices, dominant nonlinear scattering systems will be presented in this chapter, including $Mo_6S_{4.5}I_{4.5}$ nanowires, phthalocyanine nanoparticles, and carbon nanotubes. This scattering response can contribute greatly to, and dominate, the overall nonlinear extinction (NLE) process.

Numerous groups continue to examine and review the nonlinear optical response from novel nanostructured materials with a view to understanding the nonlinear extinction of light and thus optimising the optical limiting capabilities. [7, 15-19] Tutt et al.[20] reviewed the OL mechanisms for a variety of materials including nonlinear absorbing and scattering centres. Carbon Black Suspensions, organometallics, fullerenes and semiconductor materials are reviewed. They outlined the processes involved in nonlinear scattering- Initially, at a certain incident intensity threshold, the nonlinear response is due mainly to the

development of vapour-liquid interfacial scattering (refractive index mismatch). As the laser irradiation is increased, thermally induced bubbling effects dominate. Finally *microplasma* formation occurs, forming larger scattering centres. They also discussed in detail the various power/fluence thresholds required for the realization of a working optical limiting device. Vivien et al. [21, 22] discussed in detail the process of optical limiting in Single-Walled Nanotubes (SWNTs) by means of Z-scan and pump-probe time-resolved measurements, in both water and chloroform. Similar to Tutt et al., they suggested the dominant nonlinear optical process to be fluence dependent for this molecular system. Firstly, at low input fluence they note fast probe perturbations which occur too late to induce any optical limiting response for the 5ns width pulse specific to their experimental set-up. This behaviour is seen as characteristic of vapour bubble formation due to heat transfer from the tube to surrounding solvent/surfactant. Secondly, at the optical limiting threshold, they suggest that actual sublimation of the nanotubes, or microplasma development forms *microbubbles* which in-turn induces a large nonlinear optical response. As one increases the input fluence, the formation and collapsing of *cavitation macrobubbles* (created through the coalescence of laser-induced microbubbles) leads to a larger nonlinear scattering response. They discuss the phase transition of the emission from nanotubes through these three fluence regimes.[21-24] Riggs et al.[25] reported a study into the OL properties of suspended and solubilised SWNTs and MWNTs at 532nm. They suggested that NL scattering is responsible for the NLO responses suspended-nanotube systems and nonlinear absorption occurs for the solubilized nanotube systems. Ispasiou et al.[26] reported on metal-dendrimer nanocomposite materials, with a large nonlinear optical response noted in Ag-dendrimer nanocomposites, comparing favourably to that reported for SWNT suspensions.[27] They suggested the main nonlinear optical mechanism to be intensity dependent nonlinear scattering due to bubble formation. O'Flaherty et al.[28, 29] reported NLO response for Multi-Walled Nanotubes, MWNT (poly(9,9-di-*n*octylfluorenyl-2,7'-diyl), PFO) composites at 532nm, probing the linear, nonlinear optical response for a series of nanotube concentrations. They also investigated the angular scattered signals, showing both Rayleigh and Mie scattering polar plot profiles for MWNT-polymer composites. Crucially this nonlinear optical

investigation of MWNT-polymer composite systems study was the first where the nanotube concentration was known. A similar investigation was undertaken by the same group for MWNT (poly(para-phenylenevinylene-co-2,5-dioctyloxy-metaphenylenevinylene, PmPV) composite materials at 532nm, reporting a Mie scattering profile for the scattered signal. By the degenerate four wave mixing experiment at 1064nm, they reported an excited state electronic contribution to the nonlinear response.[28, 30]

This chapter will discuss the linear and nonlinear optical properties of two nanomaterial systems, namely $Mo_6S_{4.5}I_{4.5}$ nanowire and phthalocyanine nanoparticle dispersions. **Section 5.2.3.1** will outline both the TEM and AFM analyses undertaken for various $Mo_6S_{4.5}I_{4.5}$ nanowire concentrations. In **Section 5.2**, the nonlinear extinction of laser irradiation from stable $Mo_6S_{4.5}I_{4.5}$ nanowire dispersion in iospropanol (IPA) is investigated. Nanowire diameter and incident laser wavelength dependencies are discussed. **Section 5.3** explores the dispersion of two commercially available zinc phthalocyanines fabricated in nanoparticle form and the resulting nonlinear optical response probed at 532nm. All NLE experiments described in this study were performed with 6-ns pulses from a *Q*-switched Nd:YAG laser. The beam was spatially filtered to remove higher-order modes and tightly focused to a 20-25μm spot for all experiments. The laser was operated at both first and second harmonics, (1064nm and 532 nm respectively), with a pulse repetition rate of 10 Hz. All $Mo_6S_{4.5}I_{4.5}$ nanowire and phthalocyanine nanoparticle dispersions were tested in 1cm quartz cuvettes. For all nonlinear extinction (NLE) experiments simultaneous open aperture Z-scan and intensity dependent scattering experiments, arranged at 45^0 to the Z-direction were performed as shown in **Figure 5.1.**

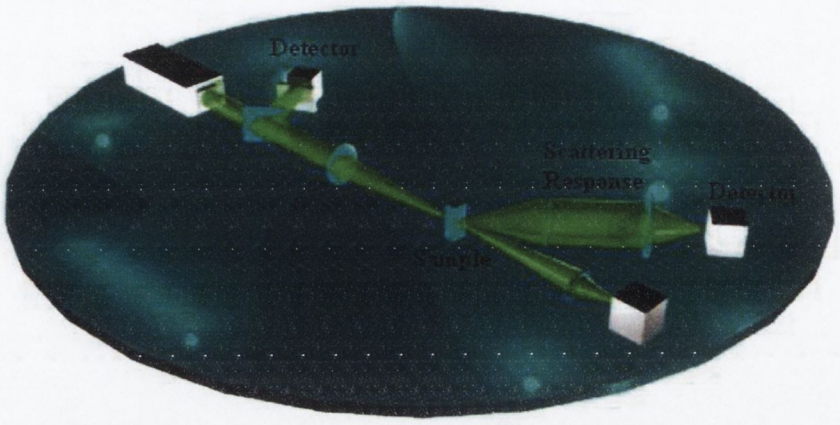

Figure 5.1 Nanosecond Z-scan experimental arrangement, with complementary intensity dependent scattering experiment, using a focusing lens set-up at 45^0 to the direct incident beam.

5.2 $Mo_6S_{4.5}I_{4.5}$ Nanowires

5.2.1 Introduction

The facile manipulation and ability to chemically tailor the material properties to suit industrial requirements has led to a huge and growing interest in inorganic nanotubes, nanoparticles and nanowires. The straight-forward synthesis, [31] easy dispersability in common organic solvents [32, 33] and uniformity in terms of both diameter and electronic behaviour makes $Mo_6S_{9-x}I_x$ nanowires one of the most interesting mono-dimensional materials available at present. In this study we report the first NLE results for $Mo_6S_{4.5}I_{4.5}$ nanowires, probed at 532 and 1064nm using the Z-scan technique. [34] We also investigate the nonlinear scattering contribution to the extinction from $Mo_6S_{4.5}I_{4.5}$ nanowires dissolved in isopropanol (IPA) compared to that of MWNT(PmPV) dispersed in toluene. Through intensity dependent scattering experiments we report a direct correlation between the observed optical extinction and the scattered intensity.[35]

5.2.2 Sample Preparation

5.2.2.1 $Mo_6S_{4.5}I_{4.5}$ Nanowire Dispersions

$Mo_6S_{4.5}I_{4.5}$ nanowires were fabricated by direct synthesis from elemental material that had been mixed in the desired stoichiometries. This resulted in a powder composed of bundles of individual nanowires, each nanowire having a diameter of 0.94 nm. [31] This powder was then washed in acetone several times to eliminate any excess iodine remaining from the synthetic step. Once the iodine had been removed, the $Mo_6S_{4.5}I_{4.5}$ powder was purified as described previously [32, 33]. Dispersions were then prepared by mixing the purified nanowire material in isopropanol at different concentrations (in the range 0.1 - 0.0125 g/l). These mixtures were sonicated for 2 minutes using a high power sonic tip (120W, 60kHz) followed by gentle agitation using a low power ultrasonic bath for 2 hours to ensure a uniform dispersion. [36] For comparison purposes, a dispersion of MWNT(PmPV) composite was prepared as previously reported. [29] Transmission Electron Microscopy (TEM) measurements were made with a Hitachi H-7000 and "holey" carbon grids. In preparation for Atomic Force Microscopy (AFM) studies (using a Nanoscope III) a small volume from each nanowire dispersion was deposited on highly ordered pyrolytic graphite (HOPG) under ambient conditions.

5.2.2.2 Determination of Diameter from AFM Studies

In Atomic Force Microscopy (AFM) a three dimensional image of the surface of a sample is constructed by scanning a tip across its surface. This tip is fixed to a cantilever, whose motion is monitored and recorded during a scan. An AFM is capable of imaging features as small as a carbon atom (~0.25 nm) and as large as the cross section of a human hair (~80 μm).

There are three different modes in which the AFM can be operated. In "contact mode" the tip scans the sample in contact with the surface. The "non contact" mode is used when a sample could be changed or destroyed by tip contact. The tip is 1 to

1.5 nm above the sample and Van der Waals forces between surface and tip are detected. The "tapping mode" technique allows high resolution imaging of a sample that can be easily damaged or is loosely held to the substrate. The cantilever oscillates with a high amplitude (typically greater than 20 nm) when the tip is not in contact with the surface. The oscillating tip is then moved toward the surface until it begins to lightly touch, or tap the surface. As the oscillating cantilever begins to contact the surface, the cantilever oscillation is damped due to energy loss caused by the tip contacting the surface. The reduction in oscillation amplitude is used to identify and measure surface features. A constant force is maintained by measuring the force with a "light lever" sensor. In the light lever method, light is reflected from the back side of the cantilever into a photo detector. A feedback loop is used to control the position of the tip with respect to the surface while scanning.

Images obtained with AFM are always a convolution of the tip geometry and the shape of the features being imaged. If the tip size is much smaller than the features of the images being measured the tip-generated artifacts will be minimal. Therefore, the dimensional image of the sample will be accurate. Avoiding artifacts from probes is achieved by using the optimal tip for the application. For example, if the measured feature is in the 100 nm range, a tip as large as 10 nm in diameter will be adequate for getting good images with almost no artifacts. If the feature is smaller than 100 nm artifacts are more likely to appear in the image. Common artifacts are the appearance of objects being either too large or too small, depending whether you look at particles on a surface or holes in the surface. One of the drawbacks of remaining in contact with the sample is that there exist large lateral forces on the sample as the drip is "dragged" over the specimen. In this thesis work all diameter measurements based on AFM images were performed by considering the height of the considered object and not its width; this has been done to avoid affecting our measurements with tip convolution artifacts. These are in fact one of the most important error source in AFM and arises when the radius of curvature of the tip is comparable with, or greater than, the size of the imaged feature.

5.2.2.3 MWNT(PmPV) Composite System

The MWNT(PmPV) composites were prepared as follows. A 20g l^{-1} solution of PmPV in spectroscopic grade toluene was prepared. To this, a mass of MWNT soot equal to half the total mass of the PmPV in solution was added. This was ultrasonically agitated with a high power sonic tip over 40 seconds to accelerate the dispersion of the soot in the solution. This also facilitates the interaction process between polymer and nanotubes. The sample was then transferred to a low-power sonic bath, where it was gently agitated for a number of hours. The solution was then left to stand undisturbed for a number of days. This allows the graphitic particles to fall out of the solution, [37] leaving a PmPV coated MWNT suspension. This purified nanotube-polymer composite solution was then separated from the sediment by decantation. The composite was blended with a known amount of pure PmPV solution, and was then diluted down to a specific concentration for these experiments. Previously published work on this MWNT-composite preparation[28, 38] included Thermo-Gravimetric Analysis (TGA) to calculate the percentage mass of MWNT's in the final composite sample. In this technique the sample is heated in air and the decrease in sample mass is monitored as it is oxidized.

5.2.3 Results & Discussion

5.2.3.1 Microscopy Analysis

Nanowire information concerning bundle size was determined by both AFM and TEM analysis on the range of concentrations. Representative TEM images for $Mo_6S_{4.5}I_{4.5}$ nanowires at concentrations of 0.1, 0.05, 0.025 and 0.0125 g/l are shown respectively in **Figures 5.2(a)-(d)**. In addition, for each of the four nanowire concentrations prepared, AFM measurements were carried out. From the AFM images, the diameters of a large number of nanowire bundles were calculated. The average bundle diameter tended to decrease with concentration as shown in **Figure 5.3**. This *debundling* effect is in agreement with previous observations reported for

both single wall carbon nanotubes[39] and MoSI nanowires.[33] Lengths do not appear to change within error for the various concentrations investigated (and sonication regimes). An average length of (3.8 ± 1.7) μm was estimated from TEM data.

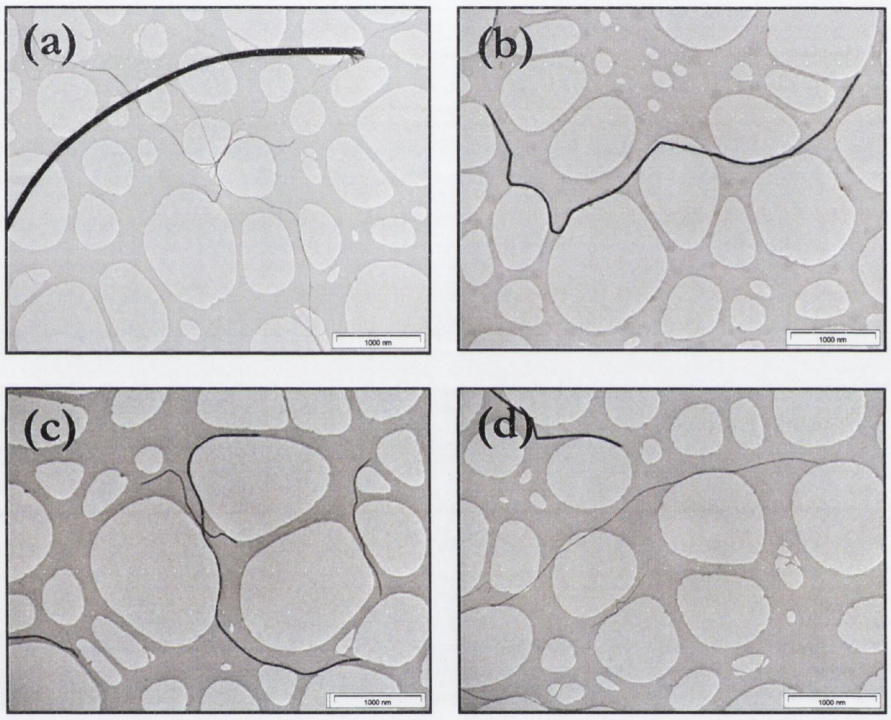

Figure 5.2 TEM images of a series of $Mo_6S_{4.5}I_{4.5}$ nanowire in IPA. Concentrations vary from 0.1g/l (a), 0.05g/l (b), 0.025g/l (c), 0.0125g/l (d). The scale bar for each image represents 1μm.

5.2.3.2 Linear Optical Investigation

Absorption coefficients, ε, as defined by the Lambert Beer law, $\ln(I/I_0)=-\varepsilon Cl$ were measured at 532nm and 1064nm for each sample. In this equation I/I_0 defines the ratio of transmitted to incident laser light, C is the molar concentration and l is the sample thickness. The ε value measured for $Mo_6S_{4.5}I_{4.5}$ nanowires in IPA (532nm) at 0.1g/l was 1.1 $lg^{-1}cm^{-1}$, 1.8 $lg^{-1}cm^{-1}$ for 0.05g/l and 1.6 $lg^{-1}cm^{-1}$ for 0.025g/l. The linear absorption coefficient for the 0.0125g/l nanowire dispersion at 532nm was undetectable using our setup as the linear transmission at such a low concentration was close to 100%. At 1064nm the values calculated for ε were 1.3 $lg^{-1}cm^{-1}$, for the 0.1g/l nanowire dispersion and 2.4 $lg^{-1}cm^{-1}$ for the 0.05g/l sample. The two lower concentrations (0.025g/l and 0.0125g/l) did not exhibit a NLE response at 1064nm and consequentially the optical data from these samples have been omitted in the interest of brevity.

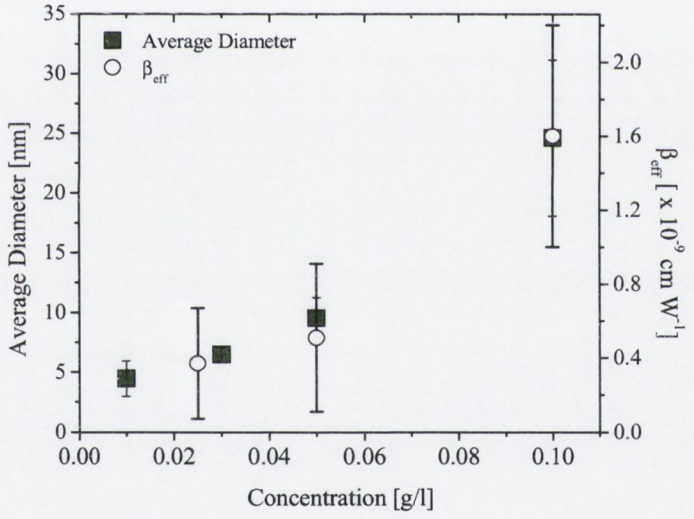

Figure 5.3 This plot is presented as the mean nanowire diameter (measured from at least 50 nanowire or nanowire bundles per sample), as a function of concentration. (*Filled squares*) Also plotted is the effective nonlinear absorption coefficient, β_{eff}, as a function of nanowire concentration. (*Circles*)

5.2.3.3 Nonlinear Optical Investigation

In order to probe the resulting NLE response at 532 and 1064nm, for a variety of $Mo_6S_{4.5}I_{4.5}$ nanowires concentrations, the open-aperture of the Z-scan technique was employed. **Figure 5.4** plots the normalized transmission as a function of laser energy density for the four $Mo_6S_{4.5}I_{4.5}$ nanowire concentrations in solution, at 532nm. All four curves displayed a characteristic NLE profile, where above a certain incident energy threshold, the degree of transmitted light detected is greatly reduced, due to the intensity dependent nonlinear response of the material to incident irradiation. To quantify the magnitude of the optical dissipation we estimate the NLE coefficient, β_{eff}, from theoretical fitting of the Z-Scan spectra. [34] **Table 4** presents the calculated values for α_o and β_{eff} at specific focal intensities for four concentrations at 532nm and two concentrations at 1064nm. The value for β_{eff} measured for $Mo_6S_{4.5}I_{4.5}$ nanowires was $(1.6 \pm 0.6) \times 10^{-9}$ cm W^{-1} for 0.1g/l, $(5.1 \pm 0.4) \times 10^{-10}$ cm W^{-1} for 0.05g/l and $(3.7. \pm 0.3) \times 10^{-10}$ cm W^{-1} for 0.025g/l. At concentrations of 0.1g/l and 0.05g/l, studied at 1064nm, β_{eff} values of $(1.1 \pm 0.3) \times 10^{-10}$ and $(1.2 \pm 0.2) \times 10^{-10}$ cm W^{-1} were measured for the nonlinear absorption coefficient respectively. At the lower concentrations no NLE response was observed under 1064nm irradiation.

Table 4 Nonlinear optical coefficients for $Mo_6S_{4.5}I_{4.5}$ nanowires at various concentrations, at 532nm and 1064nm, including focal intensity (I_0), linear absorption coefficient (α_0) and effective nonlinear absorption coefficient (β_{eff}).

Wavelength [λ]	Concentration [g/l]	I_0 [GW cm^{-2}]	α_0 [cm^{-1}]	β_{eff} [cm W^{-1}]
532	0.1	1.0	0.11	$(1.6 \pm 0.6) \times 10^{-9}$
	0.05	1.0	0.09	$(5.1 \pm 0.4) \times 10^{-10}$
	0.025	0.9	0.04	$(3.7 \pm 0.3) \times 10^{-10}$
1064	0.1	1.6	0.13	$(1.1 \pm 0.3) \times 10^{-10}$
	0.05	1.6	0.12	$(1.2 \pm 0.2) \times 10^{-10}$

Further analysis revealed a $Mo_6S_{4.5}I_{4.5}$ nanowire diameter dependent NLE of incident irradiation. In **Figure 5.4** normalized transmission is presented as a function of energy density (Jcm^{-2}) for the four nanowire dispersions at different concentrations. It can be noted from this plot that the NLE response of the $Mo_6S_{4.5}I_{4.5}$ nanowires at 532nm falls into one of two distinct regimes. The weaker NLE responses are from the two lower concentrations of 0.025g/l and 0.0125g/l. From AFM imaging studies, this corresponds to an average nanowires bundle diameter of <6nm.

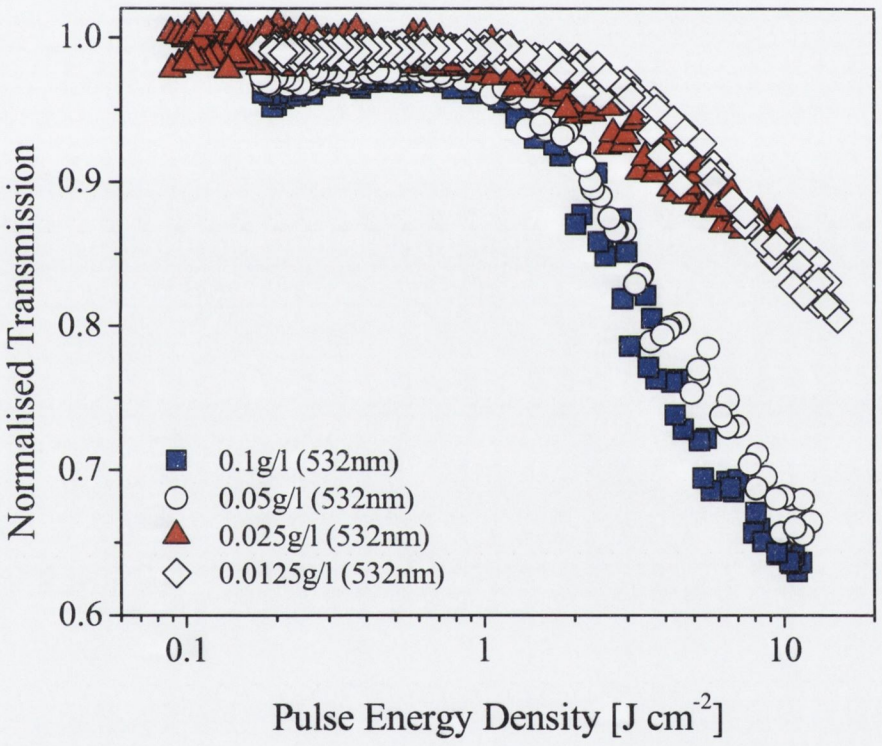

Figure 5.4 Plot of normalized transmission against laser pulse energy density for $Mo_6S_{4.5}I_{4.5}$ nanowires at 0.1g/l, 0.05g/l, 0.025g/l and 0.0125g/l at 532nm.

At these concentrations, for a normalized extinction at an energy density of ~12 J cm^{-2}, the nonlinear optical dissipation was 20%. At the higher nanowire concentrations, the nonlinear optical dissipation was 35%, for a normalized extinction occurring at an energy density of ~ 12 J cm^{-2}. Shown in **Figure 5.3** are both nanowires bundle diameter and β_{eff}, plotted as a function of concentration. The concentration dependence of these parameters is strikingly similar. The variation of β_{eff} is clearly non-linear with concentration indicating that it does not simply scale with the total amount of nanowires material in solution. The fact that its concentration dependence is so similar to that of the bundle diameter suggest that β_{eff} is in fact related to bundle size and not simply to concentration. **Figure 5.5** presents a plot of normalized transmission against laser pulse energy density for both materials at 532 and 1064nm at 0.1g/l and 0.05g/l. A clear distinction can be noted between NLE at 532nm and 1064nm NLO extinction for the $Mo_6S_{4.5}I_{4.5}$ nanowires. If one considers this plot in terms of an investigation into broadband responses, it can be seen that the nonlinear intensity dependent behaviour is far stronger at 532nm than it is at 1064nm.

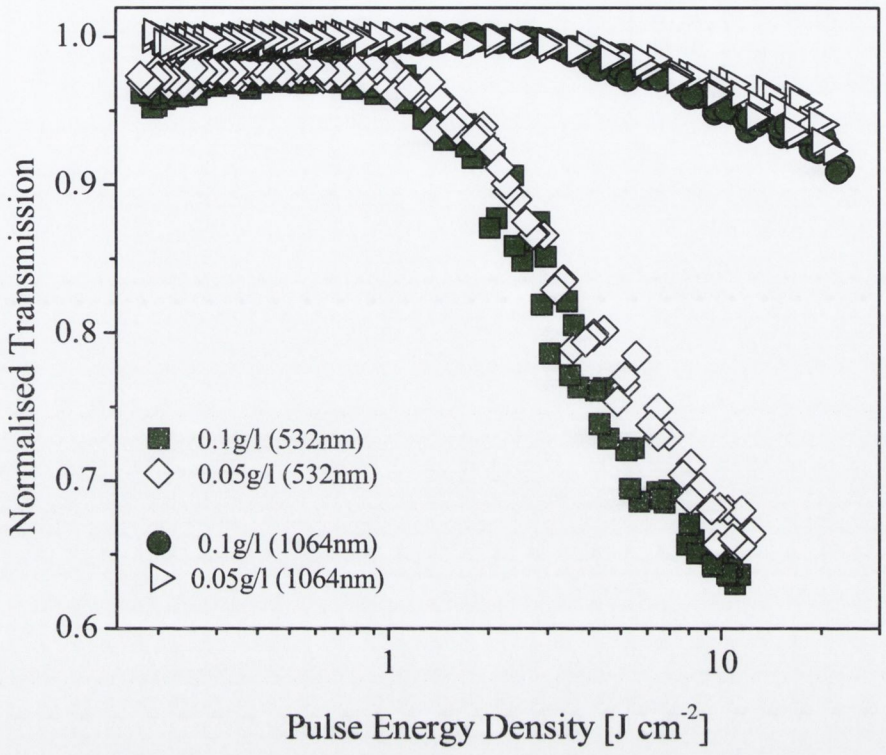

Figure 5.5 Plot of normalized transmission against laser pulse energy density for $Mo_6S_{4.5}I_{4.5}$ nanowires (at 0.1g/l and 0.05g/l) at 532nm and 1064nm.

Much effort has been afforded to understanding the nonlinear optical extinction process resulting from carbon nanotubes.[40-42] As mentioned in Section **5.1**, Riggs et al.,[25] using 532nm nanosecond laser irradiation, reported a study into the nonlinear optical properties of suspended and solubilised SWNTs and MWNTs at 532nm. They suggested that nonlinear scattering is responsible for the NLE responses suspended-nanotube systems and nonlinear absorption occurs for the solubilized nanotube systems. Li et al. [43] investigated the optical limiting properties of two polymer-functionalized MWNT dispersion systems. They noted an enhancement of the NLE response for both poly(N-vinylcarbazole)-MWNT (PVK-MWNT) and

polybutadiene-MWNT (PB-MWNT) when compared to C_{60}-fullerene. The report concluded that the strong electron-donating and accepting abilities of the bound polymer increases intramolecular electron transfer in soluble nanotube systems, leading to enhanced nonlinear absorption.

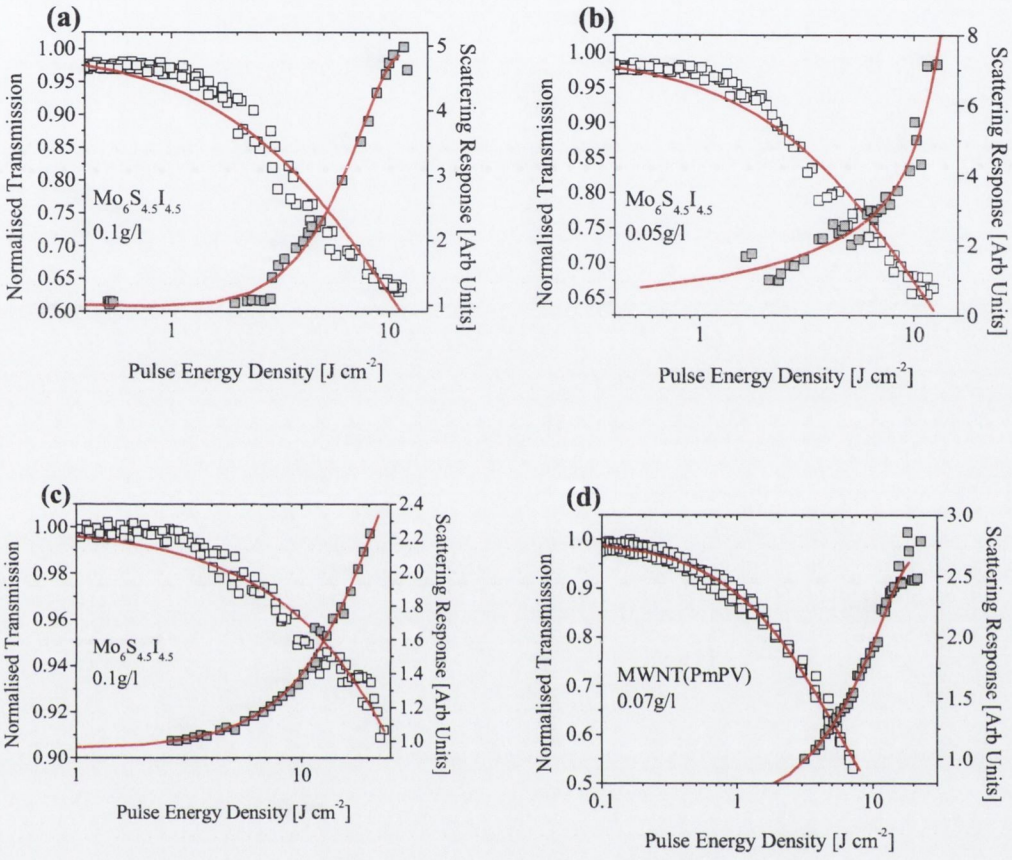

Figure 5.6 Plot of normalized transmission (Y1 axis) and scattered signal (Y2 axis, shaded squares) against laser pulse energy density for $Mo_6S_{4.5}I_{4.5}$ nanowires at concentrations of 0.1g.l, 532nm (a), 0.05g/l, 532nm (b), 0.1g/l, 1064nm (c) and MWNT(PmPV) composite dispersion at 0.07g/l, 532nm (d) respectively. The solid line is intended as a visual guide to the eye.

The general consensus for the NLE of carbon nanotubes in dispersion, is that of a dominant nonlinear scattering response from suspended tubes [22-24] and a complementary nonlinear absorption response from solubilised tubes.[28, 29] This "two-component" system exploits both nonlinear processes, with an enhanced broadband OL response. [41] Compared to phthalocyanine-based study presented in

chapter 4, the exploitation of both nonlinear absorption and scattering processes is a viable alternative to the phthalocyanine systems for optimising the NLE response. It must be highlighted that scattering from thermal induced bubbles is unachievable in solid state form.

In order to investigate the mechanism underlying the observed extinction in the $Mo_6S_{4.5}I_{4.5}$ nanowire system, it was necessary to perform intensity dependent scattering experiments. In the specific angular geometry used for these experiments, if the NLE is solely due to non-linear absorption effects, then the intensity of scattered light should scale linearly with incident light intensity. Any nonlinearity in the response indicates the presence of intensity dependent scattering processes. The scattered signal was collected at 45 degrees to the incident irradiation direction. The results are presented in **Figure 5.6(a)-(d)** where we have simultaneously collected data measuring the direct optical extinction and the scattered intensity for $Mo_6S_{4.5}I_{4.5}$ nanowires at 0.1g/l (532nm, **Figure 5.6a** and 1064nm, **Figure 5.6c**), and 0.05g/l (532nm, **Figure 5.6b**). For comparison purposes, **Figure 5.6d** presents the results of a similar investigation for MWNT(PmPV) composite dispersion at 0.07g/l (at 532nm). In all cases the scattered intensity was highly non-linear with incident intensity. For both nanowire concentrations there is a clear correlation between the initiation of the NLE and the onset of the nonlinear scattered signal at 532nm, with a similar trend noted at 1064nm (**Figures 5.6a-c**). From this investigation it is clear that scattering processes play a critically important role in the NLE response exhibited by $Mo_6S_{4.5}I_{4.5}$ nanowires for all concentrations, at both wavelengths of 532nm and 1064nm. The NLE of nanosecond laser pulses was characterized for a series of $Mo_6S_{4.5}I_{4.5}$ nanowire concentrations at both 532nm and 1064nm using the Z-scan technique. At 532nm, two main NLE regimes were noted for a series of nanowire concentrations, which also exhibit two distinct nanowire diameter distributions. Intensity dependent nonlinear scattering experiments were performed and a correlation between the NLE and the scattering response was observed for both wavelengths.

Future investigations would include fabricating $Mo_6S_{4.5}I_{4.5}$ nanowire-polymer composite, and evaluating the NLE in the solid-state form. If scattering is the dominant process in the NLE, one would expect negligible response in the

composite films. However if there exists a nonlinear absorption component, such as in carbon nanotubes, one may then consider exploiting $Mo_6S_{4.5}I_{4.5}$ nanowires for introduction into OL device structures.

5.3 Phthalocyanine Nanoparticles

5.3.1 Introduction

Among the large number of non-linear optical absorbers that have been identified, phthalocyanines and their derivatives have emerged as promising materials due to their large optical nonlinearities, ultrafast response times and easy processability.[9-12, 44-50] In **chapter 4** the nonlinear optical properties of phthalocyanine-polymer composite systems were investigated and discussed, with particular regard to the various chemical modifications to the phthalocyanine macrocycle. As an alternative to such phthalocyanine systems the fabrication of nanoparticle dispersions may offer opportunities to enhance the nonlinear dissipation of high intensity light and would be of great potential interest for incorporating into nonlinear optical devices.

5.3.2 Sample Preparation

The nanoparticle preparation procedure for both phthalocyanine compounds was as follows: 200µl of the acetone solution was injected into 20ml of vigorously stirred deionised water at room temperature. After injection, the aqueous nanoparticle dispersion was irradiated immediately using a microwave oven (Sharp Compact R-230A; 2.45 GHz, 800W) at 560W for 30s. The treatment with microwaves is considered to be a homogeneous irradiation of the entire droplet liquid dispersion system formed after reprecipitation. Experimentally, this implies that after injecting the organic solvent solution (phthalocyanine dissolved in acetone in this case) into water, microwaves are employed to heat the dispersion and hence force the organic

solvent to evaporate rapidly. The rapid evaporation aims to prevent aggregation between droplets. The compound, which was dissolved in the droplet before evaporation, will then form regular shaped particles of nanometre dimensions. Thus, the final nanoparticle dispersions were at mass concentrations of 0.007 and 0.01 g/l for the $(SPh)_4PcZn$ and tBu_4PcZn nanoparticles, respectively, and to allow the execution of comparable experiments solutions of the two compounds were prepared at the same mass concentrations in dimethylformamide (DMF).

For the TEM investigations approximately 2ml of the freshly prepared nanoparticle-water dispersion was dropped onto a Formvar coated copper grid. The water was evaporated under reduced pressure (7–10 mbar) at room temperature. The resulting samples were observed using a Hitachi H-7000 transmission electron microscope equipped with a Megaview 2 CCD camera from SIS for electronic picture storage. Due to the low contrast between the Formvar coated gird and the phthalocyanine nanoparticles (both consist mainly of carbon) most pictures were taken slightly off focus. AFM samples were prepared by dropping approximately 3ml of freshly prepared nanoparticle-water dispersion onto a $1cm^2$ silicon substrate. The substrate was immediately placed in a vacuum oven and the water evaporated under reduced pressure (7–10 mbar) at room temperature. The samples were observed using a Digital Instruments Nanoscope IIIa in tapping mode. The nanoparticles were dispersed in deionised water and the molecules dissolved in DMF (Aldrich; analytical grade) and sonicated using a low power ultrasonic bath (50W) for 30 min. All samples were measured for nonlinear optical absorption in quartz cells with a 1 cm path.

5.3.3 Results & Discussion

5.3.3.1 Microscopy Analysis

Typical TEM images of the nanoparticles are depicted in **Figures 5.7(a), 5.7(c)** and the spherical geometry of the nanoparticles can be observed. The nanoparticle size was confirmed by tapping mode atomic force microscopy imaging shown in **Figures 5.7(b), 5.7(d)**. The nanoparticle clustering effect, which can be seen in the TEM, was also observed in the AFM studies, although this is not shown in the images presented.

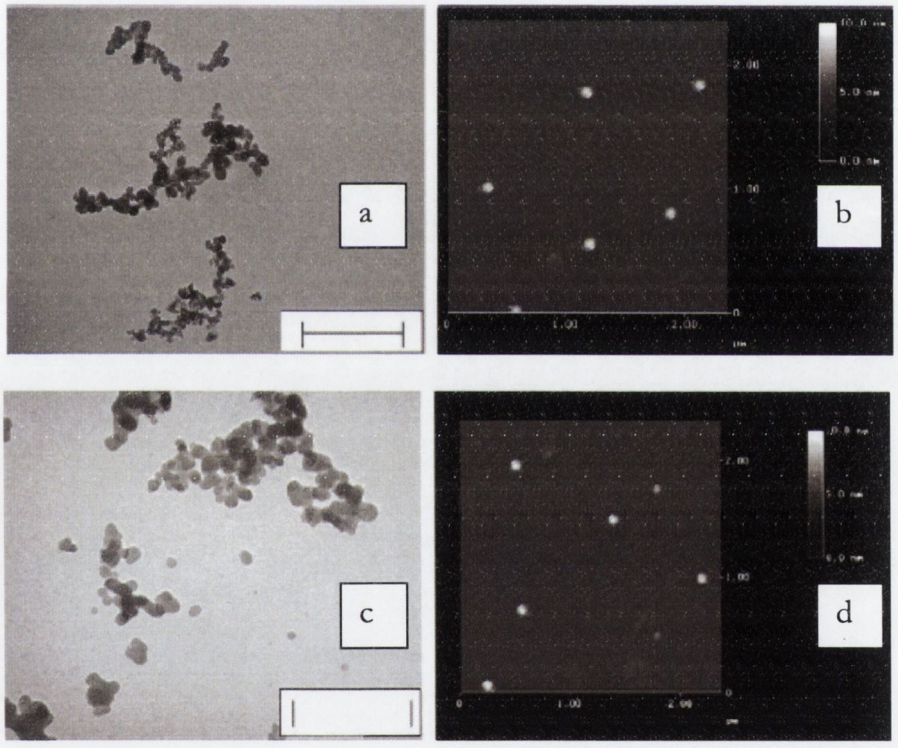

Figure 5.7 (a) TEM and **(b)** AFM images of tBu$_4$PcZn nanoparticles, **(c)** TEM and **(d)** AFM images of (SPh)$_4$PcZn nanoparticles. The scale bars in the TEM images represent 0.5 μm.

The average nanoparticle size was found to be of order 50 nm for the tBu$_4$PcZn nanoparticles and of order 65 nm for the (SPh)$_4$PcZn nanoparticles.

5.3.3.2 Linear Optical Investigation

The linear absorption spectra of phthalocyanine compounds exhibit two main features: a Q-band in the region of 670–690 nm and a B-band (or Soret band) in the region of 320–370 nm, sensitive to molecular substitutions and the environment in which the phthalocyanine resides.[10] The linear absorption spectra of the molecular solutions and the nanoparticle dispersions are depicted in **Figure 5.8(a)&(b)**. The typical Q-band and B-band peaks were located in both molecular cases and are in good agreement with those found by Wrobel and Boguta.[51]

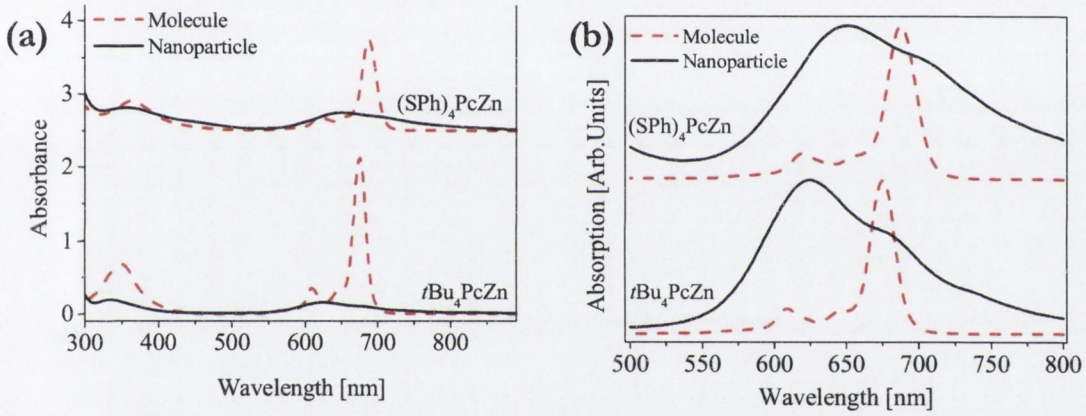

Figure 5.8 (a) UV–Vis spectra of (SPh)$_4$PcZn and tBu$_4$PcZn molecular solutions in DMF (dashed lines) and nanoparticles in water (solid lines). The concentrations of the molecule and nanoparticle pairs are equal by mass (0.01 g/l for tBu$_4$PcZn and 0.007 g/l for (SPh)$_4$PcZn). **(b)** Adjusted view of the UV–Vis spectra in the Q-band region.

The areas under the Q-bands exhibited a significant reduction by a factor of approximately 1.5 for (SPh)$_4$PcZn and of 4.0 for tBu$_4$PcZn when comparing molecular to nanoparticle phases. Furthermore, a broadening of the Q-band was observed as well as a double peak shift to red and blue in the area between 500 and

800 nm. This broadening phenomenon is clearly represented in **Figure 5.8b** where the Q-band absorptions have been normalized to their peaks. This broadening is probably due to a mixture of cofacially and edge-to-edge stacked molecules within the nanoparticle.[52, 53]

Visibly, the intense green or blue colour, characteristic of these phthalocyanine solutions, was found to be much lighter for the nanoparticle samples. The B-band absorption was also seen to increase in the nanoparticle state, with a peak in the region of 270 nm (*not shown in the figure*). We attribute this to acetone, which seems to be trapped within the particle. This is caused during the rapid solvent evaporation in the preparation phase where the nanoparticle formation appears to prevent complete evaporation of the acetone. Endo et al.[53] and Balaban et al.[54] have previously reported this type of behaviour for similar molecules.

5.3.3.3 Nonlinear Optical Investigation

Optical attenuation measurements were performed using the open aperture Z-scan technique.[34] Both nanoparticle dispersion or molecular solution samples exhibited a reduction in the transmission about the focus of the lens, typical of an induced positive nonlinear extinction of the incident light, in the case of the molecular solutions this can certainly be attributed to reverse saturable excited state absorption. The effective nonlinear extinction coefficients (β_{eff}) determined for each sample are quoted in **Table 5**. It should be noted that in both cases, for the $(SPh)_4PcZn$ and $t Bu_4PcZn$ nanoparticle dispersions, their effective nonlinear extinction coefficients β_{eff} are significantly larger than that for their associated molecular solutions despite the equivalent mass concentrations.

Table 5 Optical data collected from UV–Vis absorption spectroscopy and nonlinear optical attenuation experiments. The reference (M) denotes the molecule in solution and (NP) implies the nanoparticle form.

Sample	Concentration (g/L)	α_0 (532nm)	β_{eff} (532nm)
$(SPh)_4PcZn$ (M)	0.01	0.14	$(4.0\pm0.8)\times10^{-10}$
$(SPh)_4PcZn$ (NP)	0.01	0.15	$(2.1\pm0.4)\times10^{-9}$
tBu$_4$PcZn (M)	0.007	0.10	$(4.9\pm1.0)\times10^{-10}$
tBu$_4$PcZn (NP)	0.007	0.095	$(1.6\pm0.3)\times10^{-9}$

The $(SPh)_4PcZn$ molecular solution exhibited $\beta_{eff} \approx (4.0\pm0.8)\times10^{-10}$ cm W^{-1} while its associated nanoparticle exhibited a β_{eff} coefficient approximately 5.3 times larger. For the tBu$_4$-substituted zinc phthalocyanine the β_{eff} difference between the molecule and nanoparticle samples was by a factor of approximately 3.7. Thus, the engineering of phthalocyanine monomer solutions into nanoparticle dispersions appears to be an effective method of increasing the non-linear optical dissipative effect exhibited by the system.

Characteristic curves representing the optical limiting response exhibited by the systems where transmitted energy density (J cm^{-1}) has been plotted against the incident energy density are presented in **Figure 5.9**. In the absence of nonlinear activity in these systems the transmitted energy as a function of incident energy plots would be governed by the linear transmission and this eventuality has been represented by solid lines. It can clearly be seen in both plots that for equivalent incident energy densities that the transmitted energy density is always less for the nanoparticle dispersions than it is for the molecular solutions. This implies more effective optical limiting, which was not unexpected when one considers the nonlinear extinction coefficients as determined above.

(a)

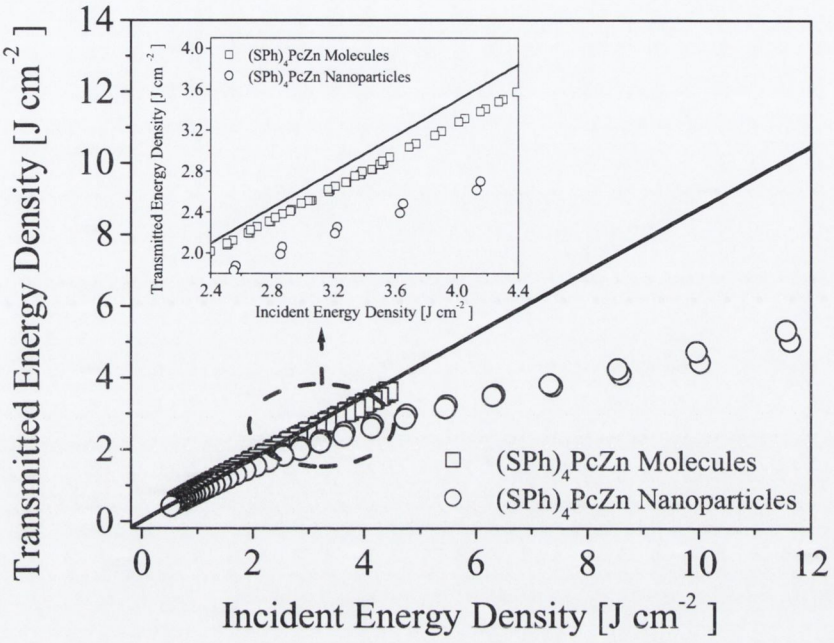

(b)

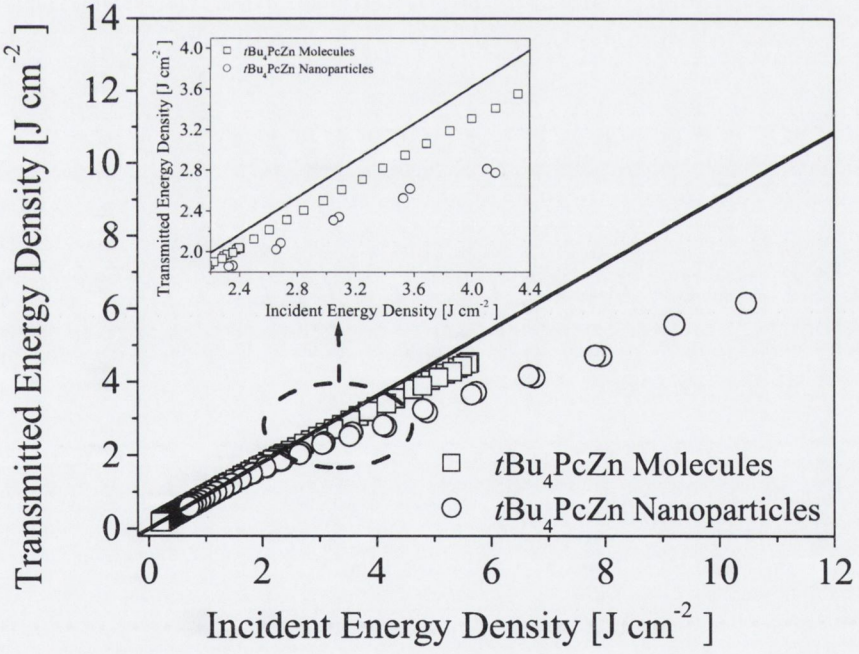

Figure 5.9 Plots of incident against transmitted energy density for **(a)** $(SPh)_4PcZn$ and **(b)** tBu_4PcZn molecular solution and nanoparticle samples, respectively. The solid lines in both plots represent transmission.

Previously, Mansour et al. [13] have reported that optical limiting exhibited by carbon black dispersions was almost entirely due to thermally induced nonlinear scattering of the incident laser pulse. In light of this the nanoparticles that were tested here with dimensions in the region of 60 nm could also exhibit appreciable nonlinear optical extinction due to scattering.

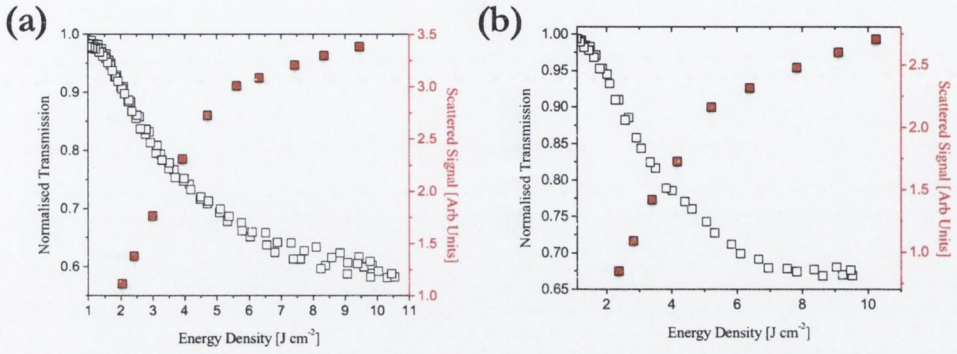

Figure 5.10 (a) $(SPh)_4PcZn$ and **(b)** $t Bu_4PcZn$ nanoparticle dispersions plotting the normalized transmission as a function of energy density. Overlaying these plots is the scattered signal, scaled inversely proportional to the onset of nonlinear optical extinction.

As outlined in **Section 5.2.3.3** for the $Mo_6S_{4.5}I_{4.5}$ nanowire system, the scattered signal was also collected for both zinc phthalocyanine nanoparticle dispersions at 45^0 to the incident irradiation direction. **Figure 5.10(a)&(b)** presents the normalized transmission as a function of energy density, overlaid with the intensity dependent scattered signal, for $(SPh)_4PcZn$ nanoparticle dispersion (**Figure 5.9a**) and the $t Bu_4PcZn$ nanoparticle dispersion (**Figure 5.9b**). From both graphs it can be clearly noted that the scattered signal scales inversely proportionally to the NLE response. Light scattering clearly plays a critical role in the nonlinear extinction for both zinc phthalocyanine nanoparticle dispersions under 532nm irradiation.

Conclusion

A systematic study was undertaken to probe the linear optical properties and nonlinear extinction of high intensity laser irradiation from two nanostructured systems. In the case of $Mo_6S_{4.5}I_{4.5}$ nanowire dispersions, four sequentially decreasing concentrations were prepared and the resulting nonlinear optical properties investigated at 532nm. All four dispersions displayed characteristic nonlinear dissipation curves, graphically presented by plotting normalized transmission as a function of the incident energy density. The two highest nanowire concentration dispersions were also examined at 1064nm, showing a clear wavelength dependent nonlinear extinction at various incident energies.

The linear and nonlinear optical properties of two commercially available zinc phthalocyanines in solution form and in nanoparticle form have been characterized. Using TEM and AFM analysis average nanoparticle size was found to be ~50nm for the tBu$_4$PcZn nanoparticles and ~65nm for the (SPh)$_4$PcZn nanoparticles. The fabrication of the zinc phthalocyanine nanoparticle dispersions increased the nonlinear dissipation of laser irradiation by a factor of ~4, when compared to the molecular phthalocyanine solution. The ease of fabrication, reproducibility and enhanced nonlinear optical properties at 532nm suggests much potential interest as a complementary dispersion to phthalocyanine solution-based systems.

The origin of the nonlinear extinction was probed using an intensity dependent scattering method, by isolating the partial scattering response at an angle of 45^0 to the incident irradiation. A highly nonlinear scattered intensity response was collected for both the $Mo_6S_{4.5}I_{4.5}$ nanowire, MWNT(PmPV) composite samples and the two zinc phthalocyanine nanoparticle dispersions. This optical scattering contributes greatly to the overall optical nonlinear extinction for $Mo_6S_{4.5}I_{4.5}$ nanowire and zinc phthalocyanine nanoparticle dispersions as noted in **Figures 5.5 & 5.9**.

References

1 P. A. Miles, *Applied Optics* **33**, (30), 6965-6979 (1994).

2 P. Miles, *Applied Optics* **38**, (3), 566-570 (1999).

3 F. Henari, J. Callaghan, H. Stiel, W. Blau, and D. J. Cardin, *Chemical Physics Letters* **199**, (1-2), 144-148 (1992).

4 S. R. Mishra, H. S. Rawat, M. P. Joshi, and S. C. Mehendale, *Applied Physics a-Materials Science & Processing* **63**, (3), 223-226 (1996).

5 S. R. Mishra, H. S. Rawat, and S. C. Mehendale, *Applied Physics Letters* **71**, (1), 46-48 (1997).

6 W. J. Blau, H. J. Byrne, D. J. Cardin, T. J. Dennis, J. P. Hare, H. W. Kroto, R. Taylor, and D. R. M. Walton, *Physical Review Letters* **67**, (11), 1423 (1991).

7 S. R. Mishra, and S. C. Mehendale, *Handbook of advanced electronic and photonic materials and devices.* Academic Press: San Diego, CA ; London, 2001; Vol. 9, p 347-364.

8 S. R. Flom, *Porphyrin and Phthalocyanine Handbook.* Academic Press: Boston, MA, 2003.

9 H. S. Nalwa, and J. S. Shirk, *Phthalocyanines: Properties and Applications* John Wiley&Sons: New York, 1996; Vol. 4, p 83.

10 N. B. McKeown, *Phthalocyanine Materials: Synthesis, Structure and Function (Eds: B. Dunn, J.W. Goodby, A.R. West).* Cambridge University Press: 1998.

11 D. R. Coulter, V. M. Miskowski, J. W. Perry, T. H. Wei, E. W. V. Stryland, and D. J. Hagan, *SPIE Proc.* **1105**, 42 (1989).

12 J. W. Perry, K. Mansour, S. R. Marder, K. J. Perry, D. J. Alvarez, and I. Choong, *Optics Letters* **19**, (9), 625-627 (1994).

13 K. Mansour, P. Fuqua, S. R. Marder, B. Dunn, and J. W. Perry, *Proceedings of SPIE-The International Society for Optical Engineering* **2143**, 239 (1994).

14 M. Tian, S. Yanagi, K. Sasaki, T. Wada, and H. Sasabe, *J. Opt. Soc. Am. B* **15**, 846 (1998).

15 S. R. Mishra, Mehendale S.C. , *Organic Materials For Optical Limiting.* ed.; Academic Press: 2001; Vol. 9, p 347-363.

16 H. S. Nalwa, *Handbook of Nanostrctured Materials & Nanotechnology.* 1st ed.; Academic Press,: San Diego, CA ; London 2000; Vol. 5, p 433.

17 R. H. Xie, *Handbook of advanced electronic and photonic materials and devices: .* Academic Press: San Diego, CA ; London 2001 Vol. 9, p 267-304.

18 B. Champagne, and B. Kirtman, *Handbook of advanced electronic and photonic materials and devices: .* Academic Press: San Diego, CA ; London 2001; Vol. 9, p 63-119.

19 Y. Chen, Y. Lin, N. He, J. J. Doyle, X. Zhuang, J. Bai, Y. Liu, and W. J. Blau, *Journal of Nanoscience and Nanotechnology* **Accepted**, (2006).

20 L. W. Tutt, and T. F. Boggess, *Progress in Quantum Electronics* **17**, (4), 299-338 (1993).

21 L. Vivien, E. Anglaret, D. Riehl, F. Bacou, C. Journet, C. Goze, M. Andrieux, M. Brunet, F. Lafonta, P. Bernier, and F. Hache, *Chemical Physics Letters* **307**, (5-6), 317-319 (1999).
22 L. Vivien, E. Anglaret, D. Riehl, F. Hache, F. Bacou, M. Andrieux, F. Lafonta, C. Journet, C. Goze, M. Brunet, and P. Bernier, *Optics Communications* **174**, (1-4), 271-275 (2000).
23 L. Vivien, P. Lancon, D. Riehl, F. Hache, and E. Anglaret, *Carbon* **40**, (10), 1789-1797 (2002).
24 L. Vivien, D. Riehl, F. Hache, and E. Anglaret, *Physica B: Condensed Matter* **323**, (1-4), 233-234 (2002).
25 J. E. Riggs, D. B. Walker, D. L. Carroll, and Y. P. Sun, *J. Phys. Chem. B* **104**, (30), 7071-7076 (2000).
26 R. G. Ispasoiu, L. Balogh, O. P. Varnavski, D. A. Tomalia, and T. G. Goodson, *J. Am. Chem. Soc.* **122**, (44), 11005-11006 (2000).
27 S. R. Mishra, H. S. Rawat, S. C. Mehendale, K. C. Rustagi, A. K. Sood, R. Bandyopadhyay, A. Govindaraj, and C. N. R. Rao, *Chemical Physics Letters* **317**, (3-5), 510-514 (2000).
28 S. A. O'Flaherty, R. Murphy, S. V. Hold, M. Cadek, J. N. Coleman, and W. J. Blau, *Journal of Physical Chemistry B* **107**, (4), 958-964 (2003).
29 S. M. O'Flaherty, S. V. Hold, M. E. Brennan, M. Cadek, A. Drury, J. N. Coleman, and W. J. Blau, *Journal of the Optical Society of America B-Optical Physics* **20**, (1), 49-58 (2003).
30 M. E. Brennan, in *Physics*, Trinity College Dublin: Dublin, Ireland, 2001; Vol. PDoctor of Philosophy, p 180.
31 D. Vrbanic, M. Remskar, A. Jesih, A. Mrzel, P. Umek, M. Ponikvar, B. Jancar, A. Meden, B. Novosel, S. Pejovnik, P. Venturini, J. C. Coleman, and D. Mihailovic, *Nanotechnology* **15**, (5), 635-638 (2004).
32 V. Nicolosi, D. Vrbanic, A. Mrzel, J. McCauley, S. O'Flaherty, D. Mihailovic, W. J. Blau, and J. N. Coleman, *Chemical Physics Letters* **401**, (1-3), 13-18 (2005).
33 V. Nicolosi, D. Vrbanic, A. Mrzel, J. McCauley, S. O'Flaherty, C. McGuinness, G. Compagnini, D. Mihailovic, W. J. Blau, and J. N. Coleman, *Journal of Physical Chemistry B* **109**, (15), 7124-7133 (2005).
34 M. Sheik-Bahae, A. A. Said, T. H. Wei, D. J. Hagan, and E. W. Vanstryland, *IEEE Journal of Quantum Electronics* **26**, (4), 760-769 (1990).
35 J. J. Doyle, V. Nicolosi, S. M. O'Flaherty, D. Vengust, A. Drury, D. Mihailovic, J. N. Coleman, and W. J. Blau, *Submitted Aug 2006, Chemical Physics Letters*, (2006).
36 V. Nicolosi, J. N. Coleman, W. J. Blau, and D. Mihailovic, *Abstracts of Papers of the American Chemical Society* **227**, U1260-U1260 (2004).
37 J. N. Coleman, D. F. OBrien, B. McCarthy, B. Lahr, A. Drury, R. C. Barklie, W. J. Blau, and A. B. Dalton, *Chemical Communications* **20**, 2001-2002 (2000).
38 K. P. Ryan, S. M. Lipson, A. Drury, M. Cadek, M. Ruether, S. M. O. Flaherty, V. Barron, B. McCarthy, H. J. Byrne, W. J. Blau, and J. N. Coleman, *Chemical Physics Letters* **391**, 329 (2004).

39 J. N. Coleman, A. Fleming, S. Maier, S. O'Flaherty, A. I. Minett, M. S. Ferreira, S. Hutzler, and W. J. Blau, *Journal of Physical Chemistry B* **108**, (11), 3446-3450 (2004).
40 L. Liu, S. Zhang, T. Hu, Z. X. Guo, C. Ye, L. Dai, and D. Zhu, *Chemical Physics Letters* **359**, (3-4), 191-195 (2002).
41 X. Sun, R. Q. Yu, G. Q. Xu, T. S. A. Hor, and W. Ji, *Applied Physics Letters* **73**, (25), 3632-3634 (1998).
42 K. C. Chin, A. Gohel, W. Z. Chen, H. I. Elim, W. Ji, G. L. Chong, C. H. Sow, and A. T. S. Wee, *Chemical Physics Letters* **409**, (1-3), 85-88 (2005).
43 C. Li, C. L. Liu, F. S. Li, and Q. H. Gong, *Chemical Physics Letters* **380**, (1-2), 201-205 (2003).
44 J. J. Doyle, B. Ballesteros, G. de la Torre, D. A. McGovern, J. M. Kelly, T. Torres, and W. J. Blau, *Chemical Physics Letters* **428**, (4-6), 307-311 (2006).
45 D. Dini, M. Hanack, W. Ji, and W. Z. Chen, *Molecular Crystals and Liquid Crystals* **431**, 559-574 (2005).
46 H. S. Nalwa, and A. Kakuta, *Thin Solid Films* **254**, (1-2), 218-223 (1995).
47 C. F. Li, L. Zhang, M. Yang, H. Wang, and Y. X. Wang, *Physical Review A* **49**, (2), 1149-1157 (1994).
48 J. S. Shirk, R. G. S. Pong, F. J. Bartoli, and A. W. Snow, *Applied Physics Letters* **63**, (14), 1880-1882 (1993).
49 Y. Chen, M. E. EI-Khouly, J. J. Doyle, E. G. A. Notaras, W. J. Blau, and S. M. O'Flaherty, *Handbook of Organic Electronics and Photonics*. American Scientific Publishers: 2005; Accepted.
50 G. de la Torre, P. Vazquez, F. Agullo-Lopez, and T. Torres, *Journal of Materials Chemistry* **8**, (8), 1671-1683 (1998).
51 D. Wrobel, and A. Boguta, *Journal of Photochemistry and Photobiology A: Chemistry* **150**, (1-3), 67-76 (2002).
52 L. Antonov, G. Gergov, V. Petrov, M. Kubista, and J. Nygren, *Talanta* **49**, 99-106 (1999).
53 K. Endo, Y. Kondo, Y. Aoyama, and F. Hamada, *Tetrahedron Letters* **44**, (7), 1355-1358 (2003).
54 T. S. Balaban, A. Eichhöfer, and J.-M. Lehn, *Eur. J. Org. Chem.*, 4047-4057 (2000).

CHAPTER 6

CONCLUSION

6.1 Closing Remarks

Chapter **1** initially presented the concept of *optical limiting*, a term indicative of the nonlinear dissipation of high intensity irradiation. The nonlinear extinction (NLE) of incident light through both absorption and scattering processes was discussed for various material systems and the mechanisms of light dissipation investigated. Chapter **4** detailed the nonlinear optical absorption for a series of polymer-phthalocyanine composite films. Three case studies were outlined representing the three main chemical modifications to the phthalocyanine macrocycle - central metal, axial and peripheral substitutions. In comparing the performance of each polymer-phthalocyanine film, surface roughness, molecular aggregation and linear and nonlinear optical coefficients were employed. In that regard, films **1** (PMMA-*t*Bu$_4$PcInCl) and **2** (PMMA- *t*Bu$_4$PcGaCl) out-performed all phthalocyanine composite films, with **1** showing the most enhanced nonlinear optical response. The calculated κ value for **1** was (4.1 ± 0.1) and for **2** was (3.7 ± 0.1). Similar FWHM ratios of ~5.5 were found for both films. The enhanced nonlinear optical response noted in **1** was compared to **2** which exhibited a F_{sat} one third that of film **1**. This is indicative of the nonlinear absorption processes occurring for relatively lower input energies for film **1**. The negative effects of aggregation on the nonlinear optical response of polymer-phthalocyanine films were highlighted in comparing films **3**-**8**. In the second case study the degree of strength of electron withdrawing capabilities of the axial ligand in **10** (largest), **9** and **2** (lowest) resulted in sequentially decreasing κ values from **10** to **2**. Film **2** had the lowest calculated F_{sat} value, of (1.6 ± 0.1) J cm^{-2}, compared to (2.3 ± 0.1) J cm^{-2} for **9** and (3.1 ± 0.2) J cm^{-2} for **10**. The highest F_{sat} value was calculated for **10** which has the less efficient, Ga-benzene-CF_3, axial ligand. For axial ligand substitution it appeared that κ may be influenced by the strength of electron withdrawing in the axial group, while F_{sat} may be mainly influenced by the efficiency of this electron transfer process.

Concerning peripheral substitutions, the highly concentrated electron withdrawing groups tended to strongly influence the resulting nonlinear optical

response of the PMMA-phthalocyanine films. The fluorine side-group in film **14** out-performed **4** and displayed comparable results to film **15.**

A series of $Mo_6S_{4.5}I_{4.5}$ nanowire dispersions were prepared for both concentration and wavelength dependent nonlinear optical studies. The average bundle diameter tended to decrease with concentration as presented diagrammatically in chapter **5**. The NLE response of the $Mo_6S_{4.5}I_{4.5}$ nanowire dispersions at 532nm fell into one of two distinct regimes. The weaker NLE response was noted for the two lower concentrations of 0.025g/l and 0.0125g/l, corresponding to an average nanowires bundle diameter of <6nm. At these concentrations for a normalized extinction at an energy density of ~12 J cm^{-2}, the nonlinear optical dissipation was 20%. Detailing the two higher nanowire concentrations of 0.1g/l and 0.05g/l, the nonlinear optical dissipation was 35% for a normalized extinction occurring at an energy density of ~ 12 J cm^{-2}. Also presented in chapter **5** was a plot of normalized transmission against laser pulse energy density for $Mo_6S_{4.5}I_{4.5}$ nanowire dispersion concentrations of 0.1g/l and 0.05g/l, at 532nm and 1064nm. A clear distinction was noted between the NLE at 532nm and 1064nm for the $Mo_6S_{4.5}I_{4.5}$ nanowire system. An intensity dependent scattering investigation was undertaken to probe the mechanism underlying the observed extinction in the $Mo_6S_{4.5}I_{4.5}$ nanowire system. From this study at 532nm and 1064nm, a clear correlation between the initiation of the NLE and the onset of the nonlinear scattered signal was observed for 0.1g/l and 0.05g/l nanowire dispersions. In conjunction with this investigation, a polymer-multiwalled carbon nanotube composite dispersion was employed as reference system for all nonlinear extinction and nonlinear scattering experiments. Included in this chapter were sample preparation and experimental NLE results of two zinc phthalocyanine nanoparticles dispersions. The average nanoparticle size was found to be ~50 nm for the tBu$_4$PcZn nanoparticles and ~65 nm for the (SPh)$_4$PcZn nanoparticles. Both phthalocyanine nanoparticle dispersions and molecular solution samples exhibited a reduction in the transmission about the focus of the lens, typical of an induced positive nonlinear extinction of the incident light. For the (SPh)$_4$PcZn and tBu$_4$PcZn nanoparticle dispersions, the effective nonlinear extinction coefficients β_{eff} were significantly larger than that for their associated molecular solutions despite the

equivalent mass concentrations. The intensity dependent scattered signal was collected for both zinc phthalocyanine nanoparticle dispersions at 45^0 to the incident irradiation direction and yielded interesting results. Two graphs were presented plotting the normalized transmission as a function of energy density. Overlaying these plots is the scattered signal which scaled inversely proportional to the onset of nonlinear optical extinction. Light scattering played a critical role in the nonlinear extinction for both zinc phthalocyanine nanoparticle dispersions under 532nm irradiation.

With sustained growth in photonic technologies, enormous interest remains in this dynamic research field with the ongoing necessity for protection of such optical sensors as the human eye. Future scientific directions in this research field may see the integration of polymer-phthalocyanine films, and polymer doped phthalocyanine nanoparticle and $Mo_6S_{4.5}I_{4.5}$ nanowire dispersions for further incorporation into optical limiting device structures. The integration of nonlinear optically responsive media into working optical limiting device geometries, capable of meeting industrial criteria for protection of optical sensors, is fast approaching.

Appendix I

List of Publications

Yu Chen, James J. Doyle, Ying Liu, Adam Strevens, Y. Lin, Mohamed E. EI-Khouly, Yasuyuki Araki, Werner J. Blau, Osamu Ito, "Optoelectronic and nonlinear optical properties of tBu$_4$PcTiO/polymer composite materials", *Journal of Photochemistry and Photobiology A: Chemistry*, 185,263-270, **2007**.

Yu Chen, Ying Liu, Sean M.O'Flaherty, Yasuyuki Araki, Jinrui Bai, James Doyle, Werner J.Blau, Osamu Ito, "Photophysical And Nonlinear Optical Properties Of m-Oxo-Bridged Indium And Gallium Phthalocyanines" *Inorganic Chemistry : An Indian Journal* **1**(1-2), 17-23, **2006.**

James J. Doyle, B. Ballesteros, G. de la Torre, D. A. McGovern, J. M. Kelly, T. Torres, W. J. Blau, "Combination of phthalocyanine and fullerene moieties for optical limiting" *Chemical Physics Letters* 428, 307, **2006**.

Aneta Slodek, Dieter Wöhrle, James J. Doyle, Werner Blau, "Metal Complexes of Phthalocyanines in Polymers as Suitable Materials for Optical Limiting" *Macromolecular Symposia* **235**(9-18), 1, **2006**.

Yu Chen, Mohamed E. EI-Khouly, James J. Doyle, Eleni G.A. Notaras, Werner J. Blau, Seán M. O'Flaherty, "Phthalocyanines and related compounds: nonlinear optical response and photoinduced electron transfer process" *Handbook of Organic Electronics and Photonics*, American Scientific Publishers, **2005.**

Christian Nitschke, Sean M. O'Flaherty, James J. Doyle, Michael Kroell, Werner J. Blau, "Material investigation and nonlinear optical properties of phthalocyanine nanoparticles" *Nonlinear Optics, Quantum Optics*, **34**(1-4), 261-264. **2005**.

Yu Chen, Yasuyuki Araki, James J. Doyle, Adam Strevens, Osamu Ito, and Werner J. Blau, "Synthesis, Characterization, and Optoelectronic Properties of a Novel Polyfluorene/Poly(p-Phenylenevinylene) Copolymer" *Chemistry of Materials* **17**, (7), 1661-1666, **2005**.

Sean M. O'Flaherty, James J. Doyle, Werner J. Blau, "Numerical Approach for Optically Limited Pulse Transmission in Polymer-Phthalocyanine Composite Systems", *Journal of Physical Chemistry B* **108**, (45), 17313-17319, **2004**.

James J. Doyle, Sean M. O'Flaherty, Yu Chen, Tadgh Hegarty, Michael Hanack, Werner J. Blau. "Polymer-phthalocyanine composite systems as solid state passive optical limiters" *Proceedings of SPIE-The International Society for Optical Engineering* **5464**, 269-279, **2004**.

Christian Nitschke, Sean M. O'Flaherty, James J. Doyle, Michael Kröll, Werner J. Blau, "Material investigation and nonlinear optical properties of phthalocyanine nanoparticles", *Chemical Physics Letters* **383**(5-6), 555-560, **2004**.

Accepted

Yu Chen, Ying Lin, Nan He, James J. Doyle, Xiaodong Zhuang, Jinrui Bai, Ying Liu, Werner J. Blau, "Carbon nanotube-based functional materials for optical Limiting" *Journal of Nanoscience and Nanotechnology*, Invited Review, (In press) **2006**.

Ying Liu, Sean M. O'Flaherty, Yu Chen, Yasuyuki Araki, Jinrui Bai, James J. Doyle, Werner J. Blau , Osamu Ito, "Photophysical and nonlinear optical properties of μ-oxo-bridged indium and gallium phthalocyanines" *Dyes and Pigments*, (In press) **2006**.

James J. Doyle, Valeria Nicolosi, Sean M. O'Flaherty, D. Vengust, Anna Drury, Dragan Mihailovic, Jonthan N. Coleman, Werner J. Blau, "Nonlinear Optical Response of $Mo_6S_{4.5}I_{4.5}$ Nanowires" *Chemical Physics Letters*, (In press) **2006**.

Nan He, Yu Chen, James J. Doyle, Ying Liu, Werner J. Blau "Optical and nonlinear optical properties of an octasubstituted liquid crystalline copper phthalocyanine" *Dyes and Pigments*, (In press) **2006**.

Submitted

Yu Chen, James J. Doyle, Nan He, Xiaodong Zhuang, Ying Liu, Werner J. Blau, "Enhancement of optical limiting response by embedding gallium phthalocyanine into polymer host" *Optics Letters*, Submitted **2006**.

Sharon M. King, Shweta Chaure, James J. Doyle, Alan Colli, Andrea C. Ferrari, Werner J. Blau. "Scattering induced optical limiting in Si/SiO_2 nanostructure dispersions" Optics Communications, Submitted **2006**.

Yu Chen, James J. Doyle, Nan He, Xiaodong Zhuang, Ying Lin, Werner J. Blau, "The passive optical limiting performance of the gallium phthalocyanine/polymer composite materials", *Journal of Materials Chemistry*, Submitted **2006**.

Yu Chen, Xaiodong Zhuang, James J. Doyle, Mohamed E. EI-Khouly, Werner J. Blau, Yasuyuki Araki, Osamu Ito, "Optical and nonlinear optical properties of an octasubstitutued copper phthalocyanine", *Applied Physics A: Materials Science & Processing*, Submitted **2006**.

Eleni G. A. Notaras, Marijana Fazekas, James J. Doyle, Werner J. Blau and Mathias O. Senge, "A2B2–type push-pull porphyrins as reverse saturable and saturable absorbers", Chemical Communications, Submitted **2006**.